Membrane Transport 2023: Recent Research into Ion Channels, Transporters and Epithelial Physiology
24 – 25 August 2023 | University of St Andrews, UK
Abstracts

Experiments on animals and animal tissues

It is a requirement of The Society that all vertebrates (and Octopus vulgaris) used in experiments are humanely treated and, where relevant, humanely killed.

To this end authors must tick the appropriate box to confirm that:

For work conducted in the UK, all procedures accorded with current UK legislation.

For work conducted elsewhere, all procedures accorded with current national legislation/guidelines or, in their absence, with current local guidelines.

Experiments on humans or human tissue

Authors must tick the appropriate box to confirm that:

All procedures accorded with the ethical standards of the relevant national, institutional or other body responsible for human research and experimentation, and with the principles of the World Medical Association's Declaration of Helsinki.

Guidelines on the Submission and Presentation of Abstracts

Please note, to constitute an acceptable abstract, The Society requires the following ethical criteria to be met. To be acceptable for publication, experiments on living vertebrates and Octopus vulgaris must conform with the ethical requirements of The Society regarding relevant authorisation, as indicated in Step 2 of submission.

Abstracts of Communications or Demonstrations must state the type of animal used (common name or genus, including man. Where applicable, abstracts must specify the anaesthetics used, and their doses and route of administration, for all experimental procedures (including preparative surgery, e.g. ovariectomy, decerebration, etc.).

For experiments involving neuromuscular blockade, the abstract must give the type and dose, plus the methods used to monitor the adequacy of anaesthesia during blockade (or refer to a paper with these details). For the preparation of isolated tissues, including primary cultures and brain slices, the method of killing (e.g. terminal anaesthesia) is required only if scientifically relevant. In experiments where genes are expressed in Xenopus oocytes, full details of the oocyte collection are not necessary. All procedures on human subjects or human tissue must accord with the ethical requirements of The Society regarding relevant authorisation, as indicated in Step 2 of submission; authors must tick the appropriate box to indicate compliance.

SA01

The role of TRPV4 in electrolyte and fluid secretion by choroid plexus epithelia: Implications for hydrocephalus

Bonnie Blazer-Yost[1]

[1]*Indiana University, Indianapolis, United States*

Hydrocephalus is a devasting disease for which there is no pharmaceutical treatment. Currently the standard of care involves brain surgery - most usually the placement of a shunt to drain excess cerebrospinal fluid (CSF) from the brain to another area of the body. However, shunts routinely fail for a variety of reasons including infection, blockage and equipment malfunction predisposing the patient to multiple brain surgeries. While pediatric hydrocephalus is perhaps the most recognizable form, there are multiple causes of this condition in older children and adults including traumatic brain injury, stroke, infection. Regardless of the precipitating factors, there is an enlargement of the cerebral ventricles and an excess of CSF in the brain. It is our hypothesis that pharmaceuticals that could decrease CSF production on an as-needed basis would be helpful in treating most forms of hydrocephalus. Rational drug design for such potential treatments is based on a more detailed understanding of the production of CSF by the choroid plexus epithelium (CPe). The small tissue comprising the choroid plexus produces approximately 500 ml of CSF per day, the composition of which varies according to physiological, diurnal, and pathophysiological influences.

In a genetic rat model of hydrocephalus, we have shown that antagonists of the transient receptor potential vanilloid 4 (TRPV4) channel ameliorate the development of hydrocephalus, implicating this channel as a key component of CSF production. Preliminary studies indicate that TRPV4 antagonists are also effective in rodent models of post hemorrhagic and post traumatic hydrocephalus. In addition to pre-clinical animal models, we use a human CPe cell model, the HIBCPP (human choroid plexus papilloma) to identify the transepithelial electrolyte and fluid fluxes that occur in response to TRPV4 stimulation. Ussing-style electrophysiology combined with imaging, qRT-PCR and western blotting, have shown that the HIBCPP cells form a moderately tight barrier epithelium consistent with the blood-CSF barrier and express important transporters found in the native epithelium with the correct polarization. Addition of a TRPV4 agonist causes a multicomponent change in transepithelial electrolyte flux as well as a substantial but reversible change in transepithelial permeability. The TRPV4-mediated electrolyte flux appears to result from secondary activation of multiple transport proteins stimulated in response to the TRPV4-mediated influx of Ca^{2+} and Na^{+} and is a complex mixture of movement of both cations and anions. This flux is accompanied by a statistically significant secretory movement of fluid in response to the TRPV4 agonist. Although *in vivo* the choroid plexus is one of the most secretory epithelia in the body, the degree of fluid secretion by this cell line is unique. The HIBCPP cell line is being used to dissect pathways involved in CSF production. Our results have uncovered unexpected levels of fluid movement in response to TRPV4 stimulation that can inform the role of opposing electrolyte movements and electroneutral transporters that are difficult to measure using electrophysiological techniques.

SA02

Nutraceutical targeting of the Farnesoid X Receptor for regulation of CFTR expression in the colonic epithelium

Jessica Smyth[1], Ciara Fallon[1], Sudipto Das[1], Stephen Keely[1]

[1]*Royal College of Surgeons in Ireland, Dublin, Ireland*

Introduction: The nuclear bile acid receptor, farnesoid X receptor (FXR), is an important regulator of colonic epithelial function and the therapeutic potential for targeting FXR in the treatment of chronic intestinal disease is well documented. We have previously shown that bile acids, acting via FXR, inhibit colonic epithelial Cl^- secretion by downregulating expression of the CFTR Cl^- channel. We have also shown that the pentacyclic triterpene (PCT), hederagenin (HG), a plant-derived bioactive phytochemical, enhances the expression and activity of FXR in colonic epithelial cells and potentiates the effects of FXR on CFTR. Peroxisome proliferator-activated receptors (PPARs), described as nutrient sensors, have recently been shown to modulate FXR expression. Here, we investigated molecular mechanisms underlying FXR regulation of CFTR expression in colonic epithelial cells, and a potential role for PPARs in mediating HG actions on FXR expression and activity.

Methods: Monolayers of T_{84} colonic epithelial cells were treated with HG, PPARγ, PPARα, or PPARδ agonists, rosiglitazone, WY14643, and GW501516, and antagonists, GW9662, GW6471, and GSK3787, respectively. GW4064 was employed as an FXR agonist and FGF19 used as an index of FXR activation. Levels of FGF19, NF-κB p65, FXR, and ANGPTL4, a PPAR target gene, were measured by qRT-PCR, western blotting, or ELISA. FXR binding to the CFTR promoter was investigated by chromatin immunoprecipitation (ChIP).

Results: FXR activation did not alter expression, phosphorylation, or nuclear translocation of the NF-κB p65 subunit, while preliminary ChIP-qPCR analysis demonstrated enhanced binding of FXR to the CFTR promoter upon GW4064 treatment. Treatment with HG significantly increased mRNA expression of the PPAR target gene, ANGPTL4, to 5.7 ± 1 fold ($n = 5$; $p < 0.05$) of untreated cells after 3 hours. The effects of HG on FXR expression were mimicked by rosiglitazone (1 μM), WY14643 (10 μM), and GW501516 (0.5 μM), respectively. The PPARα antagonist, GW6471 (1 μM), reduced HG-induced FXR mRNA and protein expression from 2.8 ± 0.4 to 0.9 ± 0.1 ($n = 5$; $p < 0.05$) and 1.8 ± 0.3 to 1 ± 0.1 ($n = 3$) fold of untreated controls, respectively, whereas the PPARγ and PPARδ antagonists, GW9662 (5 μM) and GSK3787 (1 μM), did not prevent upregulation of FXR by HG.

Conclusion: FXR regulates colonic epithelial CFTR expression and function by a mechanism which appears to involve direct binding of FXR to the CFTR promoter. The bioactive phytochemical, HG, regulates colonic epithelial FXR expression through mechanisms that involve activation of PPARα. By virtue of their ability to upregulate FXR expression, and thereby enhance its antisecretory actions, plant extracts containing HG have excellent potential to be developed as FXR-targeted nutraceuticals for the treatment and prevention of intestinal disease.

SA03

Aldosterone-independent ENaC activity: A paradigm shift for renal salt homeostasis

Christoph Korbmacher[1]

[1]*Friedrich-Alexander-Universität Erlangen-Nürnberg, Erlangen, Germany*

The focus of this presentation will be on emerging evidence for site-specific regulation of the epithelial sodium channel (ENaC) and its role in Na^+ and K^+ homeostasis [1]. In most textbooks ENaC function is discussed in the context of the cortical collecting duct (CCD). ENaC is localised in the apical membrane of CCD principal cells and is the rate-limiting step for Na^+ absorption. It is inhibited by the K^+ sparing diuretic amiloride and regulated by aldosterone. Aldosterone binds to a cytosolic mineralocortioid receptor (MR) and by complex transcriptional regulation and signaling pathways stimulates ENaC. This is evident in primary hyperaldosteronism or Conn syndrome. In simplified terms, inappropriately increased ENaC activity due to hyperaldosteronism results in enhanced NaCl absorption, expansion of extracellular fluid volume and hypertension. Conn syndrome is mimicked by gain-of-function mutations of ENaC causing Liddle syndrome, a rare genetic form of salt-sensitive hypertension. This highlights the importance of ENaC in Na^+ homeostasis and long-term control of blood pressure. Hyperaldosteronism and Liddle syndrome are usually associated with hypokalemia due to a tight functional link between ENaC activity and renal K^+ secretion *via* the renal outer medullary K^+ channel ROMK. The classical concept that ENaC is strictly aldosterone-dependent was challenged by our patch-clamp studies exploring the site-specific regulation of ENaC in microdissected mouse tubules with a focus on two clearly distinguishable regions: The transition zone from the late convoluted tubule (CNT) to the CCD referred to as CNT/CCD, and the transition zone from the late distal convoluted tubule (DCT2) to the early connecting tubule referred to as DCT2/CNT. In an aldosterone synthase deficient mouse model we confirmed the aldosterone dependence of ENaC in CNT/CCD, but made the surprising observation that ENaC activity is aldosterone-independent in DCT2/CNT [2]. Using a mouse model with inducible nephron-specific MR deficiency, we demonstrated that aldosterone-dependent ENaC activity in CNT/CCD was completely MR dependent as expected. Interestingly, MR deficiency also largely reduced aldosterone-independent ENaC activity in DCT2/CNT [3], where MR can probably be stimulated by glucocorticoids due to low expression of 11β-hydroxysteroid dehydrogenase 2 (11β-HSD2). Aldosterone-independent but MR-dependent ENaC activity in DCT2/CNT probably explains, why MR antagonists are efficient blood pressure lowering drugs even when aldosterone levels are not elevated. Moreover, in DCT2/CNT baseline apical ROMK activity is high and a low-K^+ diet reduces ENaC activity, which highlights the important role of this nephron segment in regulating K^+ secretion in an aldosterone-independent manner [4]. Future studies are needed to explore whether other hormones or local factors also regulate ENaC activity in a site-specific manner. In this context proteolytic channel activation, a unique feature of ENaC, may be of particular interest. To address this, the physiologically relevant endogenous proteases need to be elucidated. Recently, we identified TMPRSS2 as a candidate protease involved in proteolytic ENaC activation [5], but its role in the kidney remains to be determined. Finally, high resolution cryo-EM structures of ENaC are now available. These structural data open up exciting new horizons to study ENaC function and site-specific regulation at the molecular level.

1. Pearce D et al. (2022). Pflügers Arch 474: 869-884 2. Nesterov V et al. (2012). Am J Physiol Renal Physiol 303: F1289–F1299 3. Nesterov V et al. (2021). Am J Physiol Renal Physiol 321: F257-F268 4. Nesterov V et al. (2022). Am J Physiol Renal Physiol 322: F42–F54 5. Sure F et al. (2022). J Biol Chem 298:102004

SA04

Structural insights into the trimeric assembly of epithelial sodium channels

Isabelle Baconguis[1], Alexandra Houser[3]

[1]Vollum Institute, Oregon Health & Science University, Portland, OR, United States, [2]Oregon Health & Science University, Portland, OR, United States, [3]Neuroscience Graduate Program, Oregon Health & Science University, Portland, OR, United States

My group studies the ion channel superfamily of Epithelial sodium channel (ENaC)/Degenerin (DEG) channels. Currently, we focus our efforts on understanding ENaC function. ENaC plays a key role in Na^+ reabsorption in epithelial cells. In the kidneys, it regulates blood volume and blood pressure. In the lungs, it regulates airway surface liquid layer. To understand its role in physiological and pathophysiological conditions, we use a combination of biochemical and biophysical techniques to define the molecular basis of oligomeric assembly. We find that ENaC arranges in a preferred counterclockwise configuration to form a stable trimeric assembly. Our findings highlight the importance of diverse subunit compositions in fine-tuning ion channel properties.

SA05

CFTR structure and function: insight from chimeric channels

David Sheppard[1]

[1]*University of Bristol, Bristol, United Kingdom*

A powerful approach to investigate ion channel structure-function relationships is to exploit functional differences between orthologues from divergent species. Here, this approach is used to study the epithelial anion channel cystic fibrosis transmembrane conductance regulator (CFTR). Mouse CFTR has 79% shared amino acid identity with human CFTR. Its function differs from human CFTR in several important respects: altered gating pattern distinguished by prolonged residence in a sub-conductance state, reduced single-channel conductance and strong inward rectification (1,2). Transfer of the regulatory (R) domain of mouse CFTR to human CFTR was without effect, whereas transfer of both nucleotide-binding domains (NBDs) endowed human CFTR with greatly prolonged channel openings without conferring human CFTR with the sub-conductance state, single-channel conductance and inward rectification of mouse CFTR (3). To test the idea that the membrane-spanning domains (MSDs) govern the conduction properties of human and murine CFTR, the human-murine CFTR (hmCFTR) chimeras hmTM1-6, hmTM7-12 and hmTM1-6:TM7-12 containing MSD1, MSD2 and MSD1+MSD2 of mouse CFTR on a human CFTR background were synthesized. To study the single-channel behaviour of these hmCFTR chimeras, a large Cl^- concentration gradient ($[Cl^-]_{int}$, 147 mM; $[Cl^-]_{ext}$, 10 mM) was imposed across inside-out membrane patches excised from transiently transfected CHO cells and voltage clamped at -50 mV, whereas to analyse macroscopic currents, membrane patches were bathed in symmetrical 147 mM Cl^- solutions and voltage clamped at 0 mV. All intracellular solutions contained protein kinase A (PKA; 75 nM) and ATP (1 mM) to activate and sustain CFTR channel activity; temperature was 37 °C. The three hmCFTR chimeras possessed a gating pattern intermediate between those of human and mouse CFTR. Like human CFTR, hmTM7-12 rarely transitioned to sub-conductance states, whereas hmTM1-6 sojourned to multiple sub-conductance states and hmTM1-6:TM7-12 resided in a tiny sub-conductance state resembling that of mouse CFTR. Consistent with hmTM1-6:TM7-12 possessing human, not mouse, NBDs, this hmCFTR chimera resided in the sub-conductance state for noticeably shorter periods than mouse CFTR. Upon quantification, both the single-channel conductance and open probability of the full open-state of hmCFTR chimeras decreased in the rank order: human CFTR > hmTM7-12 > hmTM1-6 ≥ hmTM1-6:TM7-12 ($n = 5 – 10$). Using 2-s voltage ramps from -100 to +100 mV to acquire current-voltage relationships, human CFTR Cl^- currents weakly inwardly rectified, whereas those of mouse CFTR exhibited strong inward rectification. Transfer of both MSDs of mouse CFTR to human CFTR in the chimera hmTM1-6:TM7-12 reproduced the strong inward rectification of mouse CFTR ($n = 4$). Interestingly, the inward rectification of hmTM1-6 closely resembled that of mouse CFTR, whereas that of hmTM7-12 was intermediate between human and mouse CFTR ($n = 6 – 9$). Taken together, these data demonstrate that sequences from both MSDs specify the gating, conduction and rectification properties of CFTR with sequences from MSD1 playing a dominant role in determining the different rectification behaviour of human and mouse CFTR.

(1) Lansdell KA et al. (1998) J Physiol. 508, 379-392. (2) Lansdell KA et al. (1998) J Physiol. 512, 751-764. (3) Scott-Ward TS et al. (2007) Proc Natl Acad Sci U S A. 104, 16365-16370.

SA06

Structural insights into the gating dynamics of bacterial mechanosensitive channels

Benjamin Lane[1,2], Bolin Wang[1,2], Charline Fagnen[1,3], Mariangela Dionysopoulou[1,2], Hassane El Mkami[4], Antonio Calabrese[1,5], Stephen Muench[1,2], Antreas Kalli[1,3], Christos Pliotas[1,6,7]

[1]Astbury Centre for Structural Molecular Biology, University of Leeds, Leeds, United Kingdom, [2]School of Biomedical Sciences, Faculty of Biological Sciences, University of Leeds, Leeds, United Kingdom, [3]Leeds Institute of Cardiovascular and Metabolic Medicine, School of Medicine, University of Leeds, Leeds, United Kingdom, [4]School of Physics and Astronomy, University of St Andrews, St Andrews, United Kingdom, [5]School of Molecular and Cellular Biology, Faculty of Biological Sciences, University of Leeds, Leeds, United Kingdom, [6]School of Biological Sciences, Faculty of Biology, Medicine and Health, Manchester Academic and Health Science Centre, University of Manchester, Manchester, United Kingdom, [7]Manchester Institute of Biotechnology, University of Manchester, Manchester, United Kingdom

Ion channels control solute flux by undergoing conformational changes which regulate their function in response to stimuli. Bacterial mechanosensitive channels sense changes in lateral tension generated in the membrane, acting as pressure-safety valves to prevent cell lysis (1). However, some of these channels also have unique features that suggest additional physiological roles. Bacterial mechanosensitive channels can be divided into two structural families: MscL and the MscS-like superfamily (1). The large-conductance (MscL) and small-conductance (MscS) mechanosensitive channels are well characterized structurally and functionally, but an understanding of the link between structure and function is missing. Lipid availability within pockets has been linked with mechanosensation in these channels (2), but the gating mechanisms and discrete subconducting states have not been fully defined. Studies on other members of the MscS-like family, such as YbiO, are limited. Several of these mechanosensitive channels have been implicated in bacterial pathogenicity and virulence, so understanding their mechanisms could provide avenues for the development of antimicrobials (3).

Previously, it was shown that lipid removal from transmembrane pockets through a point mutation (L89W) leads to the stabilization of an expanded subconducting state (2). However, whether there is a correlation between the tension-mediated state and the state derived by pocket delipidation in the absence of tension remained unknown. To investigate the physiological relevance of this subconducting state we probed solvent accessibility using a combination of electron paramagnetic resonance (EPR) spectroscopy and hydrogen-deuterium exchange (HDX) mass spectrometry (4). This was coupled with membrane stretching molecular dynamics (MD) which allowed the stabilization of a state under tension. This allowed us to investigate the structural changes associated with distinctively derived states. We found that pocket delipidation by either membrane tension or molecular modification causes MscL to occupy a similar structurally defined subconducting state (5). These findings revealed the mutation stabilized state is an intermediate in the channel activation pathway. They also provide support for models that implicate lipid availability in the regulation of channel gating in mechanosensitive channels. Ongoing structural work aims to investigate whether lipid availability within transmembrane pockets is also a regulatory mechanism of channel gating within larger members of the MscS-like superfamily.

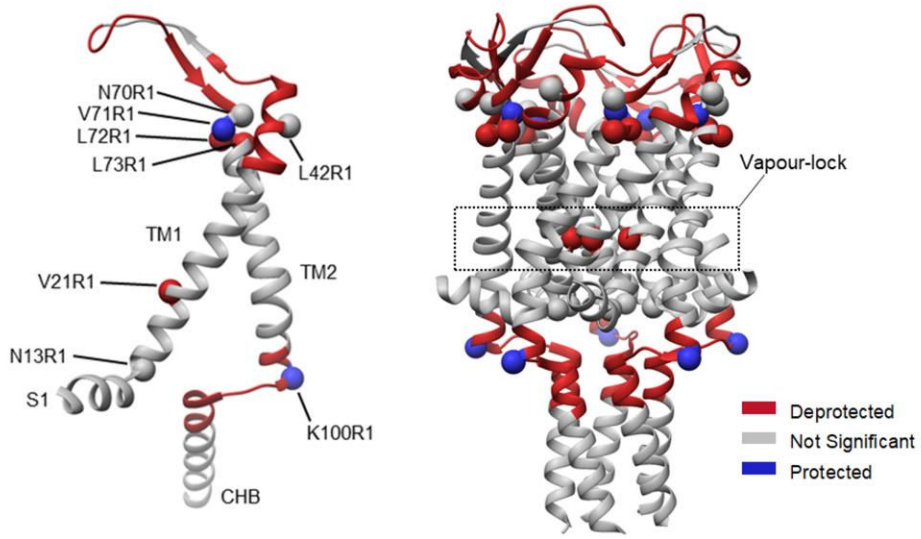

Figure 1. Differences in solvent accessibility for Mycobacterium tuberculosis MscL following the introduction of the L89W mutation. Highlighted helices are used to represent changes in solvent accessibility identified by HDX-MS following the introduction of the L89W mutation. Sites that were mutated to cysteines and then spin-labelled for 3pESEEM solvent accessibility measurements are represented by spheres. Cysteine residues that are spin-labelled are denoted as R1. Red regions are deprotected and blue regions are areas that are protected following the introduction of the L89W mutation. There were no differences in solvent accessibility of N13R1, L42R1, and N70R1 following the introduction of the L89W mutation. Accessibility increased for V21R1 and L72R1 and decreased for L71R1 and K100R1 in an L89W background.

(1) Blount P & Iscla I (2020). Microbiol Mol Biol Rev. 84, 1. (2) Kapsalis C et al. (2019). Nat Commun. 10, 4619. (3) Lane BJ & Pliotas C (2023). Front Chem. 11. (4) Lane BJ et al. (2022). STAR Protoc. 3 (5) Wang B et al. (2021). Structure. 30, 4.

SA07

Ion channel engineering: Chemical biology approaches to study function and ligand interactions in the acid-sensing ion channel

Stephanie Heusser[1]

[1]*University of Copenhagen, Dep. for Drug Design and Pharmacology, Copenhagen, Denmark*

Acid-sensing ion channels (ASICs) are proton-gated sodium channels that contribute to fast synaptic transmission, learning, and memory. ASICs have also gained attention as possible targets to treat ischemic stroke, chronic pain, and neurological disorders. To build the foundation for pharmaceutical targeting, we use chemical biology approaches and fluorometry to better understand the structure-function relationship of these channels. Here, I will present approaches of advanced conventional engineering that help us decipher single subunit contributions in peptide-ion channel interactions and that can incorporate non-canonical amino acids for binding-site identification. Further, I will showcase an intein-mediated protein semi-synthesis approach that allows us to introduce modified sidechains and small organic fluorophores into ASIC1. The results provide an understanding of the role of specific residues in proton sensing and promise insights into the conformational changes of the intracellular domain during gating.

Membrane Transport 2023: Recent Research into Ion Channels, Transporters and Epithelial Physiology
University of St Andrews, UK | 24 - 25 August 2023

SA08

Using scRNAseq datasets to explore glucose transporters in airway epithelia

Deborah Baines[1], Stanislavs Vasiljevs[1], Kameljit Kalsi[1]

[1]St George's University, London, United Kingdom

Introduction: The recent development of new technologies such as single cell RNA sequencing (scRNAseq) has enabled identification of the mRNA transcripts expressed by single cells of many tissues including the airway. We analysed recent scRNAseq studies to investigate the expression of facilitative glucose transporters (GLUTs) and sodium coupled glucose transporters (SGLTs) in the epithelial cells of the airway epithelium from trachea to alveolus.

Methods: We used six studies that reported single cell data for the human airway for interrogation based on the basis of the data availability, the lung cell types included and the range glucose transporters reported (even if not detected) (1-6). The number of cells in a cluster in which RNA transcripts were detected (frequency, normally expressed as %) and the number of RNA transcripts recorded per cell (transcripts per million) were obtained.

Results: Not all studies reported the full range of transporters. Glucose transporter mRNA transcripts were expressed at lower levels than other epithelial marker genes and there were differences between cells freshly isolated from the airways and those grown *in vitro*. Nevertheless, these studies highlighted that there were differences in cellular expression of GLUTs and SGLTs. GLUT1 was the most abundant of the broadly expressed transporters that included GLUT8, 10 and 13. GLUT9 transcripts were more common in basal cells and GLUT12 in ionocytes and ciliated cells. SGLT1 transcripts were present in alveolar and secretory cells. GLUT3 mRNA transcripts were expressed in a cell cluster that expressed monocarboxylate (MCT2) transporters.

Conclusions: The differences in cellular transporter expression potentially underlie cell specific metabolic requirements to support proliferation, ion transport, mucous secretion, environment sensing and airway glucose homeostasis. These studies also highlighted the role of glucose transporters in the movement of dehydroascorbic acid/vitamin C, myoinositol and urate which are factors important to the innate immune properties of the airways. Discrepancies in the reported detection of mRNAs, protein and function of glucose transporters in the lungs remains. Nevertheless, understanding which glucose transporters are present in the lung, their cellular location and how they change in respiratory disease will provide further insights into the function of airway cells and their contribution to cancer progression, the regulation of ASL glucose homeostasis and innate defence against infection.

1. Goldfarbmuren KC, et. al 2020. Nat Commun 11: 2485. 2. Plasschaert LW, et. al. 2018. Nature 560: 377-381. 3. Ravindra NG, et al. 2021. PLoS Biol 19: e3001143. 4. Montoro DT, et.al.2018. Nature 560: 319-324. 5. Deprez M, et. al. 2020., Am J Respir Crit Care Med 202: 1636-1645. 6. Travaglini KJ, et. al. 2020. Nature 587: 619-625.

SA09

Metabolic communication by SGLT2 inhibition

Markus Rinschen[1]

[1]Aarhus University/University Hospital Hamburg Eppendorf, Aarhus, Denmark

Our research goal is to understand the fundamental mechanisms of kidney disease in order to develop novel therapies for renal failure. To this end, we use integration of mass-spectrometry based proteome and metabolome analyses in order to pinpoint the precise mechanisms determining glomerular fate and kidney tissue heterogeneity, and to investigate their impact in a hypothesis-driven manner from mouse to man.

Here, I will present a global view on mechanistic actions of SGLT2 (Slc5a2) inhibitors by multi-layered omic integration. SGLT2 inhibitors (SGLT2i) can protect the kidneys and heart, but the underlying mechanism remains poorly understood. Previous studies have only analyzed individual organs, and the late-stage pathology potentially reflected tissue remodeling secondary to metabolic benefits. Here, we performed an in-depth proteomics, phosphoproteomics, and metabolomics analysis after one week of SGLT2i treatment of non-diabetic as well as early diabetic mice, by integrating signatures from multiple metabolic organs and body fluids. The results revealed that metabolic communication by the SGLT2i reduced circulating waste products like p-cresol sulfate and thereby the need for renal detoxification, which combined with less proximal tubule glucotoxicity and a broad downregulation of apical transport activity provides a metabolic explanation for kidney and cardiovascular protection.

SA10

Cryptic calcium signals for intestinal membrane transport – utility of ex vivo 3D culture systems

Mark Williams[1]

[1]*University of East Anglia, Norwich, United Kingdom*

The main functions of the human intestinal epithelium are to form a vital selective barrier between the systemic circulation and the luminal contents of the gut, whilst facilitating digestion and absorption of nutrients. Preservation of barrier function is underpinned by rapid stem cell-driven tissue renewal, and by secretion of a protective mucus layer. These physiological processes are regulated through the bilateral convergence of systemic and luminal signals which enable the gut epithelium to adapt to changes in the gut microenvironment. Not surprisingly, loss of gut epithelial tissue homeostasis precedes the onset of major intestinal conditions such as inflammatory bowel disease and cancer. Until relatively recently, investigation of the molecular and cellular processes that regulate and enact the physiological functions of the of the human gut epithelium in health and disease has been hampered by the lack of appropriate 3D ex vivo model systems.

The human colonic epithelial monolayer invaginates millions of times to form a carpet of crypts that line the gut lumen. At the base of each crypt, a population of 5-10 active LGR5-positive stem cells divides on a daily basis and gives rise to progenitor cells that migrate along the crypt-axis and differentiate into absorptive colonocytes or secretory goblet cells, enteroendocrine cells and tuft cells. Tissue renewal is completed by shedding of differentiated cells from the surface epithelium into the gut lumen. Significantly, the cellular hierarchy of tissue renewal aligns with the topology of the crypt-axis, as do the processes of fluid secretion and absorption.

Secretion of fluid from stem/progenitor cells located in the lower half of the crypt is coupled to the secretion of mucus from crypt-base-goblet-cells which combine to periodically flush the microenvironment of the stem cell niche and the macroscopic crypt lumen. Regulation and coordination of mucus and fluid secretion from collaborating goblet and stem/progenitor cells is achieved in part via the polarised expression of the associated molecular machinery across these gut epithelial cell types.

Recent advances in 3D ‘near-native’ and organoid model systems have made significant progress in recapitulating the topology and the polarity of the molecular machinery that orchestrates intestinal epithelial membrane transport along the crypt-axis. I will showcase the utility of cultured colonic crypts and organoids, in conjunction with fixed clinical specimens, for the study of calcium-dependent excitation-mucus/fluid secretion coupling in the human colon.

SA11

Identification of novel TMEM175 modulators using high throughput automated patch clamp and solid supported membrane- (SSM-) based electrophysiology platforms

Alison Obergrussberger[1], Laura Hutchison[2], Maria Barthmes[1], Claire Brown[2], Andre Bazzone[1], Lesley Gerrard[2], Niels Fertig[1], David Dalrymple[2], Ian McPhee[2], Davide Pau[2]

[1]Nanion Technologies GmbH, Munich, Germany, [2]SB Drug Discovery, Glasgow, United Kingdom

TMEM175 is a novel, constitutively active ion channel involved in regulating lysosomal pH and autophagy. Mutations in this gene impair normal lysosomal and mitochondrial function, thereby increasing aggregation of insoluble proteins such as phosphorylated α-synuclein, leading to symptoms typical of Parkinson's Disease (PD). Consequently, TMEM175 demonstrates significant potential as a key player in the treatment of PD. The lack of specific pharmacological tools has hampered further investigation into the exact role of TMEM175 in normal lysosomal function and pathological processes.

Advancements in high-throughput screening technologies have allowed rapid assessment of large numbers of compounds against ion channel drug targets using automated patch-clamp. We have successfully developed recombinant cell lines expressing wild-type (WT) TMEM175, a gain of function (Q65P), and loss of function (M393T) mutants using stably transfected HEK cells. Here, we report the characterization of the WT TMEM175 cell line performed using high-throughput automated patch-clamp electrophysiology and show reproducible concentration-response curves with the potassium channel inhibitor 4-aminopyridine (4-AP). A rapid and robust, automated high-throughput electrophysiology screening assay was subsequently developed to enable the identification of both activators and inhibitors of TMEM175.

Additionally, we have used solid-supported membrane- (SSM-) based electrophysiology (SSM-E) for TMEM175 recordings from lysosomal membranes purified and prepared from the WT TMEM175 cell line. Dose-dependent signal enhancement and inhibition of TMEM175 currents were successfully characterized. The SSM-E approach allows for stable and robust recordings from proteins residing in organellar membranes with a throughput of up to 10,000 data points per day.

In summary, the TMEM175 stable cell line was characterized using an automated patch-clamp and SSM-based electrophysiology. We developed and executed robust, high throughput, and high content direct electrophysiological intracellular screening assays, with unusually high success rates. The successful development of TMEM175 electrophysiology assays capable of identifying novel pharmacological tools will enable investigation of the role of this exciting target in normal physiology and in disease.

SA12

The role of a newly identified Ca2+-permeable channel in cardiac dysfunction

Samantha Pitt[3], Amy Dorward[2], Claire Sneddon[1], Colin Murdoch[1]

[1]School of Medicine, University of Dundee, Dundee, United Kingdom, [2]School of Medicine, University of St Andrews, St Andrews, United Kingdom, [3]School of Medicine, University of St Andrews, St Andrews, United Kingdom

In the failing heart, Ca^{2+}-cycling is profoundly altered leading to leak of Ca^{2+} from the sarcoplasmic reticulum (SR). Mitsugumin 23 (MG23) is a non-selective cation channel located with abundance on ER/SR membranes. Previously, we have suggested that MG23 mediated Ca^{2+}-release in cardiac tissue becomes more apparent under pathophysiological conditions (Reilly O'Donnell 2017 JBC). This raises the question that MG23 may play a role in the progression of heart failure. The aim of this study was to investigate whether MG23 functions as Ca^{2+}-leak channel and to probe its role in the failing heart.

Ca^{2+}-store levels in fluo-4 loaded cardiomyocytes isolated from WT and MG23 KO hearts were assessed by the application of caffeine. To induce pressure-overload, MG23 knock out (KO) and wild type (WT) mice had Angiotensin II (1.1mg/kg/day) osmotic pumps implanted. Dynamic cardiac functions were measured *in vivo* using pressure-volume catheters placed in the left ventricle using a closed chest approach. Using histological approaches assessment of ventricular fibrosis following angiotensin treatment was made in WT and MG23 KO animals.

Cardiomyocytes isolated from MG23 KO animals had a reduced Ca^{2+}-store load compared to WT controls. Knock out of MG23 protected hearts against angiotensin II induced hypertrophy. In contrast to WT hearts, MG23 KO hearts displayed no change in cardiac compliance following angiotensin II treatment. MG23 KO animals also had significantly reduced ventricular fibrosis compared to WT controls.

These data for the first time show that MG23 contributes to leakage of Ca^{2+} from SR stores and plays a key role in driving the early pathological stages of pressure-overload induced heart failure.

SA13

Circadian regulation and dysregulation of the thiazide-sensitive sodium chloride co-transporter (NCC)

Jessica Ivy[1]

[1]*University of Edinburgh, Edinburgh, United Kingdom*

The sodium chloride cotransporter (NCC) in the distal convoluted tubule (DCT) reabsorbs approximately 7% of the total sodium load and plays a key role in blood pressure control. Thiazide diuretics, which target NCC, are a mainstay of hypertension treatment. NCC activation has a diurnal rhythm, which is dampened by chronic glucocorticoid treatment. Radiotelemetry experiments showed this dampened rhythm is accompanied by non-dipping blood pressure that could be rescued by thiazide treatment[1]. The receptor mechanisms through which glucocorticoids activate NCC are not fully elucidated. We have previously demonstrated that chronic GR blockade prevents the corticosterone-induced activation of NCC[2]. This pharmacological approach inhibits the GR expressed in all tissues throughout the body, therefore it is unclear if this is a direct result of GR blockade in the DCT or an indirect effect of GR blockade in other tissues. We hypothesised that GR in DCT contributes directly to the activation of NCC. To test this hypothesis, we generated a novel tamoxifen-inducible DCT-specific GR knock out mouse (DCT-GRKO). This talk will explore our latest data on NCC activation and sodium handling in these DCT-GRKO mice. These data have implications for rhythmic blood pressure control particularly in individuals receiving iatrogenic glucocorticoids or in conditions of chronic stress.

1. Ivy JR, Oosthuyzen W, Peltz TS, Howarth AR, Hunter RW, Dhaun N, Al-Dujaili EA, Webb DJ, Dear JW, Flatman PW and Bailey MA. Glucocorticoids Induce Nondipping Blood Pressure by Activating the Thiazide-Sensitive Cotransporter. Hypertension (Dallas, Tex : 1979). 2016;67:1029-37 2. Ivy JR, Jones NK, Costello HM, Mansley MK, Peltz TS, Flatman PW and Bailey MA. Glucocorticoid receptor activation stimulates the sodium-chloride cotransporter and influences the diurnal rhythm of its phosphorylation. Am J Physiol Renal Physiol. 2019;317:F1536-F1548.

SA14

Mechanisms of disturbed fluid and bicarbonate transport in the intestine in Cystic Fibrosis and In-flammatory Bowel Disease, and potential treatment options

Ursula Seidler[1]

[1]*Medizinische Hochschule Hannover, Hanover, Germany*

Maldigestion and –absorption, constipation and intestinal obstructive episodes (DIOS) are major health problems in cystic fibrosis patients. The defective Cl^- channel results in reduced fluidity and low pH of the pancreatic ducts and the gut lumen, which leads to ductal obstruction, maldigestion, mucus hyperviscosity, dysbiosis, mucosal inflammation, and slow intestinal transit.

In a strategic research center funded by the Cystic Fibrosis Trust the ability of three FDA-approved drugs against constipation-prone irritable bowel syndrome, i.e. the guanylyl cyclase and cGMP-linked agonist Linaclotide, and the prostaglandin E1 analogue Lubiprostone, and the NHE3-selective inhibitor Tenapanor, was tested for their ability to restore luminal fluidity and pH in CF mouse models. In parallel, the effect of these compounds on the activity of the NHE3 (SLC9A3) Na/H exchanger, the major intestinal sodium absorptive transporter and regulator of fluid absorption, was measured in stem cell-derived human intestinal organoids generated from ileal biopsies donated by homozygous F508del CF patients. Tenapanor was chosen for an intervention trial in CFTR null mice. Following retraction of their daily osmotic laxative, mice were gavaged twice daily with 30µg tenapanor or vehicle for 21 days, and carefully monitored for the occurrence of an intestinal obstruction. After the end of the intervention, or if a suspicion of an intestinal obstruction arose, the mice were sacrificed, the intestine excised, the microbial composition of the luminal contents and the mucosa-adherent mucus layer was analysed, and the mucosa was studied histologically. The results suggested that an intestine-specific inhibition of NHE3 results not only in an increase in gut fluidity and pH, but also reduces mucus hypersecretion and prevents intestinal obstruction.

A hallmark of inflammatory bowel disease (IBD) is chronic or recurrent “inflammatory diarrhea”. Reduced epithelial Na^+ and fluid absorption is a prominent feature. Fluid absorption in the ileocolonic region is predominantly mediated by the Na^+/H^+ exchanger NHE3, the H^+-short chain fatty acid (SCFA) cotransporter MCT1, the Cl^-/HCO_3-exchanger SLC26A3 (DRA), and the epithelial Na^+ channel (ENaC). We asked the question whether the downregulation of specific absorptive ion transporters or a general defect in enterocyte differentiation correlates with the degree of diarrhea and inflammation. mRNA expression and/or protein abundance was systematically studied of a panel of genes that determine or correlate with the differentiation state of the colonic epithelium, including the transport genes named above, in the different segments of the ileocolon of healthy individuals and IBD patients with mildly, moderate-severely, or noninflamed colonic mucosa. Clinical scores for disease activity and diarrhea were obtained. The results from a comparison of the IBD and healthy control biopsies suggested that inflammation results in a dysregulation of differentiation, with an aberrant proliferative response, an elongation of the proliferative zone, and an incomplete differentiation of the surface enterocytes. This results in a dramatically reduced expression of the colonic absorptive transporters and an increased expression of the poreforming “leaky” claudin2, resulting in diarrhea. This dysregulation is reversible, and noninflamed IBD colon

has the same differentiation pattern as that of healthy controls. Thus, anti-inflammatory treatment appears as the only option to improve inflammatory diarrhea.

SA15

Impaired Renal Bicarbonate Excretion in Cystic Fibrosis: Its Physiology and Clinical Implications

Peder Berg[1]

[1]Aarhus University, Aarhus, Denmark, [2]Aarhus University, Aarhus, Denmark

Intro: Cystic fibrosis (CF) is a lethal inherited multi-organ disease caused by loss-of-function mutations in the cystic fibrosis transmembrane conductance regulator (CFTR) anion channel. Respiratory insufficiency is the primary cause of mortality in CF, but additional complications such as alkalosis and a Bartter-like phenotype have been observed, potentially contributing to end-stage hypercapnic respiratory failure. The mechanism behind the development of alkalosis in CF has been unclear.

Methods: This study utilized various molecular techniques (immunoblotting, immunostainings, *in vitro* cell studies, etc.), *ex vivo* renal tubule perfusion, *in vivo* whole animal studies, and clinical investigations involving individuals with CF and healthy controls.

Results: The function of renal β-intercalated cells, which are responsible for physiological regulation of renal HCO_3^- excretion, is reliant on CFTR. Loss of CFTR function leads to dysfunctional pendrin regulation and impaired renal HCO_3^- excretion, resulting in exacerbated metabolic alkalosis and hypoventilation during acute base loading. Individuals with CF exhibit a significantly reduced ability to excrete an oral HCO_3^- load. The level of challenged urine HCO_3^- excretion correlates with important disease features such as lung function, pancreatic insufficiency, mutation type, and risk of persistent pulmonary infections. Treatment with the CFTR modulator drug Elexacaftor/Tezacaftor/Ivacaftor significantly improves urine HCO_3^- excretion. Furthermore, CFTR modulator therapy may restore pendrin function, reducing the risk of electrolyte disorders and metabolic alkalosis. This is highlighted by the correction of the salt-wasting phenotype in persons with CF following CFTR modulator treatment.

Conclusions: This research provides insights into the role of CFTR in renal HCO_3^- excretion and the development of alkalosis in CF. Mechanistically, Loss of CFTR causes dysfunctional pendrin regulation and CFTR is necessary for alkalosis-induced pendrin activation. Pendrin is the HCO_3^--secretory pathway in the distal renal tubular system and is furthermore important for renal fluid and NaCl conservation. CFTR modulator therapy shows promise in improving urine HCO_3^- excretion and correcting electrolyte imbalances. Acute renal HCO_3^- excretion may serve as a useful measure of CFTR function and as a prognostic marker in persons with CF. The precise mechanism by which CFTR regulates pendrin function remains unresolved.

• Berg P, Sørensen MV, Rousing AQ, Olesen HV, Jensen-Fangel S, Jeppesen M, Leipziger J. Urine bicarbonate excretion as a measure of CFTR function in cystic fibrosis. Annals of Internal Medicine, 2022. • Berg P, Andersen JF et al. Alkalosis-induced hypoventilation in cystic fibrosis: the importance of efficient renal adaptation. Proc Natl Acad Sci U S A 2022;119(8). • Berg P, Svendsen SL, Sorensen MV, Schreiber R, Kunzelmann K, Leipziger J. The molecular mechanism of CFTR- and secretin-dependent renal bicarbonate excretion. J Physiol 2021;599:3003-11. • Berg P, Jeppesen M,

Leipziger J. Cystic fibrosis in the kidney: new lessons from impaired renal HCO3- excretion. Curr Opin Nephrol Hypertens 2021;30:437-43. • Berg P, Svendsen SL, Hoang TTL, Praetorius HA, Sorensen MV, Leipziger J. Impaired renal HCO3− secretion in CFTR deficient mice causes metabolic alkalosis during chronic base-loading. Acta Physiol (Oxf) 2021;231:e13591. • Berg P, Svendsen SL, Sorensen MV, et al. Impaired Renal HCO3 (-) Excretion in Cystic Fibrosis. J Am Soc Nephrol 2020;31:1711-27.

SA16

The kidneys' inner workings and needs – lessons from inhibiting a glucose transporter

Volker Vallon[1]

[1]*University of California San Diego, San Diego, United States*

Healthy kidneys filter ~160 g of glucose per day (~30% of calorie intake). To prevent this energy from being lost, the proximal tubule avidly reabsorbs filtered glucose up to ~450 g/day, primarily by the sodium glucose cotransporter SGLT2 in the early proximal tubule. When SGLT2 is inhibited, the kidneys' reabsorptive capacity for glucose declines to ~80 g/day, mediated by SGLT1 in the late proximal tubule, and glucose is spilled into the urine. SGLT2 inhibitors (SGLT2i) not only improve glycemic control in all stages of type 2 diabetes, but can protect the kidneys of patients with and without type 2 diabetes from failing. The basic idea for their therapeutic use is to lower the body's glucose burden, but the rationale to protect the kidneys goes much further. The hypoglycemia risk of SGLT2i is low because they naturally stop working when the filtered glucose load falls to the reabsorption capacity of SGLT1, and they don't otherwise interfere with metabolic counter regulation. Through glucosuria, SGLT2i induce a modest osmotic diuresis as well as a fasting-like response associated with lesser body fat and weight and a shift in substrate utilization from carbohydrates to lipids and ketone bodies, which serve as energy sources for many organs. Because SGLT2 reabsorbs Na along with glucose and is positively coupled to other transporters in proximal tubule brush border, like NHE3 and URAT1, SGLT2i are natriuretic, uricosuric, and antihypertensive. And, because they work in the proximal tubule, they increase delivery of fluid and NaCl to the macula densa, thereby activating tubuloglomerular feedback and increasing tubular back pressure, which acutely lower glomerular pressure and filtration, thereby reducing the physical stress on the filtration barrier, the exposure to tubulotoxic substances, and the oxygen demand for tubular reabsorption. This improves cortical oxygenation, which, together with lesser tubular gluco-toxicity and improved mitochondrial function and autophagy, can reduce pro-inflammatory and pro-fibrotic signaling and preserve tubular function and GFR in the long-term. By shifting transport downstream, SGLT2i more equally distribute transport work along the nephron but may also simulate systemic hypoxia at the kidney outer medullary oxygen sensor and stimulate erythropoiesis, which improves oxygen delivery to kidneys and other organs. We are only beginning to understand the integrated kidney and body response to inhibiting SGLT2. Much needs to be learned including i) the effects on the inner workings of early proximal tubule cells, ii) the likely contrasting consequences on downstream segments that are exposed to more glucose, fluid and NaCl, iii) consequences of increasing macula densa glucose delivery, which is sensed by SGLT1, iv) glomerular hemodynamic effects via the efferent arteriole, and v) potential off-target effects of SGLT2i, which all hold potential for further clues how to protect the kidneys and heart. Moreover, can we identify transporters with characteristics similar to SGLT2 that can serve as new therapeutic targets to treat metabolic and kidney disease?

C01

Succinate enhances mucociliary clearance in the murine tracheal epithelium by triggering acetylcholine release from chemosensory cells

Alexander Perniss[1,2], Moritz Thiel[1], Sarah Tonack[3], Silke Wiegand[1], Uwe Pfeil[1], Burkhard Schuetz[4], Stefan Offermanns[3], Wolfgang Kummer[1]

[1]Institute for Anatomy and Cell Biology, German Center for Lung Research, Cardio-Pulmonary Institute (CPI), Justus Liebig University, Giessen, Germany, Giessen, Germany, [2]Division of Allergy and Clinical Immunology, Brigham and Women's Hospital and Department of Medicine, Harvard Medical School, Boston, MA, USA, Boston, United States, [3]Department of Pharmacology, Max Planck Institute for Heart and Lung Research, Bad Nauheim, Germany, [4]Department of Molecular Neurosciences, Institute of Anatomy and Cell Biology, Philipps-University, Marburg, Germany, Marburg, Germany

Introduction: Solitary cholinergic chemosensory cells (SCCC) are rare tracheal epithelial cells, which are considered as a part of the innate immune system sensing invading pathogens within the airways. They express a wide range of GPCR including taste receptors and their signaling machinery (TRPM5, PLCβ2 and ITP3R3) and the acetylcholine (ACh) producing enzyme ChAT. We previously identified bacterial formylated signal peptides as activators of SCCC, which subsequently release ACh and thereby alter ciliary activity. The receptor recognizing these formylated peptides, however, remained unknown. In the intestine it was shown that tuft cells, the counterpart of tracheal SCCC, can be activated by the microbial metabolite succinate. We here investigated if tracheal SCCC are also equipped with the succinate recognizing receptor SucnR1 and if succinate triggers innate defense mechanism through activation of tracheal SCCC.

Material and Methods: Expression of the succinate receptor SucnR1 was analyzed in isolated tracheal epithelial cells by RT-PCR and by analyzing existing single cell sequencing data sets. Particle transport speed (PTS) and ciliary beat frequency (CBF) were examined in response to metabolites. Ussing chamber experiments were performed with explanted tracheas to investigate ion transport processes across the tracheal epithelium.

Results: SucnR1 was exclusively expressed by a subset of SCCC within the tracheal epithelium, and there was no epithelial Sucnr1 expression in mice lacking SCCC ($Pou2f3^{-/-}$). Succinate, but neither butyrate nor acetate, increased CBF and, consequently, PTS in a dose-dependent manner. This effect required Sucnr1 (lost in SucnR1-deficient mice) and SCCC (lost in Pou2f3- and Trpm5-deficient mice). In mice with SCCC-specific deletion of ChAT ($ChAT^{fl}$-$Avil^{cre}$) and in the presence of the muscarinic antagonist atropine, the effect of succinate was reduced by 71 and 87%, respectively. In mice lacking muscarinic receptor M3, which is expressed by ciliated cells, the succinate effect was also abrogated by 77%. In Ussing chamber experiments, succinate induced a sharp increase in ion flux across the tracheal epithelium, which was reduced in SucnR1-, Pou2f3- and Trpm5-deficient mice by 81, 82 and 76%, respectively. The succinate-induced increase could be reduced by blocking cholinergic signaling (atropine + mecamylamine, 4-DAMP) and by the general chloride channel inhibitor NPPB (85, 94 and 98%, respectively). Furthermore, the gap junction blocker Gap27 reduced both, the succinate-induced increase in PTS and ion secretion (79 and 74%, respectively).

Conclusion: Succinate activates SCCC by binding to SucnR1, thereby triggering release of ACh. This increases ciliary activity of neighboring ciliated cells most likely via gap junctions and induces secretion of chloride ions into the periciliary fluid. Secretion of chloride ions is required for sufficient production of periciliary fluid. Hence, these effects are synergistic in terms of mucociliary clearance. Interestingly, succinate is produced in high quantities by epithelial cells during infection with *Pseudomonas aeruginosa*, a common pathogen especially in cystic fibrosis patients. Thus, the present data extend the molecular spectrum surveilled by tracheal SCCC beyond microbial factors to host-derived factors.

C02

Purinergic P2Y2 receptors are coupled to calcium-dependent mucus and fluid secretion in the human colonic stem cell niche

Alvin Lee[1], Victoria Jones[1], Nicolas Pelaez-Llaneza[1], Sean Tattan[1], Mark Williams[1]

[1]School of Biological Sciences, University of East Anglia, Norwich, United Kingdom

The human colonic stem cell niche provides a safe harbour for long-lived stem cells. Intestinal stem cells are responsible for driving tissue renewal and cellular differentiation that underpins intestinal barrier function. Neuronal and non-non-neuronal (i.e. crypt autonomous) neurotransmitters are emerging as key regulators of physiological function in the stem cell niche. Similarly, downstream calcium signals are emerging as central integrators of signals that regulate the physiology of the stem cell niche. The aim of this study was to determine the mechanism of purinergic coupled calcium signals in the human colonic stem cell niche and investigate their physiological consequences. Methods: Human colonic crypts were isolated from colorectal tissue samples obtained at surgical resection (NREC approval) and cultured as crypts in the short term (or propagated as crypt-like organoids over the long-term (5 years). The spatio-temporal characteristics of intracellular calcium was monitored by Fura-2/Fluo-4/Calbryte-630 imaging and the mechanism of receptor-mediated calcium mobilisation was characterised by pharmacological and knockdown gene approaches. Calcium signalling toolkit expression was investigated by bulk RNAseq and visualised by fluorescence immunolabelling and super-resolution imaging. Mucus secretion was visualised by Muc2 immunofluorescence depletion assays and real-time imaging of fluorescently tagged mucin-2, using MUC2::mNEON crypt-like organoids generated by CRISPR-HOT. An organoid swelling assay was used as a proxy for fluid secretion. Results: Bulk RNA seq demonstrated mRNA expression of metabotropic P2Y1 (P2RY1), P2Y2 (P2RY2), P2Y11 (P2RY11) and P2Y13 (P2RY13) in native human colonic mucosa, isolated crypts, and cultured organoids. A focus on P2Y2 immunolocalisation revealed expression on basolateral membranes lining the colonic crypt-axis. P2Y2 co-labelled with LGR5+ stem cells along their basolateral membranes at the crypt-base, in addition to labelling MUC2-positive goblet cells, and sparse numbers of chromogranin-positive enteroendocrine cells. Both ATP and UTP, a P2Y2-selective ligand, stimulated intracellular calcium levels in the absence of extracellular calcium, and was inhibited by the InsP3R receptor antagonists 2-APB (100 mM), but not by inhibitors of two pore channels, NED19 (250 μM or tetrandrine (20 μM). UTP induced a reduction of intracellular MUC2 immunofluorescence intensity in colonic crypt-bases and crypt-like organoids. Similarly, UTP stimulated a decrease in intracellular MUC2-mNEON fluorescence and a concomitant increase in luminal MUC2-mNEON fluorescence. UTP also promoted an increase in the cross-sectional area of closed organoids. UTP effects on intracellular calcium, intracellular and luminal MUC2 levels and organoid cross sectional area were abolished by the P2Y2 antagonist, AR-C118925XX (5 μM). These functional observations of fluid secretion are supported by basal expression of NKCC1 and apical expression of ANO1. Conclusions: Puringeric input stimulates P2Y2 receptor mediated calcium mobilisation from intracellular stores, mucus secretion and fluid secretion. These effects suggest that purinergic input regulates the microenvironment of the human colonic stem cell niche.

C03

Multiplatform analysis of kidney tubule-specific mechanisms during low dietary potassium intake

Adrienne Assmus[1], Qi Wu[1], Robert Little[1], Søren Poulsen[1], Robert Fenton[1]

[1]*Department of Biomedicine, Aarhus University, Aarhus, Denmark*

Western diets are typically high in sodium, widely regarded to increase blood pressure (BP). They are also characterised by a relatively low potassium (K) intake, also linked to higher BP. Previous studies have shown that the ability of low dietary K to increase BP is almost fully accounted for by an increase in the abundance and activity of the thiazide-sensitive sodium-chloride transporter (NCC) in the kidney distal convoluted tubule (DCT). However, there is a gap in knowledge for how NCC is increased, but also in the mechanisms underlying an accompanying hypertrophy of the DCT. This study aims to increase our understanding of the specific effects of low K intake on the molecular landscape of the DCT.

Methods: Due to the relatively low abundance of DCT cells *vs*. whole kidney, many DCT-specific changes are undetectable when analysing whole kidney or cortex samples. To uncover these mechanisms, Parvalbumin-GFP+ mice (GFP expressed only in DCT) were fed control (1% K) or a low K (0.2% K, n=7) diet for 4 days. Kidneys were collected on day 5, a single cell suspension prepared and GFP^- and GFP^+ (DCT) cells separated using FACS. Cells were prepared for both bulk RNAseq and protein mass spectrometry. In parallel, kidney samples were embedded in paraffin, tubules were isolated using a laser microdissection system (LMD) and a protocol optimised to analyse these samples with mass spectrometry.

Results: Compared to control diets, mice on 0.2% K intake had increased NCC (+44%) and phosphorylated (active) NCC (+51%), and decreased expression of α-ENaC (-20%) and cleaved γ-ENaC (-10%). Mice on 0.2% K also had higher BP by tail cuff plethysmography (SBP 121.4 ± 2.1 vs. 110.8 ± 1.1 mmHg), reduced urine volume and urinary K excretion (5.5-fold). Plasma K was slightly decreased compared to control diets (4.06 *vs*. 4.35mmol/l). FACS of living GFP^+ cells was optimised to 95 ± 2% purity and enrichment of DCT cells confirmed at the protein and RNA level for various DCT specific genes of interest. Mass spectrometry returned 1426 identified proteins and 75 proteins with TTest<0.05 (Control *vs*. LK). LK diet increases NCC as expected. Kir5.1 and Parvalbumin also increase, while V-ATPase subunits C and E decrease. Other potentially interesting proteins are involved in zinc transport, glycolysis and tubular structure. More generally, results suggest a remodelling of the DCT with DCT1 expanding and DCT2/CNT shrinking.

LMD sample analysis is ongoing. LMD studies are addressing the specific proteomes of proximal tubule cells and collecting duct cells subsequent to 0.2% K intake.

Perspectives: Understanding the mechanisms of K handling and their effects on BP may offer new targets for prevention or treatment of hypertension, both through drug and dietary intervention. We have developed a multiplatform approach to study DCT cells by proteomics, transcriptomics and coupled it to functional studies. We have also developed a protocol for processing laser microdissection samples that allows for a good recovery of proteins from a low number of tubules.

C04

Conserved hydrophobic interactions play a critical role in inhibiting the epithelial sodium channel (ENaC) by α- and γ-inhibitory peptides

Florian Sure[1], Alicia Kißler[1], Christoph Korbmacher[2], Alexandr V. Ilyaskin[1]

[1]Institute of Cellular and Molecular Physiology, Friedrich-Alexander-Universität Erlangen-Nürnberg, Erlangen, Germany, [2]Institute of Cellular and Molecular Physiology, Friedrich-Alexander-Universität Erlangen-Nürnberg, Erlangen, Germany

ENaC is a heterotrimeric ion channel typically formed by α-, β-, and γ-subunits [1, 2]. Channel activation requires proteolytic release of inhibitory tracts from the extracellular domains of α- and γ-ENaC [1-3]. In good agreement with this, applying synthetic inhibitory peptides corresponding to key inhibitory sequences within the α- or γ-inhibitory tracts was shown to reduce ENaC activity [4, 5]. Recently published structural data of ENaC (PDB-ID: 6WTH; [2]) provided information regarding the putative binding pockets of the inhibitory peptides. However, the functional importance of individual residues belonging to these binding pockets is still incompletely understood. We performed atomistic molecular dynamic (MD) simulations to predict critical interactions between the inhibitory peptides and their binding sites in α- and γ-ENaC. Computer predictions were verified by combining site-directed mutagenesis with two-electrode voltage clamp current measurements of human wild-type or mutant αβγ-ENaC heterologously expressed in *Xenopus laevis* oocytes. ENaC function was assessed by measuring amiloride-sensitive currents (ΔI_{ami}). Values are presented as mean ± SEM. One-way ANOVA with Bonferroni posthoc test was used for statistical analysis. MD simulations demonstrated that α- and γ-inhibitory peptides form stable interactions with a central hydrophobic patch in their respective binding site. Interestingly, these hydrophobic patches are formed by four amino acid residues, which are conserved in α- (α_{F226}, α_{W251}, α_{H255}, α_{Y447}) and γ-ENaC (γ_{F204}, γ_{W229}, γ_{H233}, γ_{Y425}). To assess the functional importance of these residues, we individually replaced them by an alanine and compared the effects of synthetic α or γ inhibitory peptides on channels with corresponding mutations in α or γ ENaC with those on wild-type ENaC. Except for $\alpha_{F226A}\beta\gamma$- and $\alpha\beta\gamma_{Y425A}$-ENaC, which for unknown reasons could not be functionally expressed, all other ENaC mutants produced measurable ΔI_{ami} in oocytes. Compared to its inhibitory effect on wild-type ENaC (−76±2 %, n=41) the inhibitory effect of the synthetic α-peptide (30 μM) was strongly reduced in $\alpha_{W251A}\beta\gamma$-ENaC (−28±4 %, n=14, p<0.001) and to lesser extents in $\alpha_{H255A}\beta\gamma$-ENaC (−61±4 %, n=12, p<0.001) and $\alpha_{Y447A}\beta\gamma$-ENaC (−47±4 %, n=14, p<0.001). To investigate the effect of the γ-inhibitory peptide on ENaC, oocytes were pre-treated with chymotrypsin to remove the endogenous γ-inhibitory tract, which otherwise would have occupied its binding site in γ-ENaC. Compared to its inhibitory effect on wild-type ENaC (−58±2 %, n=44), the inhibitory effects of the synthetic γ-peptide (10 μM) on $\alpha\beta\gamma_{F204A}$-ENaC (−15±1 %, n=13, p<0.001), $\alpha\beta\gamma_{W229A}$- (−17±6 %, n=12, p<0.001) and $\alpha\beta\gamma_{H233A}$-ENaC (−24±1 %, n=17, p<0.001) were significantly reduced. Consistent with these findings, we found that hydrophobic amino acid residues belonging to the endogenous γ-ENaC inhibitory tract are critical for its inhibitory effect on the channel. The leucine residue γ_{L160}, which is expected to interact with γ_{W229}, appeared to be particularly important. Its substitution by an alanine increased baseline currents by ~2-fold, mimicking the stimulatory effect of chymotrypsin on the channel. These findings highlight the functional importance of conserved hydrophobic interactions of synthetic inhibitory peptides or endogenous inhibitory

tracts with their corresponding binding pockets in α- and γ-ENaC. This adds to our molecular understanding of proteolytic ENaC activation.

1. Kellenberger and Schild (2015). Pharm Reviews 67, 1-35 2. Noreng et al. (2020). Elife 9:e59038 3. Rotin and Staub (2021). Compr Physiol 11, 2017-2045 4. Kashlan et al. (2010). J Biol Chem 285, 35216-35223 5. Passero et al. (2010). Am J Physio Renal Physio 299, F854-F861

C05

N-linked glycosylation contributes to the absence of protease-sensitivity in epithelial sodium channels containing the δ-subunit

Rene Lawong[1], Fabian May[1], Etang Collins Etang[1], Dagmar Kockler[1], Mike Althaus[1]

[1]Bonn-Rhein-Sieg University of Applied Sciences, Institute for Functional Gene Analytics, Rheinbach, North Rhine-Westphalia, Germany, Rheinbach, Germany

Introduction

There are four epithelial sodium channel (ENaC) subunits (α, β, γ, δ) which form heterotrimeric αβγ- or δβγ-ENaCs that are vital in the salt and water homeostasis in vertebrates. As they mature through the secretory pathway, the ENaC subunits undergo N-linked glycosylation. αβγ-ENaC open probability is tightly coupled to the processing of its α- and γ-ENaC subunits by both intracellular and extracellular proteases. We have previously shown that guinea pig or *Xenopus laevis* αβγ-ENaC is potently activated by chymotrypsin, whereas δβγ-ENaC is not (Gettings et al., 2021; Wichmann et al., 2018). Since ENaC activation by chymotrypsin requires cleavage of the γ-ENaC subunit, it is unknown how the presence of the δ-ENaC subunit prevents ENaC activation by the protease. Glycosylation of ENaC subunits has been shown to impact the channel's activation by proteases (Kashlan et al., 2018). As such, we aimed to investigate whether glycans in the δ-ENaC subunit contribute to the observed differences in the activation of ENaC isoforms by chymotrypsin.

Methods

N-linked glycosylation sites were predicted on guinea pig δ-ENaC using the NetNGlyc 1.0 server. With site-directed mutagenesis, the glycosylated asparagines (N) in the δ-ENaC subunit extracellular domain were substituted with alanine (A). We heterologously expressed wild type αβγ-ENaC, wild type δβγ-ENaC or δβγ-ENaC containing the N/A substituted δ-ENaC subunits in *Xenopus laevis* oocytes. ENaC activity was measured using the two-electrode voltage-clamp technique at – 60 mV.

Results

Extracellular chymotrypsin (2 µg/ml) significantly stimulated αβγ-ENaC currents by 2.8 ± 0.34-fold (n=11) in comparison with control experiments without chymotrypsin (0.82 ± 0.07-fold, n=12; $p<0.0001$, unpaired t-test). There was no difference in the fold-activation of δβγ-ENaC currents without (0.97 ± 0.02-fold, n=10) and with chymotrypsin (0.95 ± 0.03-fold, n=13, p=0.6, unpaired t-test). The NetNGlyc 1.0 server predicted three glycosylated asparagines in the extracellular loop of the guinea pig δ-ENaC subunit: N129, N174 and N344. When these asparagines were substituted one at a time by alanine, none of the channels were activated by chymotrypsin (δ_{N129A}βγ-ENaC: with chymotrypsin 0.92 ± 0.03-fold, n=12, without chymotrypsin 0.84 ± 0.06, n=8; p=0.2080, unpaired t-test; δ_{N174A}βγ-ENaC: with chymotrypsin 0.97 ± 0.05-fold, n=9, without chymotrypsin 0.87 ± 0.04, n=8; p=0.1482, unpaired t-test; and δ_{N344A}βγ-ENaC: with chymotrypsin 0.91 ± 0.04-fold, n=8, without chymotrypsin 0.89 ± 0.05, n=9; p=0.8438, unpaired t-test). When all three asparagines were substituted, extracellular chymotrypsin significantly stimulated the mutant $\delta_{N129,174,344A}$βγ-ENaC by 1.72 ± 0.14-fold (n=15) in comparison with the control experiments without chymotrypsin (0.9 ± 0.03-fold, n=7; p=0.0007, unpaired t-test).

Conclusion

Taken together, these data indicate that removal of glycans in the δ-ENaC subunit renders guinea pig δβγ-ENaC sensitive to activation by chymotrypsin. N-glycans in the δ-ENaC subunit might alter the accessibility of the γ-ENaC subunit to proteases.

References Gettings, S. M., Maxeiner, S., Tzika, M., Cobain, M. R. D., Ruf, I., Benseler, F., Brose, N., Krasteva-Christ, G., Vande Velde, G., Schönberger, M., & Althaus, M. (2021). Two functional epithelial sodium channel isoforms are present in rodents despite pronounced evolutionary pseudogenisation and exon fusion. Molecular Biology and Evolution, 1, 1–42. https://doi.org/10.1093/molbev/msab271 Kashlan, O. B., Kinlough, C. L., Myerburg, M. M., Shi, S., Chen, J., Blobner, B. M., Buck, T. M., Brodsky, J. L., Hughey, R. P., & Kleyman, T. R. (2018). N-linked glycans are required on epithelial Na + channel subunits for maturation and surface expression. American Journal of Physiology - Renal Physiology, 314(3), F483–F492. https://doi.org/10.1152/ajprenal.00195.2017 Wichmann, L., Vowinkel, K. S., Perniss, A., Manzini, I., & Althaus, M. (2018). Incorporation of the Delta-subunit into the epithelial sodium channel (ENaC) generates protease-resistant ENaCs in Xenopus laevis. Journal of Biological Chemistry, 293(18), 6647–6658. https://doi.org/10.1074/jbc.RA118.002543

C06

Structural Insight to Human Urea Transporter Function and Implications for Medicines

Gamma Chi[1], Larissa Dietz[1], Haiping Tang[1], Carol Robinson[1], Wouter van Putte[3], Katharina Duerr[2]

[1]University of Oxford, Oxford, United Kingdom, [2]OMass Therapeutics, Oxford, United Kingdom, [3]Puxano BV, Ghent, Belgium

Introduction: Urea is a key molecule in several physiological processes including urea cycle and urine volume regulation (1). These functions require urea transport across the plasma membrane, which in humans is facilitated by two urea transporters, UT-A (also called UT-2 or SLC14A2) and UT-B (UT-1, SLC14A1) (1). UT-A isoforms are expressed in various compartments of the loops of Henle to reabsorb urea from glomerular filtrate to tubular cells and eventually to blood (1), thereby regulating urine volume via the osmotic gradient. In contrast, UT-B is widely expressed in human tissues and so is involved in a wider range of physiological processes (2). Additionally, UT-B has a unique clinical implication as the primary antigen for the Kidd blood group system (3), where its Asp/Asn amino acid variation at residue 280 determines its Jk blood group phenotype. These make UT-A and UT-B important targets not only from drug discovery perspective but also for clinical applications.

Aims: This study aimed to determine high-resolution structures of human UT-A and UT-B to understand structural aspects of their function, and to enable the development of therapeutics targeting these urea transporters.

Methods: Human urea transporters were expressed in HEK293 cells and purified in detergents for structural studies. Atomic-resolution (2.3 – 2.9 Å) structures of apo UT-A and UT-B, and inhibitor-bound UT-B, were determined by X-ray crystallography and cryo-electron microscopy. Computational tools such as APBS electrostatics, ICM-Pro and MOLE were used to analyse the proteins' surface charges, inhibitor binding, and channel pore radius, respectively.

Results: In this talk, I present insights into the molecular mechanisms of human UT-A and UT-B function from our high-resolution structures of the proteins in apo and inhibitor-bound states. These structures reveal UT-A's extracellular surface to be more negatively charged than UT-B, and that its surface charge can significantly vary within the pH ranges of 5.5 and 7.5 observed in the tubular lumen. This suggests that the function of UT-A may be regulated by the pH of the convoluted tubules, in contrast to UT-B. The divergent surface properties between the two transporters also establish the basis for structure-guided drug discovery programs which target each protein individually. Lastly, the position of UT-B's antigenic surface raises interesting questions about the epitope targeted by anti-Jk antibodies.

Conclusion: The urea transporter structures further our physiological understanding of urea transport and advance efforts for therapeutic development programs targeting them.

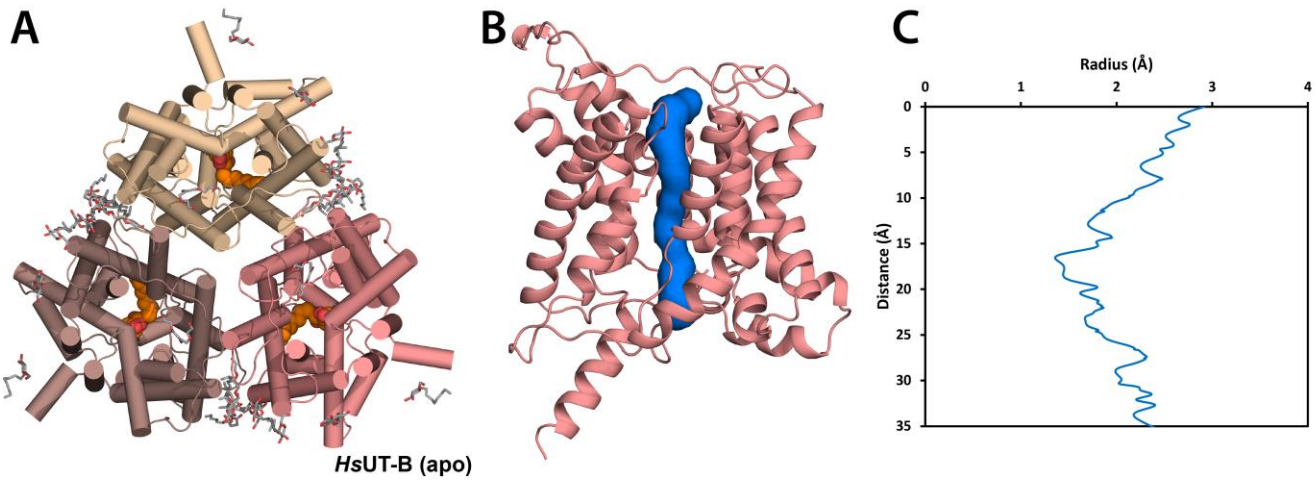

(1) Stewart G. The emerging physiological roles of the SLC14A family of urea transporters. British journal of pharmacology. 2011;164(7):1780-92. (2) Sands JM, Blount MA. Genes and proteins of urea transporters. Sub-cellular biochemistry. 2014;73:45-63. (3) Lucien N, Sidoux-Walter F, Roudier N, Ripoche P, Huet M, Trinh-Trang-Tan M-M, et al. Antigenic and Functional Properties of the Human Red Blood Cell Urea Transporter hUT-B1*. Journal of Biological Chemistry. 2002;277(37):34101-8.

C07

Flotillins, nicotinic acetylcholine receptors, endothelial NO synthase, and the P2X7 receptor interact to control interleukin-1β release

Katrin Richter[1], Antje Banning[2], Juliane Liese[1], J. Michael McIntosh[3], Ritva Tikkanen[2], Veronika Grau[1]

[1]Laboratory of Experimental Surgery, Department of General and Thoracic Surgery, Cardiopulmonary Institute (CPI), German Centre for Lung Research (DZL), Justus-Liebig-University Giessen, Giessen, Germany, [2]Institute of Biochemistry, Medical Faculty, Justus-Liebig-University Giessen, Giessen, Germany, [3]Department of Biology, University of Utah, Salt Lake City, United States

Objective: The pro-inflammatory cytokine interleukin (IL)-1β contributes to the pathogenesis of diverse inflammatory diseases. An example of high clinical relevance is life-threatening systemic inflammation caused by accidental trauma or major surgery that is *inter alia* induced by extracellular ATP originating from damaged cells. Extracellular ATP activates the P2X7 receptor (P2X7R) and thereby triggers the maturation and release of IL-1β. Therefore, mechanisms controlling ATP-mediated IL-1β release are of substantial clinical interest. We identified a cholinergic mechanism that inhibits the damage-mediated release of IL-1β by human monocytes via flux-independent signaling of nicotinic acetylcholine receptors (nAChRs) containing subunits α7, α9 and/or α10 **[1]**. Stimulation of nAChRs activates endothelial NO synthase and inhibits the P2X7R by cysteine nitrosylation. Here, we investigate if the lipid raft-associated flotillins are involved in this pathway.

Methods: Human monocytic THP-1 cells, THP-1 cell-derived macrophages, murine peripheral blood mononuclear cells (PBMCs), and murine bone marrow-derived macrophages (BMDMs) isolated from wild-type and flotillin-1 (*Flot1*) and/or -2 (*Flot2*) gene-deficient mice were primed with lipopolysaccharide. The ATP-induced release of IL-1β was studied in the presence and the absence of classical (e.g. acetylcholine) and unconventional (e.g. phosphocholine) nAChR agonists. To test for the involvement of nAChRs, the conopeptides [V11L;V16D]ArIB (specific for subunit α7) and RgIA4 (specific for subunits α9/α10) were used. Animals received humane care according to NIH "Guide for the Care and Use of Laboratory Animals".

Results: Classical and unconventional nAChR agonists efficiently inhibited the ATP-mediated release of IL-1β by monocytic cells and exert similar functions in THP-1 cell-derived macrophages and BMDMs ($n \geq 5$, $P \leq 0.05$, Friedman followed by Wilcoxon signed-rank test). This inhibitory effect was reversed by the specific conopeptides indicating an involvement of nAChR subunits α7, α9 and/or α10 in mononuclear phagocytes. When investigating the ATP-induced IL-1β release by murine PBMCs and BMDMs, classical and unconventional nAChR agonists efficiently inhibited the ATP-induced IL-1β release by cells from wild-type mice ($n \geq 5$, $P \leq 0.05$, Friedman followed by Wilcoxon signed-rank test). This inhibitory effect was completely reversed in in mice with a double-deficiency in *Flot1* and *Flot2* and partially reversed in cells from either *Flot1* or *Flot2* gene-deficient mice ($n \geq 5$, $P \leq 0.05$, Kruskal Wallis followed by Mann Whitney rank sum test).

Conclusion: We provide first evidence that the lipid raft-related proteins flotillin-1 and -2 are required for the cholinergic control of ATP-mediated IL-1β release by mononuclear phagocytes.

Flotillins have been shown to be associated with several signal transduction pathways. Their exact physiological function is, however, at best partially understood. In the light of the high clinical relevance of the control of ATP-mediated IL-1β release, the exact molecular mechanisms of the interaction of nAChRs, the endothelial NO synthase, the P2X7R, and flotillins deserve further investigation.

[1] Richter K. et al. (2023). Front Immunol 14:1140592.

C08

The Effect of Microgravity and Galactic Cosmic Radiation on Renal Structure and Function

Keith Siew[1], Viola D'Ambrosio[1,3], Elizabeth R Wan[1], Chutong Zhong[1], Zhongwang Li[1], Vaksha Patel[1], Alessandra Grillo[1], Stephen B Walsh[1]

[1]University College London, London, United Kingdom, [2]Università Cattolica del Sacro Cuore, Rome, Italy, [3]Università Cattolica del Sacro Cuore, Rome, Italy

Background: Missions into Deep Space (DS) are planned for the next two decades; a permanent orbital lunar station by end of the 2020s and first manned trip to Mars by late 2030s. The biology of kidney function in spaceflight has been largely overlooked. We suspect that kidney physiology may be disturbed in spaceflight, either by microgravity (MG) and/or Galactic Cosmic Radiation (GCR) potentially leading to kidney injury and stone formation.

MG exposed astronauts have unusually high rates of kidney stones. Indeed, MG associated changes in urinary biochemistry favour stone formation, and current thinking suggests this is secondary to bone demineralisation due to unloading. However, the compartmental fluid shifts associated with MG cause changes in differential perfusion pressures in tissue beds and changes in baroreceptor activation. We predicted this would cause physiological changes in renal sodium and calcium transporter expression (which tend to be physiologically linked), resulting in elevated urinary calcium loss, kidney stone formation and decreased bone mineral density as kidney-driven primary events.

The kidney is an exquisitely radiation sensitive organ; it is the dose limiting organ in abdominal radiotherapy. Chronic kidney dysfunction can occur with acute low linear energy transfer (LET) radiation doses as low as <0.5 Gy; the LET dose expected on a Mars Mission. However, GCR is comprised of low-LET x- and γ-rays, protons and high energy ions of heavier elements 'HZE' (e.g. iron). We hypothesise that GCR may cause renal damage within the timeframe and dose expected for a mission to Mars.

Methods: We performed biomolecular (Epigenomic, bulk and spatial mRNA and miRNA transcriptomic, proteomic, phosphoproteomic, metabolomic, metagenomic), clinical chemistry (electrolytes, endocrine and biochemistry biomarkers) and imaging (histology, immunofluorescence, miRNA FISH, 3D morphometry) analyses using samples and datasets available from 11 spaceflight-exposed mouse (13-75 days on ISS/shuttle) and 5 human (3-180 days on ISS/Shuttle) collections of missions, and 4 simulated GCR-exposed mouse experiments (0.5-0.75Gy ≈ 1.5-2.5-year dose / necropsy 1-180 days post-exposure). In total the study encompassed approximately ~100 humans / ~155 mice (n per group). All animal and human studies had local ethical committee approval and licenses where appropriate.

Results: Historical human data showed hypercalciuria, hyperphosphaturia and reduced urine volume during spaceflight. Multiomic pathway enrichment analysis indicated changes in kidney gene products associated with nephrolithiasis. MG-exposed animals had significant dephosphorylation of thiazide-sensitive SLC12A3 and furosemide-sensitive SLC12A1 canonical

transporters known to impact nephrolithiasis and bone mineral density, as well as dysbiosis of faecal microbial genera known to influence nephrolithiasis.

Pathway analysis of human and mouse plasma and kidney samples showed enrichment of gene products associated with renal fibrosis, inflammation, glomerular and tubular injury (Fig.1). GCR-exposed animals had decreased mitochondrial protein expression, and elevation in pathogenic miRNA species. Spatial transcriptomics revealed immune cell infiltration of the cortex, biochemistry revealed elevated urinary protein loss and histopathological investigation revealed incidences of thrombotic microangiopathy.

Conclusion: Our data provide strong evidence that prolonged exposure to DS will induce significant harm to renal health and function that may prove mission critical. Development of mitigation strategies will be essential for long-term missions to the moon, mars and beyond.

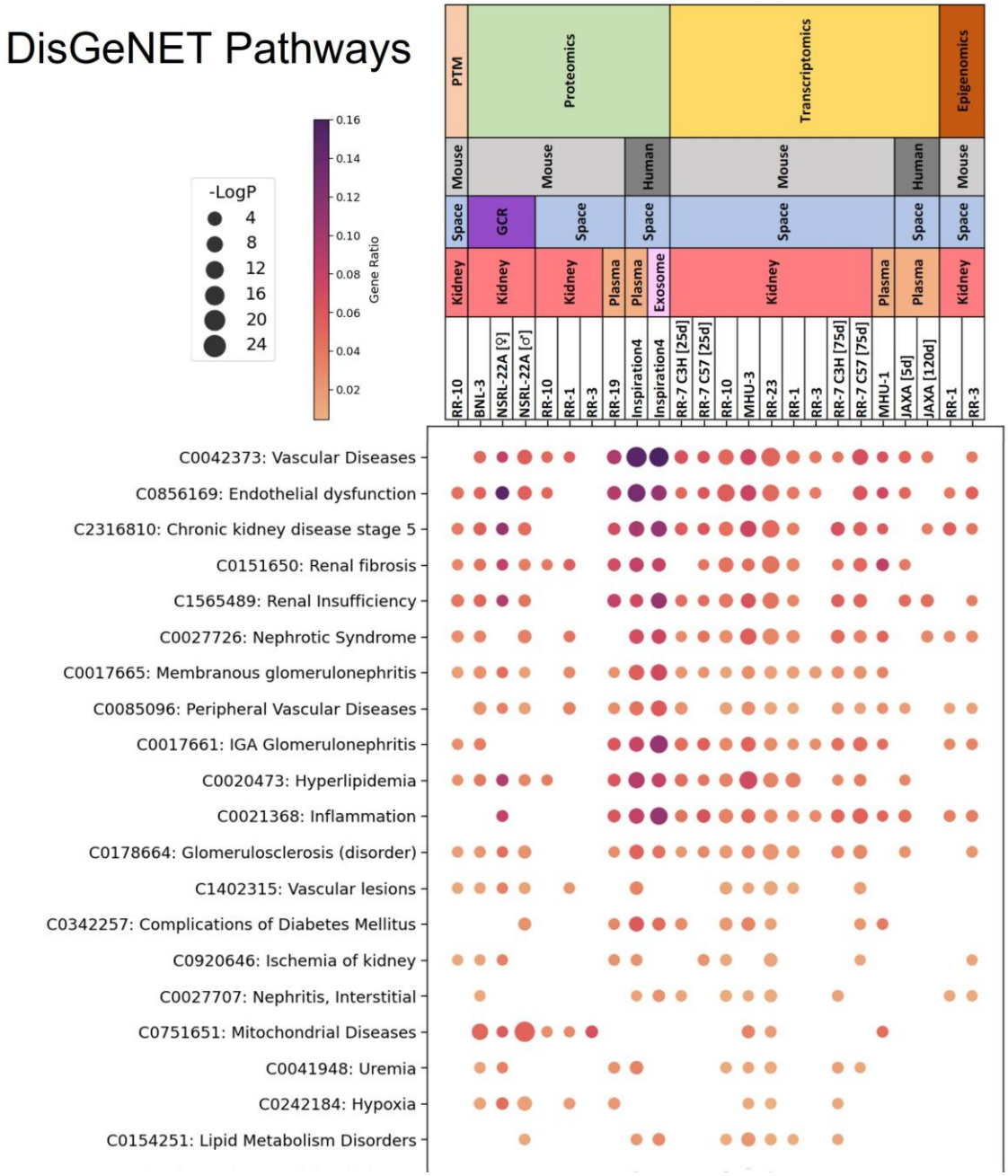
DisGeNET Pathways
-LogP
4
8
12
16
20
24
Gene Ratio
0.16
0.14
0.12
0.10
0.08
0.06
0.04
0.02
PTM
Proteomics
Transcriptomics
Epigenomics
Mouse
Human
Space
GCR
Kidney
Plasma
Exosome
RR-10
BNL-3
NSRL-22A [♀]
NSRL-22A [♂]
RR-1
RR-3
RR-19
Inspiration4
RR-7 C3H [25d]
RR-7 C57 [25d]
MHU-3
RR-23
RR-7 C3H [75d]
RR-7 C57 [75d]
MHU-1
JAXA [5d]
JAXA [120d]
C0042373: Vascular Diseases
C0856169: Endothelial dysfunction
C2316810: Chronic kidney disease stage 5
C0151650: Renal fibrosis
C1565489: Renal Insufficiency
C0027726: Nephrotic Syndrome
C0017665: Membranous glomerulonephritis
C0085096: Peripheral Vascular Diseases
C0017661: IGA Glomerulonephritis
C0020473: Hyperlipidemia
C0021368: Inflammation
C0178664: Glomerulosclerosis (disorder)
C1402315: Vascular lesions
C0342257: Complications of Diabetes Mellitus
C0920646: Ischemia of kidney
C0027707: Nephritis, Interstitial
C0751651: Mitochondrial Diseases
C0041948: Uremia
C0242184: Hypoxia
C0154251: Lipid Metabolism Disorders

C09

Early versus late effects of aldosterone on sodium transport and the transcriptome of cultured mouse cortical collecting duct cells

Sara Afonso[1], Marko Bertog[1], Alexandr Ilyaskin[1], Christian Büttner[2], Arif Ekici[2], Christoph Korbmacher[1]

[1]Friedrich-Alexander-Universität Erlangen-Nürnberg, Institute of Cellular and Molecular Physiology, Erlangen, Germany, [2]Universitätsklinikum Erlangen, Institute of Human Genetics, Erlangen, Germany

The epithelial sodium channel (ENaC) is the rate-limiting transport mechanism for Na^+ reabsorption in the distal nephron and is critical for maintaining sodium homeostasis. In the cortical collecting duct (CCD) ENaC activity is tightly regulated by aldosterone. Its stimulatory effect on ENaC requires the presence of the mineralocorticoid receptor (1) and involves transcriptional regulation of a complex set of genes which are not yet fully characterized. In particular, a better understanding of the early versus late transcriptional effects of aldosterone is needed (2,3). To address this issue, we used mRNA sequencing (RNAseq) for a comprehensive transcriptome analysis of a highly differentiated and aldosterone sensitive mouse cortical collecting duct ($mCCD_{cl1}$) cell line. Cells were grown on permeable supports and exposed to 3 nM aldosterone for 2 h or 24 h. To confirm the hormone's stimulatory effect on ENaC-mediated transepithelial sodium transport, equivalent short-circuit current (I_{SC}) measurements were performed as previously described (4). In the 2 h incubation experiments I_{SC} was continuously recorded in modified Ussing chambers. In the 24 h incubation experiments I_{sc} was monitored by repeated transepithelial voltage and resistance measurements with two sticks "STX" electrodes and an epithelial volt-ohm-meter. The ENaC-mediated I_{SC} component ($\Delta I_{SC\text{-}ami}$) was determined by application of 10 µM amiloride. In cells treated with aldosterone for 2 h $\Delta I_{SC\text{-}ami}$ was 2.2-fold higher than in controls (27.1±0.9 µA·cm^{-2} vs. 12.3±0.8 µA·cm^{-2}; n=6; mean ± SEM; p<0.001). Similarly, compared to controls $\Delta I_{SC\text{-}ami}$ was 3.2-fold higher in cells treated with aldosterone for 24 h (23.1±2.7 µA·cm^{-2} vs. 7.2±1.1 µA·cm^{-2}; n=7; mean ± SEM; p<0.001). Subsequently, mRNA was prepared from cells harvested from each individual permeable support for RNAseq analysis. The mRNA libraries were prepared using the Illumina TruSeq and Stranded mRNA kits and sequenced on the Illumina Hiseq 2500 and Illumina Novaseq 6000 platforms. In cells treated for 2 h or 24 h we identified a total of 94 (66 up- and 28 downregulated) or 453 (347 up- and 106 downregulated) aldosterone-regulated protein coding transcripts, respectively. A set of 49 transcripts was found to be aldosterone-regulated in both the 2 h and 24 h groups. The well-known aldosterone-regulated serum and glucocorticoid-regulated kinase 1 (*Sgk1*) was upregulated by a factor of 9.0 (n=6; p<0.001) and 6.4 (n=7; p<0.001) after 2 h and 24 h aldosterone incubation, respectively. The transcript of the α-subunit of ENaC (*Scnn1a*) was also upregulated after both short-term (1.23-fold; p<0.001) and long-term (1.54-fold; p<0.001) aldosterone treatment. No effect was observed on β- and γ-ENaC transcripts consistent with previous reports. Interestingly, the transcript for the transmembrane serine protease 2 (*Tmprss2*), which has recently been shown to be involved in proteolytic ENaC activation (5), was upregulated (1.1-fold; p<0.01) after 24 h aldosterone treatment. This work highlights the differential transcriptional effects of acute vs. chronic aldosterone exposure. Further studies are needed to explore the physiological role and molecular interplay of newly identified early vs. late aldosterone-regulated genes in renal ENaC regulation.

1. Nesterov V et al. (2021). Am J Physiol Renal Physiol. 321(3):F257–68. 2. Swanson EA et al. (2019). Physiol Genomics. 51(4):125–35. 3. Loughlin S et al. (2023). Kidney360. 4(2):226–40. 4. Mansley MK et al. (2020). J Gen Physiol. 152(8):1–15. 5. Sure F et al. (2022). J Biol Chem. 298(6):102004.

C10

The impact of acute potassium chloride infusion on renal haemodynamics and sodium excretion in anaesthetised rats.

Atta Arshad[1], Kevin Stewart[1], Jessica Ivy[1], Neeraj Dhaun[1], Matt Bailey[1]

[1]*The University of Edinburgh, Edinburgh, United Kingdom*

Introduction: Modern diets are high in sodium chloride, which raises blood pressure and has negative health consequences (Hunter et al., 2022). Additionally, dietary potassium intake is often comparatively low. Dietary sodium and potassium have a well-known influence on blood pressure. Interventions that increase potassium intake reduce blood pressure in clinical trials (Filippini et al., 2020), and oral potassium salts were historically used as diuretics (Keith et al., 1935) to reduce extracellular fluid volume and decrease blood pressure. In mice, oral delivery of potassium chloride (KCl), dephosphorylates and deactivates the sodium chloride cotransporter (NCC) of the distal convoluted tubule (Penton et al., 2016). The goal of this study was to evaluate the impact of an acute rise in plasma potassium concentration on sodium excretion and NCC expression in the kidney.

Methods: Male and female Sprague-Dawley rats (n=19) aged 12-15 weeks were anaesthetised (Thiopental sodium 50mg/kg IP). The jugular vein and carotid artery were cannulated, a tracheotomy performed and the bladder catheterised (Ivy et al., 2018). An arterial blood sample was taken for measurement of plasma electrolytes, and rats were then randomised to receive an IV administration of either 140mmol/L NaCl (control) or 140mmol/L KCl at a rate of 1mL/hr/100g body weight. Both solutions also contained 0.25% FITC-inulin (for determining glomerular filtration rate; GFR) and 10mmol/L Na-aminohippurate (for measurement of renal plasma flow; RPF). After 1 hour, urine was collected for a 60-minute period, with a second arterial blood sample. Rats were then euthanised through anaesthetic overdose, and the left kidney was removed for western blot analysis of total NCC (tNCC) and T53-phosphorylated NCC (pNCC) expression.

Results: Outputs from male and female rats were pooled for analysis; comparisons between groups treated with control (NaCl) or KCl infusion were performed using unpaired t-tests, and significance values were set at $p<0.05$. Results are presented as mean±SD. Plasma sodium, potassium and chloride concentrations measured before randomisation were not different between groups. Following 2 hours of infusion, plasma potassium was significantly higher in rats infused with KCl than those treated with an NaCl control (Control: 3.9±0.6mmol/L/ KCl: 5.2±0.9mmol/L; $p<0.0001$). No significant statistical differences were found in arterial blood pressure, haematocrit, RPF or GFR between groups. Urine flow was significantly higher in the potassium infusion group (Control=10.3±7.9µl/min; KCl=19.3±15.9µl/min; $p=0.03$) with a higher excretion rate of sodium ($p=0.03$), potassium ($p=0.0014$), and chloride ($p=0.0014$) in males. Pooling both control and KCl-treated rats, correlation between plasma potassium concentration and urinary sodium excretion was not significant. Western blot analysis showed a lower expression of both total NCC ($p=0.02$) and phospho-NCC ($p=0.03$), Negative correlation was found between plasma potassium concentration and expression of tNCC (r=-0.55; $p=0.02$) and pNCC (r=-0.53; $p=0.02$).

Conclusion: An acute increase in plasma potassium within the physiological range following 2 hours of KCl infusion reduced the kidney expression of total and activated NCC leading to the observed diuretic and natriuretic effects associated with an elevated plasma potassium load. These are preliminary findings, and the acute effect of increasing plasma potassium on extracellular fluid volume balance has to be studied further.

References: Filippini, T., Naska, A., Kasdagli, M.I., Torres, D., Lopes, C., Carvalho, C., Moreira, P., Malavolti, M., Orsini, N., Whelton, P.K. and Vinceti, M., 2020. Potassium intake and blood pressure: a dose-response meta-analysis of randomized controlled trials. Journal of the American Heart Association, 9(12), p.e015719. Hunter, R.W., Dhaun, N. and Bailey, M.A., 2022. The impact of excessive salt intake on human health. Nature Reviews Nephrology, 18(5), pp.321-335. Ivy, J.R., Evans, L.C., Moorhouse, R., Richardson, R.V., Al-Dujaili, E.A., Flatman, P.W., Kenyon, C.J., Chapman, K.E. and Bailey, M.A., 2018. Renal and blood pressure response to a high-salt diet in mice with reduced global expression of the glucocorticoid receptor. Frontiers in physiology, 9, p.848. Keith, N.M. and Binger, M.W., 1935. Diuretic action of potassium salts. Journal of the American Medical Association, 105(20), pp.1584-1591. Penton, D., 2016. Extracellular K (+) rapidly controls NCC phosphorylation in native DCT by Cl (-)-dependent and-independent mechanisms. J Physiol.Hunter, R.W., Dhaun, N. and Bailey, M.A., 2022. The impact of excessive salt intake on human health. Nature Reviews Nephrology, 18(5), pp.321-335.

C11

Renal adaptation to high salt diet in mice with conditional deletion of Hsd11b2 in the brain

Celine Grenier[1], Kevin Stewart[1], Matthew Bailey[1]

[1]Edinburgh Kidney Research Group, Centre for Cardiovascular Science, The University of Edinburgh, Edinburgh, United Kingdom

HSD11B2 encodes the glucocorticoid-metabolising enzyme 11β-hydroxysteroid dehydrogenase type 2 (11βHSD2), which in is mainly expressed in the principal cell of the aldosterone-sensitive distal nephron. Loss of function mutations cause the rare hypertensive Syndrome of Apparent Mineralocorticoid Excess. Overactivation of the mineralocorticoid receptor by endogenous glucocorticoid is causative (Bailey, 2017). Hypertension is salt-sensitive, attributed to enhanced ENaC-mediated sodium reabsorption and renal sodium retention (Mullins et al, 2015). However, 11βHSD2 is also expressed in a subset of neurons in the nucleus of the solitary tract that regulate the behavioural drive to consume salt in rodents (Geerling & Loewy, 2008). We used a cre-lox approach to generate mice with conditional knockout of *Hsd11b2* in the brain (*Hsd11b2*.BKO). These mice had >90% knockdown of 11βHSD2 activity in the brainstem and displayed enhanced salt appetite and salt-sensitive hypertension (Evans et al, 2016). The mechanisms of salt-sensitivity are unknown and here we examined renal sodium excretion in male Hsd11b2.BKO mice and control littermates.

Mice (n=5-8) mice per genotype/diet were fed diets containing either 0.3% (control) or 3% sodium by weight for 7-10 days. Urine was collected for 24h and mice were then anaesthetised (thiobutabarbital sodium, 120mg/kg IP) and instrumented for measurement of renal function. Sodium excretion was measured at baseline and then again following ligation of peripheral arteries to acutely raise arterial blood pressure by ~15mmHg. At the end of the experiment, a blood sample for measurement of aldosterone and mice then killed. Data are shown as mean±SD and comparisons were by t-test or two-way ANOVA.

High salt diet significantly reduced plasma aldosterone in control mice (634±201pg/ml vs 115±35pg/ml; $p<0.001$). In *Hsd11b2*.BKO mice, aldosterone was already supressed on control diet and was the further reduced induced by high salt intake (131±66pg/ml vs 60±14pg/ml) was not statistically significant. In all mice, urinary sodium excretion was increased by high salt intake. However, sodium excretion was significantly lower in *Hsd11b2*.BKO mice than in controls after high salt feeding. Urinary excretion of 8-isoprostane was measured as a marker of production of reactive oxygen species in the kidney. This was not significantly affected by high salt diet in control mice (3.29±2.33 vs 4.22±2.68 ng/24h). In *Hsd11b2*.BKO mice, high salt significantly increased 8-isoprostane excretion (2.43±2.87 vs 12.21±5.52; $p<0.01$). In the anaesthetised preparation, sodium excretion rate was not different between genotypes. The acute elevation in arterial blood pressure increased fractional sodium excretion fourfold in control mice ($p<0.01$), indicative of down-regulation of tubular epithelial sodium reabsorption. In Hsd11b2.BKO mice, the pressure-induced natriuresis was not statistically significant (1.3±0.7 vs 1.8+0.9mmol/min).

Deletion of *Hsd11b2* in the brain amplifies leads to suppression of aldosterone production. Despite this, the normal renal tubular adaptation to high salt intake is compromised. This may reflect enhanced production of reactive oxygen species.

Bailey MA (2017) Current Hypertension Reports 19: 100-106. Evans LC et al. (2016) Circulation 133: 1360-1370 Geerling JC and Loewy AD (2008) Exp Physiol. 93:177-209.

C12

Complications and Treatment of Hypercalciuria in Familial Hyperkalaemic Hypertension (FHHt)

Viola D'Ambrosio[1,2], Olivia McKnight[2], Elizabeth R Wan[2], Robert Speller[2], Robert Moss[2], Keith Siew[2], Stephen B Walsh[2]

[1]Università Cattolica del Sacro Cuore, Rome, Italy, [2]University College London, London, United Kingdom

Background

Hypertension is frequently associated with hypercalciuria[1,2], nephrolithiasis[3] and low bone mineral density[4]. Familial Hyperkalaemic Hypertension (FHHt) causes hypercalciuria[5], although complications of this are not reported.

Methods

We examined a cohort of 9 patients with genetically confirmed FHHt. Biochemical, radiological, and clinical data was obtained in patients before and after thiazide treatment. All patients gave informed consent. The study had ethics committee approval (REC 05/Q0508/6). Data were compared using paired t tests or Wilcoxon paired rank tests.

Results

5 of the 9 patients were female (median age 41.7 years). The genetic diagnosis was confirmed in all patients, 5 patients had variants in KLHL3, 3 patients had variants of WNK4, and one had a variant of WNK1 (table 1).

Pre-treatment potassium was high (median 5.6 IQR 5.2-6.2 mmol/L). Pre-treatment calcium was in the normal range (2.34 IQR 2.29-2.38 mmol/L). There was significant hypercalciuria with a raised urinary calcium/creatinine ratio (0.69 IQR 0.41-1.13). However, PTH (4 IQR 3.95-4.35 pmol/L), phosphate (1.15 IQR 1.25mmol/L) and alkaline phosphatase (57 IQR 45-84 mmol/L) were all in the normal range.

Thiazide treatment significantly reduced hypercalciuria (calcium/creatinine ratio 0.15 IQR 0.05-0.29 p=0.04) as well as the serum potassium (3.9 IQR 3.5-4.4 mmol/L p=0.0167) (table 1).

Patients also developed complications of hypercalciuria. 3 patients had kidney stones demonstrated on cross-sectional imaging (figure 1). One of these patients (male, 30 years old) had DXA criteria for osteoporosis (T score Femoral neck -1.5, lumbar spine -2.4).

Conclusion

This is the first case series to demonstrate complications of hypercalciuria (i.e. kidney stones) in patients with FHHt. We demonstrate that thiazide treatment normalises urinary calcium excretion.

Thiazide treatment may have clinical utility in FHHt even if hypertension or hyperkalaemia are not problematic in order to avoid the complications of hypercalciuria.

Table 1: Demographics, pre- and post-thiazide treatment laboratory results

Demographic Data	**Frequency (n of patients)**		
Total cohort	9		
Female	4		
Genetic mutation			
KLHL3	5		
WNK4	3		
WNK1	1		
Thiazide diuretic	3		
Nephrolithiasis	3		
Osteoporosis	1		
Laboratory Data	**Pre-thiazide**	**Post-thiazide**	**p-value**
K (mmol/L) *median*	5.6	3.9	0.0167
uCa/Cr *median*	0.69	0.15	0.04

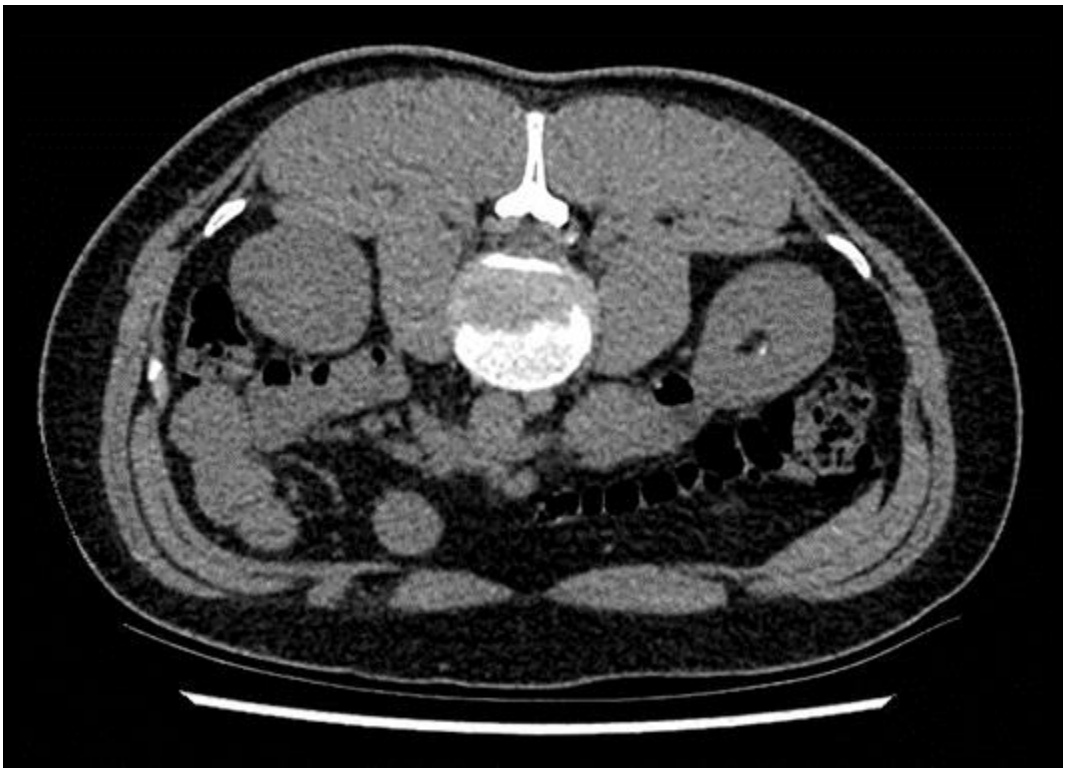

1. Mente, A., Honey, R. J. D. A., McLaughlin, J. M., Bull, S. B. & Logan, A. G. High Urinary Calcium Excretion and Genetic Susceptibility to Hypertension and Kidney Stone Disease. JASN 17, 2567–2575 (2006). 2. Cappuccio, F. P., Kalaitzidis, R., Duneclift, S. & Eastwood, J. B. Unravelling the links between calcium excretion, salt intake, hypertension, kidney stones and bone metabolism. J. Nephrol. 13, 169–177 (2000). 3. Kittanamongkolchai, W. et al. Risk of Hypertension among First-Time Symptomatic Kidney Stone Formers. CJASN 12, 476–482 (2017). 4. Tsuda, K., Nishio, I. & Masuyama, Y. Bone mineral density in women with essential hypertension*. American Journal of Hypertension 14, 704–707 (2001). 5. Mayan, H. et al. Hypercalciuria in Familial Hyperkalemia and Hypertension Accompanies Hyperkalemia and Precedes Hypertension: Description of a Large Family with the Q565E WNK4 Mutation. JCEM 89, 4025–4030 (2004).

C13

Enteroids as a model for the intact intestinal epithelium: differentiation is key

Christina Windhaber[1], Georg Csukovich[1], Barbara Pratscher[1], Iwan A. Burgener[1], Nora Biermann[1], Franziska Dengler[1]

[1]*University of Veterinary Medicine Vienna, Vienna, Austria*

The gastrointestinal epithelium is not only a central hub for nutrient uptake and an important barrier shielding the organism from external hazards, but also the site of many pathophysiological processes putting the epithelial functions at risk. Hence, a thorough understanding of the defensive, protective, and adaptive mechanisms the epithelium employs under different circumstances is decisive for improving the prophylactic and therapeutic options to treat gastrointestinal disease. With organoids, or, more specifically, enteroids, i.e., intestinal epithelial organoids, modern *in vitro* techniques have recently been developed that allow investigating epithelial pathophysiology without the need for animal experiments and with a high cellular resolution. However, there is only little evidence that the enteroids cultivated from intestinal stem cells under the influence of manifold growth factors actually reflect the intestinal epithelium *in situ*. Therefore, our study aimed to define growth conditions for equine jejunum and colon enteroids (eqJE and eqCE) mimicking the cellular composition and differentiation grade of the respective original tissue.

To cultivate eqJE and eqCE, intestinal epithelial crypts were isolated from intestinally healthy horses euthanized for unrelated reasons. After propagation, eqJE and eqCE ($N \geq 4$) were cultivated either with proliferation medium (PM) or one of four differentiation media (DM1-4) with varying compositions. The enteroids were characterized histomorphologically, on gene expression and protein level, and functionally using the Ussing chamber technique in comparison to the native epithelium of the donor horses.

Morphologically, enteroids cultivated in PM and DM1 and 2 showed extensive budding, whereas DM3 and 4 appeared to induce rather spherical growth. Together with an increased number of goblet cells this might indicate a wider variety and higher grade of differentiation of epithelial cell types. In line with this, eqJE and eqCE cultivated in DM3 and 4 showed the highest similarity to the tissue *in situ* regarding the mRNA expression of specific markers for stem cells (olfactomedin), goblet cells (mucin 2) and enterocytes (villin, Na^+/K^+-ATPase, epithelial cell adhesion molecule, Na^+ coupled glucose transporter). Ussing chamber analyses revealed that the electrophysiological parameters (short-circuit current [I_{sc}], transepithelial conductance [G_t]) were within similar ranges for eqCE-derived monolayers (G_t: 33.47 ± 1.30 mS cm^{-2}, I_{sc} 0.30 ± 0.07 µEq cm^{-2} h^{-1}) and isolated equine colon epithelia (G_t 26.82 ± 6.22 mS cm^{-2}, I_{sc} 0.89 ± 0.15 µEq cm^{-2} h^{-1}). Incubation with Na-butyrate (10 mM), forskolin (10 µM), and ouabain (100 µM) provoked similar electrophysiological responses of the organoid-derived monolayers and isolated epithelium, indicating the presence of transepithelial Na^+-dependent transport, cAMP-dependent Cl^- secretion and Na^+/K^+-ATPase activity to a similar extent in eqCE and the *ex vivo* epithelium.

In conclusion, we succeeded in isolation, propagation and differentiation of eqJE and eqCE consisting of multiple cell types that resembled the equine jejunum and colon epithelium *in situ*.

Thus, enteroids can serve as a suitable model to investigate the pathomechanisms underlying (equine) gastrointestinal disorders. However, the influence of growth conditions on the cellular composition and differentiation must not be neglected when enteroids are used for *in vitro* experiments meant to be translated to the *in vivo* situation.

C14

Acute activation of human ENaC by SGK1 depends on a highly conserved serine residue S594 in the channel's α-subunit and requires prior cleavage of the γ-subunit at a putative furin cleavage site

Alexei Diakov[1], Florian Sure[1], Alexandr Ilyaskin[1], Christoph Korbmacher[1]

[1]*Friedrich-Alexander-Universität Erlangen-Nürnberg (FAU), Institute of Cellular and Molecular Physiology, Erlangen, Germany*

Serum and glucocorticoid inducible kinase 1 (SGK1) is a key regulator of the epithelial sodium channel (ENaC) in its αβγ subunit configuration. We demonstrated that in rat ENaC the serine residue 621 (S621) localised in an SGK consensus motif (RXRXX(S/T)) in the channel's α-subunit is critically important for acute channel activation by SGK1 and the kinases PKBα and DYRK2 (1, 2, 3). Phosphorylation at S621 probably affects ENaC gating and turns previously silent channels into channels with a high open probability. Interestingly, this is reminiscent of proteolytic ENaC activation observed in single-channel recordings from outside-out patches exposed to trypsin or chymotrypsin (4, 5). Proteolytic channel activation is a unique feature of ENaC, but the underlying molecular mechanisms and a possible interplay with channel regulation by phosphorylation remain incompletely understood. The aim of the present study was to explore whether human ENaC can also be activated acutely by SGK1 and whether this activation depends on the highly conserved serine residue S594 in human αENaC. In addition, we investigated whether ENaC activantion by SGK1 depends on the cleavage state of γENaC. Human αβγENaC and mutant ENaC constructs were heterologously expressed in *Xenopus laevis* oocytes. Amiloride (2 µM) was applied to determine amiloride-sensitive ENaC currents (ΔI_{ami}) in outside-out macro-patches. We demonstrated that in outside-out patches from oocytes expressing human ENaC recombinant and constitutively active SGK1 included in the pipette solution increased ΔI_{ami} from 69 ± 21 pA to 141 ± 27 pA (n=8; SEM; p<0.003, paired *t*-test) within ~24 min after patch excision. Importantly, this stimulatory effect was completely abolished when the conserved serine residue S594 was replaced by an alanine in the channel's α-subunit by site-directed mutagenesis (n=8). It is well established that during ENaC maturation proteolytic cleavage occurs at three putative furin sites (two in α- and one in γENaC) before the channel reaches the plasma membrane. The final critical step in proteolytic ENaC activation probably takes place at the plasma membrane where γENaC is cleaved by membrane bound proteases and/or extracellular proteases in a region distal to the furin site. By Western blot analysis we confirmed for human γENaC the previously reported finding (4, 5) that in the oocyte expression system γ-ENaC is fully cleaved at its furin cleavage site by endogenous convertases. Interestingly, replacing in human γENaC all four residues of the putative furin cleavage site by alanines (135AAAA138) completely abolished the stimulatory effect of SGK1 (n=10). In contrast, the stimulatory effect of the small ENaC activator S3969 (10 µM) was preserved indicating that the mutant channel is functional and can be activated by an SGK1 independent mechanism. In conclusion, our findings highlight the importance of the conserved serine residue S594 in human αENaC for mediating the acute channel activation by SGK1. Moreover, our data indicate that ENaC activation by SGK1 requires prior cleavage of γENaC at its furin cleavage site. Thus, these findings suggest an interdependence of proteolytic channel processing and acute channel activation by SGK1.

1. Diakov A & Korbmacher C (2004). J. Biol. Chem. 279, 38134-42 2. Diakov A et al. (2010). Cell Physiol Biochem. 26, 913-924 3. Diakov A et al. (2022). Pfugers Arch. 474(7), 681-697 4. Diakov A et al. (2008). J Physiol. 586(19), 4587-608 5. Haerteis S et al. (2012). J Gen Physiol. 140(4), 375-89

C15

Modulation of Mitsugumin 23 by Zn2+ influences intracellular Ca2+ dyshomeostasis in cardiac cells.

Amy M. Dorward[1], Miyuki Nishi[2], Hiroshi Takeshima[2], Samantha J. Pitt[1]

[1]University of St Andrews, St Andrews, United Kingdom, [2]Kyoto University, Kyoto, Japan

The importance of Zn^{2+} in cardiac function was first reported in 1965, where it was demonstrated that increasing [Zn^{2+}] decreased contractility and disrupted intracellular Ca^{2+}-handling in rabbit atria [1]. [Zn^{2+}] is elevated in ischaemia and rapidly declines in reperfusion [2] and intracellular Zn^{2+} levels and protein expression of Zn^{2+} transporters are altered in the failing heart [3]. The molecular mechanisms linking disrupted Zn^{2+} homeostasis with altered intracellular Ca^{2+}-dynamics remain poorly understood. We have shown that Zn^{2+} influences intracellular Ca^{2+} dynamics in cardiomyocytes by modulating the function of the type-2 ryanodine receptor [4,5]. We have also shown that Mitsugumin 23 (MG23), a recently identified cation channel located on the sarcoplasmic reticulum (SR) and nuclear membranes, is regulated by Zn^{2+} [5].

The aim of this research was to investigate the structure-function relationship of Zn^{2+} modulation of MG23.

MG23 channels were enriched from mouse heart by affinity purification and recombinant tagged human MG23 was purified using SMA co-polymers. Site-directed mutagenesis of human MG23 was achieved using PCR. Biophysical characterisation of channel function was carried out using the planar lipid bilayer technique. Cardiomyocytes were isolated from mouse hearts by a Langendorff-free method. Live cell imaging of Zn^{2+} and Ca^{2+}-dynamics were measured using 1 μM FluoZin-3 AM or 5μM Fluo-4 AM respectively. SR Ca^{2+}-store levels were assessed by addition of 10 mM caffeine. Statistical significance was calculated with student's t-test or one-way ANOVA with Tukey's or Dunnett's post-hoc test (as specified in figure legend). The institutional ethics committee at the University of St. Andrews and Kyoto University approved the study. Work was carried out under project licence P82006EDF.

Our data show that pathophysiological [Zn^{2+}] (1 nM) increase both mouse and human MG23 channel activity, suggesting that MG23 modulation by Zn^{2+} is conserved across species ($n \geq 3$). To probe Zn^{2+} binding sites of MG23, we constructed a E79Q channel mutant. The activity of the MG23 mutant was not increased by 1 nM Zn^{2+}, suggesting this residue is important in Zn^{2+} regulation of channel activity ($n = 4$).

In isolated cardiomyocytes, we confirm that hypoxia (0.5% O_2) leads to Zn^{2+} dyshomeostasis ($n = 2$ animals). We also show that cardiomyocytes exposed to hypoxic conditions have increased MG23 protein expression ($n \geq 2$ animals) and a significant reduction in the caffeine-induced SR Ca^{2+}-release response ($n \geq 20$ cells). Under the same conditions, store levels were restored by chelation of Zn^{2+} with TPEN (10 μM). To investigate the role of MG23 in Zn^{2+}-mediated SR Ca^{2+} leak, cardiomyocytes isolated from MG23 knock-out mice were exposed to hypoxic conditions. Our data reveal that SR Ca^{2+} load was not decreased in these cells ($n \geq 20$ cells).

These preliminary data suggest MG23 is a Zn^{2+}-regulated Ca^{2+} permeable channel and provide the first evidence that MG23 is a key driver in deleterious Ca^{2+} leak in progressive deterioration of cardiac function in pathophysiology.

[1] Ciofalo FR & Thomas LJ (1965). J Gen Physiol 48(5), 825-839. [2] Ayaz M & Turan B (2005). AJP Heart Circ Physiol 290(3), H1071-H1080. [3] Olgar Y et al (2018). J Cell Mol Med 22(3), 1944-1956. [4] Woodier J et al (2015). JBC 290(28), 17599-17610. [5] Reilly-O'Donnell B et al (2017). JBC 292(32), 13361-13373.

C16

Development of a 3D organ-on-chip model of the collecting duct for disease modelling

Alessandra Grillo[1], Chutong Zhong[1], Keith Siew[1], Stephen Ben Walsh[1]

[1]*Department of Renal Medicine, University College London, London, United Kingdom*

Extracellular matrix (ECM) is a network of proteins and proteoglycans essential for supporting cellular proliferation and physiological behaviour. Particularly, it was shown that kidney basement membrane components (mainly collagen IV and laminin) play a crucial role in the function of different segments of the nephron. An example of this mechanism is hensin, an ECM protein that have shown to promote transition between α and β intercalated cells, stimulating different mechanisms of action in the collecting duct. Current models using organ-on-chip systems mainly use collagen I as scaffold for their systems, without considering segment-specific compositions. Additionally, most kidney models reproduce proximal tubule systems, with no current 3D model of the collecting duct to study physiological mechanisms *in vitro*. Therefore, the aim of the study is to develop a 3D model of the collecting duct using organ-on-chip system by integrating more physiological and biomimetic ECM components.

M1-CCD cells from collecting duct were cultured on three-lane organ-on-chip systems (OrganoPlate, Mimetas) to produce tubular structures, where the middle channel was filled with a permeable ECM formed by a mix of Collagen I, Laminin I and Collagen IV and the top channel was filled with M1-CCD.

Preliminary results of the culture of M1-CCD on low-attachment plates to verify the intrinsic ability of cells to form 3D structures, confirmed that they are able to rearrange in round 3D organizations. Next steps include culture of M1-CCD on the OrganoPlate system including different combinations of basement membrane proteins such as collagen IV and laminin to the recommended collagen I, in order to create a more biomimetic environment for collecting duct epithelial cells. The goal of the study will be to eventually incorporate patient urine-derived cells from the collecting duct to create a more accurate and personalised platform for disease modelling.

C17

Inhibition of Orai1 by a Novel Peptide (ELD607) Reduces Inflammation and Increases Survival in ßENaC-Overexpressing Mice

Robert Tarran[1], Saira Ahmad[2], Erin Worthington[3], Troy Rodgers[5], Barbara Grubb[4]

[1]KUMC, Kansas City, United States, [2]Eldec Pharmaceuticals, Durham, United States, [3]Carilion Clinic, Roanoke, United States, [4]UNC, Chapel Hill, United States, [5]UNC, Chapel Hill, United States

Cystic fibrosis is an inherited genetic disease caused by dysregulation of the CFTR anion channel. Clinical manifestations of this disease include chronic mucus plugging of the airways and unrelenting cycles of infection and inflammation. $CFTR^{-/-}$ transgenic mice which lack functional CFTR do not develop CF-like lung disease. Accordingly, mice overexpressing the beta subunit of the epithelial Na^+ channel (ßENaC mice) were generated. These mice spontaneously develop CF-like lung disease and exhibit significant mortality. Orai1 is a plasma membrane Ca^{2+} channel that regulates inflammation. Orai1 activity is increased in CF airways. We hypothesized that Orai1 inhibition would reduce inflammation in the ßENaC mice. Accordingly, we developed an Orai1-specific peptide antagonist called ELD607. Our HPLC data indicated that ELD607 was stable in proteolytically-rich CF sputum and our quartz crystal microbalance with dissipation (QCMD) data indicated that ELD607 did not stick to mucus. We added ELD607 (0.5 mg/kg) or vehicle (saline) to ßENaC mice and their WT littermate controls daily for 10 days. We assessed survival over 10 days and surviving mice were sacrificed in order to perform Ussing chamber studies and lung histology. Amiloride-sensitive currents were significantly elevated in ßENaC mice relative to WT mice (n=3 per group). However, chronic ELD607 dosing had no effect on either isoprenaline or amiloride-sensitive currents (markers of CFTR and ENaC activity respectively) in either WT or ßENaC mice (all n=3 per group). After 10 days, 100% of WT mice survived, regardless of treatment, while 50% of ßENaC mice survived. Importantly, 10 days of ELD607 exposure, significantly increased ßENaC mouse survival to 95%. In these mice, lung neutrophilia was reduced by 90% (n=9/group) while lung macrophage levels were restored to the normal range. Thus, we tentatively conclude that despite not altering ENaC activity, ELD607 increases survival by reducing neutrophilia and preventing lung damage. Such an approach may be useful for the treatment of CF lung disease by treating CF inflammation.

C18

Histamine-driven intracellular signaling and ion transport in renal epithelium.

Anastasia Sudarikova[1], Valeriia Vasileva[1], Maksim Diakov[1], Alena Cherezova[1], Daria Lysikova[2], Denisha Spires[2], Marharyta Semenikhina[3], Oleg Palygin[3], Daria Ilatovskaya[1]

[1]Medical College of Georgia, Augusta University, Augusta, United States, [2]Medical College of Georgia, Augusta University, Augusta, United States, [3]Medical University of South Carolina, Charleston, United States

Background. Histamine is a nitrogenous compound that is crucial for the progression and initiation of the local inflammation-driven response. It has been shown that the levels of histamine are increased in renal diseases such as diabetic nephropathy and acute kidney injury. Although substantial histamine levels have been reported in the kidney, renal pathological and physiological effects of this compound are not clearly defined. In this study, we **hypothesized** that histamine is a crucial regulator of renal epithelial function through its effects on ion transport and actin cytoskeleton rearrangements.

Methods. Immunostaining of cultured cells, human and rat tissues, combined with Western blotting, were employed to characterize the renal expression of histamine receptors (HRs) and histaminergic system (HiS) enzymes. The acute functional effects of histamine were tested in principle cortical collecting duct (mpkCCD) and opossum proximal tubule (OK) cells, immortalized human podocytes, and podocytes of isolated rat glomeruli. Functional confocal imaging was used to detect changes in intracellular Ca^{2+} (Fluo8/FuraRed). Actin cytoskeleton rearrangements were assessed by staining with rhodamine-phalloidin. Ion transport was probed with short-circuit current measurements and patch clamp. Differences between the groups were tested with ANOVA; $p < 0.05$ was considered significant.

Results. We showed that all four HRs, as well as HiS enzymes (histidine decarboxylase (HDC), histamine-N-methyltransferase (HNMT), and diamine oxidase (DAO)), are present in the rat and human kidney cortex, with segment-specific nephron expression in glomeruli, proximal tubules, and collecting ducts. We further demonstrated the presence of all four HRs and HiS enzymes in cultured mpkCCD and OK cells. In mpkCCD, short-circuit current studies demonstrated inhibition of ENaC (epithelial Na^+ channel)-mediated currents after 4 hours of incubation with histamine. Immunocytochemistry and qPCR confirmed this effect, showing a decrease in protein and gene expression for αENaC upon histamine treatment ($n = 7$/group, $p < 0.05$). In acute studies, single-channel patch clamp analysis revealed similar ENaC activity before and after histamine application ($n = 6$/group, $p > 0.05$). In response to histamine, we largely detected extracellular Ca^{2+} influx with a minor component of intracellular store depletion. Intracellular Ca^{2+} influx in response to acute stimulation of HR was observed in mpkCCD cells (EC50 90 ± 15 uM; pilot data allow us to speculate that the responses are mediated via HR3a and HR4), OK cells, podocytes of the freshly isolated rat glomeruli, and cultured human podocytes (at least $n = 3$/group, up to 40 replicates, $p < 0.05$). In all cell types, we observed a time-dependent formation of F-actin stress fibers and cortical polymerization of F-actin following incubation with 100 uM histamine for 1 and 4 hours ($n = 3$ experiments per group, $p < 0.05$).

Conclusions. Rat and human renal epithelia demonstrate strong expression of HiS components. Functionally, histamine elicits Ca^{2+} transients and actin reorganization in the proximal tubule, collecting duct cells, and podocytes. These data support the notion that local renal production of histamine plays a role in epithelial physiological and pathophysiological function through effects on electrolyte reabsorption, cell polarity, sheer stress response, and epithelial barrier integrity and permeability.

C19

The small molecule activator S3969 stimulates the human epithelial sodium channel (ENaC) by interacting with a specific binding pocket in the channel's β-subunit

Florian Sure[1], Jürgen Einsiedel[2], Peter Gmeiner[2], Patrick Duchstein[3], Dirk Zahn[3], Christoph Korbmacher[1], Alexandr Ilyaskin[1]

[1]Institute of Cellular and Molecular Physiology, Friedrich-Alexander-Universität Erlangen-Nürnberg, Erlangen, Germany, [2]Department of Chemistry and Pharmacy, Medicinal Chemistry, Friedrich-Alexander-Universität Erlangen-Nürnberg, Erlangen, Germany, [3]Department of Chemistry and Pharmacy, Chair for Theoretical Chemistry/Computer Chemistry Center (CCC), Friedrich-Alexander-Universität Erlangen-Nürnberg, Erlangen, Germany

Several members of the ENaC/degenerin (DEG) family of ion channels can be activated by specific ligands [1]. Interestingly, a small molecule ENaC activator (S3969) has been synthesized and shown to stimulate human but not mouse ENaC in the αβγ-subunit configuration. Moreover, it was shown that the extracellular loop of human βENaC was essential to mediate this stimulatory effect [2]. Our aim was to identify and characterize the S3969 binding site in human βENaC by combining structure-based computer simulations with site-directed mutagenesis and electrophysiological measurements. ENaC was heterologously expressed in *Xenopus laevis* oocytes. Channel function was assessed by measuring amiloride-sensitive whole-cell currents (ΔI_{ami}) using the two-electrode voltage clamp technique. A putative S3969 binding site in the channel's β-subunit was predicted by atomistic modelling, namely docking and molecular dynamics (MD) simulations based on recently published structural information of ENaC (PDB ID 6WTH; [3]). Values are presented as mean±SEM. One-tailed paired *t*-test was used for statistical analysis. We confirmed that mouse ENaC ($\alpha_m\beta_m\gamma_m$; n=19) was insensitive to S3969 in concentrations up to 10 µM, whereas S3969 activated human ENaC ($\alpha_h\beta_h\gamma_h$) by ~2-fold with an EC_{50} of ~0.3 µM (n=25). Importantly, when a portion of the extracellular loop of mouse βENaC was replaced by the corresponding portion of human β-ENaC (amino acid residues 211-404, $\alpha_m\beta_{m,h(211-404)}\gamma_m$) the chimeric channel could be activated by S3969 ~2-fold with an EC_{50} of ~0.5 µM (n=11). Functional testing of additional mouse-human chimeric βENaC constructs revealed that the β-thumb domain was critically involved in the stimulatory effect of S3969. Furthermore, structural ENaC analysis suggested that the β-thumb domain participated in forming a putative S3969 binding pocket, which was localized at the β-γ-subunit-interface. Computer simulations predicted the key residues within the binding pocket for coordinating S3969. Particularly stable interactions were observed between S3969 and an arginine βR388, a tyrosine βY406 and a phenylalanine βF391 residue. Introducing point mutations at these positions strongly reduced (βR388H, n=15; βR388A, n=12) or nearly abolished (βY406A, n=18; βF391G, n=18) the stimulatory effect of S3969 on ΔI_{ami}. MD simulations suggested that binding of S3969 to ENaC caused a conformational change of the channel, which weakened the β-γ-intersubunit interactions and increased the distance between the β-thumb and the γ-palm domains. Consistent with these predictions, the stimulatory effect of S3969 on ENaC was abolished when the β-thumb domain was covalently attached to the γ-palm domain following the introduction of two cysteine residues (βR437C – γS298C) to form a disulfide bridge (ΔI_{ami}=0.79±0.14 µA before and 0.71±0.13 µA after S3969 application, n=15, n.s.). Importantly, reducing the disulfide bond with DTT partially rescued the stimulatory effect of S3969 on ENaC currents (ΔI_{ami}=0.76±0.09 µA before and 0.98±0.10 µA after S3969 application, n=15, $p<0.001$). In conclusion, S3969

interacts with a specific binding pocket in the β-subunit of ENaC. This modifies the molecular interaction of the β- and γ-subunits probably causing a conformational change resulting in channel activation. The molecular characterization of the S3969 binding site may help to identify novel endogenous or pharmacological ENaC modulators with possible physiological and therapeutic implications.

1. Kellenberger S & Schild L (2015). Pharm Reviews 67, 1-35. 2. Lu M et al. (2008). J Biol Chem 283, 11981-11994. 3. Noreng S et al. (2020). Elife 9:e59038.

C20

Cholinergic mobilisation of juxtaposed TPC1-InsP3R3 calcium stores triggers secretion of mucus and fluid to flush the human colonic stem cell niche

Victoria Jones[1], Nicolas Pelaez-Llaneza[1], Alvin Lee[1], Sean Tattan[1], Mark Williams[1]

[1]*School of Biological Sciences, University of East Anglia, Norwich, United Kingdom*

Intestinal epithelial cells form a vital selective barrier between the mucosal immune system and a barrage of microorganisms, ligands and antigens derived from the hostile gut lumen. Preservation of barrier function is underpinned in part by calcium-dependent secretion of a protective mucus layer. The aims of the current study were to (i) unravel the mechanism of cholinergic calcium signals that initiate at the human colonic crypt base and (ii) determine the effects on secretion of mucus and fluid from crypt-base-goblet-cells GCs) and neighbouring intestinal stem cells (ISCs). Methods: Human colonic crypts were isolated from colorectal tissue samples obtained at surgical resection (NREC approval) and cultured as crypts in the short term (< 1 week), or propagated as crypt-like organoids over the long-term (up to 5 years). The spatio-temporal characteristics of intracellular calcium was monitored by Fura-2/Fluo-4/Calbryte-630 imaging and the mechanism of receptor-mediated calcium mobilisation was characterised by pharmacological and knockdown gene approaches. Calcium signalling toolkit expression was visualised by fluorescence immunolabelling and super-resolution imaging. Mucus secretion was visualised by Muc2 immunofluorescence depletion assays and real-time imaging of fluorescently tagged mucin-2, using MUC2::mNEON crypt-like organoids generated by CRISPR-HOT. An organoid swelling assay was used as a proxy for fluid secretion. Results: A microdomain of juxtaposed InsP3R3 and TPC1 expression was present at the apico-lateral pole of ISCs and GCs at the crypt (or organoid crypt-like)-base and corresponded to the site of cholinergic calcium signal initiation (Carbachol, 1-100 μM; n>10). Calcium signals propagated across to the basal pole of initiation cells and laterally to neighbouring cells. Calcium signal amplitude was reduced >50% by TPC1 antagonists NED19 (250 μM; n>10; P<0.05) and tetrandrine (20 μM; n>10; P<0.05). Caffeine (10 mM), an inhibitor of InsP3Rs, and miRNA knockdown of InsP3R3s, also reduced calcium signal amplitude by >50% (n>5; P< 0.05). Carbachol (10 μM) stimulated both MUC2 depletion from GCs in colonic crypt bases (n>200; P<0.05) and luminal secretion of MUC2-mNEON in crypt-like organoids (n>5; P<0.05). Carbachol (10 μM) also stimulated an increase in organoid cross-sectional area in organoid swelling assays. Pharmacologic inhibition of TPC1 or InsP3Rs (see above) reduced cholinergic stimulation of: MUC2 immunofluorescence depletion from crypt GCs; luminal secretion of MUC2-mNEON from crypt-like organoids; and cross-sectional area of organoids in swelling assays (n>5; P<0.05). Conclusion: Co-activation of juxtaposed TPC1 and InsP3R3 is required for generation of cholinergic calcium signals and downstream secretion of hydrated mucus, which culminates in the flushing of the human colonic stem cell niche.

C21

AI-driven Model based on Transformer Architecture for Accurate and Efficient Kidney Biopsy Analysis

Zhongwang Li[1], Keith Siew[1], Stephen Walsh[1], Simon Walker-Samuel[1]

[1]*University College London, London, United Kingdom*

Introduction

Affecting over 20 million people worldwide, kidney diseases are primarily caused by nephron lesions. The complex tubular structure of nephrons challenges accurate diagnosis through a kidney biopsy. To address this, we developed a workflow combining optical clearing and artificial intelligence, enhancing accuracy and automating the process. Optical clearing turns samples transparent, allowing precise mapping of internal tubular configurations. Light-sheet microscopy images these structures, but accurate segmentation is necessary for quantifying measurements, such as tubular length and volume. With its remarkable capabilities in medical imaging analysis, machine learning presents a promising solution for the tubule segmentation task. We propose a vision transformer-based machine learning segmentation model that automates measurements, aids clinicians in generating appropriate diagnoses, and provides valuable insights into gene location and function. This highly translational method can be extended to other tubular organs, benefiting a broader community by quickly adapting the underlying code.

Methods

We collected 36 light-sheet microscopy images, each representing a quarter of a mouse kidney. These 16-bit, 3-channel images have 2048x2048 pixels, with a depth range (Z) of 700-1200 pixels and pixel sizes of 4.08um (XY plane) and 4.0um (Z axis). Due to limited RAM and VRAM, images are split into fixed-size blocks and segmented individually. Each block is treated as a series of 2D images. Except for the 1st image, a convolutional neural network encodes and captures local features of the N^{th} image and the segmentation result of the $(N-1)^{th}$ image together, as adjacent images usually share spatial information. The transformer encoder learns high-level contextual representations while the transformer decoder reconstructs the structure. The convolutional decoder recovers spatial dimensions and generates a tubule probability map, with the final segmentation mask obtained by normalizing the output probability map using a softmax activation function. At last, these segmented blocks are reconstructed into the original size image as the segmentation result.

Results and Discussion

While the samples have been annotated, we are still in the process of building the model. Preliminary tests (Classical 3D Convolutional Neural Network) demonstrate the potential of the proposed approach to effectively segment tubular structures in the kidney, with initial results indicating improvements in segmentation accuracy compared to traditional methods. Upon completion of the model, we will conduct a comprehensive evaluation, including quantitative metrics such as Dice score, precision, recall, and intersection over union (IoU), to assess the

model's performance on the segmentation task. Additionally, we will investigate the impact of incorporating different pre-processing techniques, data augmentation strategies, and loss functions to enhance the model's accuracy and generalization further. Comparisons with existing segmentation methods, both machine learning-based and conventional, will establish the superiority of our proposed approach. Finally, we plan to analyze the model's performance in real-world clinical settings, exploring its potential for assisting clinicians in making accurate diagnoses and offering valuable insights for researchers in studying gene location and function in 3D spatial contexts.

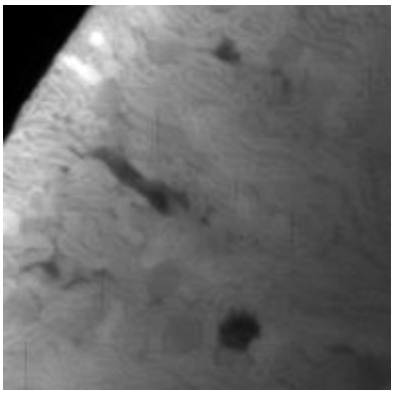

1. A. Vaswani et al., ‘Attention Is All You Need’. arXiv, Dec. 05, 2017. doi: 10.48550/arXiv.1706.03762.Mohammed Y, Sherwin SJ, Weinberg PD. J Biomech. 2017; 50:102-109.
2. A. Dosovitskiy et al., ‘An Image is Worth 16x16 Words: Transformers for Image Recognition at Scale’. arXiv, Jun. 03, 2021. doi: 10.48550/arXiv.2010.11929.Nichols WW, O’Rourke MF. McDonald's Blood Flow in Arteries. Lea & Febiger, Philadelphia; 1990.

C22

Expression of the glucose transporter GLUT12 in the A172 glioblastoma cell line and its regulation by insulin and glucose

Adrián Idoate-Bayón[3], Marta Soria[4], Neira Sáinz[6], Miguel Burgos[7], M. Pilar Lostao[8]

[1]University of Navarra, Center for Nutrition Research and Department of Nutrition, Food Sciences and Physiology, School of Pharmacy and Nutrition Pamplona, Spain., IdiSNA, Navarra Institute for Health Research, Pamplona., Spain, [2]University of Navarra, Center for Nutrition Research and Dept. of Nutrition, Food Sciences and Physiology. School of Pharmacy and Nutrition. Pamplona, Spain., IdiSNA, Navarra Institute for Health Research, Pamplona, Spain, [3]University of Navarra; Center for Nutrition Research and Department of Nutrition, Food Science and Physiology; School of Pharmacy and Nutrition., Pamplona, Spain, [4]University of Navarra, Department of Nutrition, Food Science and Physiology; School of Pharmacy and Nutrition., Pamplona, Spain, [5]University of Navarra, Center for Nutrition Research and Department of Nutrition, Food Science and Physiology; School of Pharmacy and Nutrition. Pamplona, Spain., Pamplona, Spain, [6]University of Navarra, Center for Nutrition Research and Department of Nutrition, Food Science and Physiology; School of Pharmacy and Nutrition., Pamplona, Spain, [7]University of Navarra, Center for Nutrition Research and Department of Nutrition, Food Science and Physiology; School of Pharmacy and Nutrition. Pamplona. IdiSNA, Navarra Institute for Health Research, Pamplona, Spain, [8]University of Navarra, Center for Nutrition Research and Department of Nutrition, Food Science and Physiology, School of Pharmacy and Nutrition Pamplona, Spain. IdiSNA, Navarra Institute for Health Research, Pamplona, Spain. CIBER de Fisiopatología de la Obesidad y Nutrición (CIBEROBN). Instituto de Salud Carlos III (ISCIII), Pamplona, Spain

The brain depends on glucose as the main source of energy, being GLUT1 (in astrocytes) and GLUT3 (in neurons) the most relevant glucose transporters. One of the latest members of the facilitative glucose transporter family (SLC2A) identified is GLUT12. GLUT12 is expressed in small intestine, adipose tissue, muscle, kidney and brain. Stimulus such as insulin, glucose and TNF-α induce GLUT12 expression and translocation to the membrane. However, expression and function of GLUT12 in the brain is an unexplored topic. Our group has demonstrated GLUT12 expression in different brain areas in mice, but its function has not been established yet. More interesting, we have reported upregulation of GLUT12 in the brain of mouse models of Alzheimer's disease (AD), in aged mice and senescence accelerated mice models, and in the frontal cortex of AD disease patients. Other authors have shown, among brain cells, the highest expression of GLUT12 mRNA in oligodendrocyte progenitor cells and astrocytes. Since the astrocytes are the main energy providers for the neurons, we decided to investigate GLUT12 expression and regulation by glucose and insulin in the astrocytic human glioblastoma cell line A171, to advance in the knowledge of GLUT12 function in the brain. We also studied GLUT1 expression for comparison.

Cells were incubated in the absence and presence of 50 nM insulin or 25 mM glucose for 1 and 24 h, and expression of the transporters was determined by RT-PCR and Western blot. The ANOVA test and Tukey's Post-Hoc analysis were applied.The number of samples per condition was 3-5. After 24 h incubation, glucose decreased GLUT12 mRNA by 50% ($p<0.05$), whereas insulin did not modify it. Interestingly, neither glucose nor insulin changed GLUT12 protein expression, which appeared as a dimer with a molecular weight of 140 kDa. Differently, GLUT1 mRNA was not

affected by glucose or insulin, while glucose decreased GLUT1 protein expression by 50% ($p<0.05$). After 1 h incubation, both glucose an insulin reduced GLUT12 mRNA by 50% ($p<0.05$) and 70% ($p<0.01$) respectively. Surprisingly, GLUT12 protein increased 5-fold in the presence of glucose ($p<0.05$), while insulin only induced a trend to increase the transporter expression. Finally, GLUT1 mRNA and protein were reduced by 50 % ($p<0.05$) by glucose but were not affected by insulin.

Overall, in this work we have demonstrated the expression of GLUT12 in the A172 astroglioma cell line. Of note, mRNA and protein expression were not correlated. Importantly, we found an increase in GLUT12 protein expression after high glucose incubation, while a decrease in GLUT1 expression was observed. These results will help to understand GLUT12 function in the astrocytes, who are important regulators of brain glucose metabolism.

Gil-Iturbe E et al. (2020) Mol Neurobiol 57, 798–805 Gil-Iturbe E et al. (2019) J Cell Physiol 234, 4396-4408 Gil-Iturbe E et al. (2019) Acta Physiol (Oxf) 226, e13283 Pujol-Gimenez J et al. (2014) J Alzheimers Dis 42,97–101 Rogers S et al. (2002) Am J Physiol Endocrinol Metabol 282, 733-8

C23

Interrogating the steroid receptors involved in acute corticosteroid-induced stimulation of ENaC in a cellular model of the collecting duct.

Struan R. Loughlin[1], Matthew A. Bailey[2], Morag K. Mansley[1]

[1]Cellular Medicine Research Division, University of St Andrews, St Andrews, United Kingdom,
[2]Centre for Cardiovascular Science, The University of Edinburgh, Edinburgh, United Kingdom

The volume-regulating hormone aldosterone stimulates Na^+ reabsorption *via* the epithelial Na^+ channel (ENaC) in the aldosterone-sensitive distal nephron (ASDN) [1], downstream of transcriptional processes *via* the mineralocorticoid (MR) and glucocorticoid receptor (GR). Aldosterone specificity is conferred to principal cells (PCs) of the ASDN by the enzyme 11βHSD2 which inactivates the more abundant cortisol. Both MR and GR have been localised to the ASDN [2], and recent evidence suggests that earlier portions of the ASDN contain "unprotected" ENaC [3]. However, the specific roles of these receptors in mediating steroid-induced ENaC activity remains unclear. The aim of this study was to assess the relative roles of MR and GR in mediating steroid-induced ENaC activity and the target genes involved.

$mCCD_{cl1}$ murine collecting duct (CD) cells [4] or primary CD cells (PCDs) [5] were seeded onto permeable filters for 9-11 days. Cells were treated with MR (PF-03882845, 100nM) or GR (mifepristone, 10μM) antagonists for 30min, or respective control, followed by ALDO (3nM), corticosterone (CORT, 10nM) or dexamethasone (DEX, 100nM) for 3h. For experiments involving CORT, 10μM carbenoxolone was included in the 30min treatment to inhibit 11βHSD2 activity. Changes in equivalent short-circuit current (ΔI_{eq}) were measured by epithelial volt-ohm-meter. RNA was extracted and expression of 3 ALDO-induced genes [5]: *Sgk1*, *Zbtb16* and *Rasd1* were measured by qRT-PCR. Results are mean±95% CI, statistical significance determined by two-way ANOVA and Tukey's post-hoc test.

ALDO-induced ΔI_{eq} was -5.2±1.0 $\mu A \cdot cm^{-2}$ in $mCCD_{cl1}$ cells (n=9-10, p<0.001) and -3.6±0.5 $\mu A \cdot cm^{-2}$ in PCDs (*n*=6, p<0.001). MR antagonism near abolished this in both $mCCD_{cl1}$ and PCDs (p<0.001), whereas GR antagonism did not. When pre-treated with CBX, CORT-induced ΔI_{eq} was -6.4±1.0 $\mu A \cdot cm^{-2}$ in $mCCD_{cl1}$ and -4.0±0.3 $\mu A \cdot cm^{-2}$ in PCDs (p<0.001). These were partly inhibited by MR antagonism in $mCCD_{cl1}$ (p<0.05) and PCDs (p<0.001), however GR antagonism had no effect. DEX-induced ΔI_{eq} was -9.3±1.0 $\mu A \cdot cm^{-2}$ in $mCCD_{cl1}$ cells and -4.7±0.5 $\mu A \cdot cm^{-2}$ in PCDs (p<0.001). GR, but not MR, antagonism inhibited this response in both $mCCD_{cl1}$ cells and PCDs (p<0.001).

Expression of *Sgk1*, *Zbtb16* and *Rasd1* was upregulated by ALDO, CBX+CORT and DEX (n=9-10, p<0.001 across all). MR antagonism reduced ALDO-induced expression of *Sgk1* (p<0.001), *Zbtb16* (p<0.001) and *Rasd1* (p<0.05). Interestingly GR antagonism also reduced ALDO-induced expression of *Sgk1* (p<0.001), *Zbtb16* (p<0.001) and *Rasd1* (p<0.05). MR, but not GR, antagonism reduced CORT-induced expression of *Sgk1* (p<0.0001), *Zbtb16* (p<0.05) and *Rasd1* (p<0.05). Finally, GR, but not MR, antagonism near-abolished DEX-induced expression of *Sgk1* (p<0.001), *Zbtb16* (p<0.001), *Rasd1* (p<0.001).

Whilst ALDO-induced ENaC activity was MR- but not GR-dependent, the expression of all target genes involved both MR and GR. These findings may reflect that $mCCD_{cl1}$ cells are a mixed population of principal and intercalated cells. Notably, CORT-induced ENaC activity and target gene expression was MR-dependent, with no effect of GR antagonism. In this setting, CORT may be considered a mineralocorticoid and the sole MR-dependence is at odds with the ALDO results. These findings reveal a complexity to the regulation of ENaC activity by corticosteroid hormones and the receptors involved. Further work is required to unpick these mechanisms.

[1] Loffing J and Korbmacher C (2009). Pflug Arch Eur J Phy 458: 111-135. [2] Ackermann D et al. (2010). Am J Physiol – Renal Physiol 299: F1473-F1485. [3] Nesterov V et al. (2012). Am J Physiol – Renal Physiol 303: F1289-F1299. [4] Gaeggeler HP et al. (2005). J Am Soc Nephrol 16, 878-891. [5] Loughlin S et al. (2023). Kidney360 4, 226-240.

C24

Hypoxia-mediated regulation of sodium transporters in breast cancer cell lines

Jodie Malcolm[1], Andrew Holding[1], William Brackenbury[1,2]

[1]Department of Biology, University of York, York, United Kingdom, [2]York Biomedical Research Institute, University of York, York, United Kingdom

As breast tumours grow, oxygen availability becomes limited, resulting in upregulation of key survival genes via hypoxia-inducible factors (HIFs) binding to core hypoxia response elements (HREs) [1]. Voltage gated sodium channels (VGSCs) are upregulated in several solid tumours, including breast [2]. In triple negative breast cancer (TNBC) tumours and MDA-MB-231 cells, the neonatal splice variant of $Na_v1.5$ ($nNa_v1.5$) encoded by ***SCN5A*** is overexpressed, and drives invasiveness of these cancer cells in vivo and in vitro [2,3]. In hypoxic pulmonary arterial smooth muscle cells, the HIF-1α isoform increases sodium/proton exchanger 1 (***NHE1***) expression [4]. HIF-1α also mediates expression of other membrane transporters, including ***MCT-4*** and ***GLUT1*** [5]. Due to the evidence implicating HIF-1α in modulating ion and solute transport, we wanted to investigate if VGSCs and ***NHE1*** are HIF-1α-targets in breast cancer cell lines.

To understand hypoxia-dependent dysregulation of sodium transporters, both ER +ve MCF-7 and TNBC MDA-MB-231 cells were cultured for 0, 4 or 24 hours in hypoxia (1% O2). To elucidate HIF-1α involvement, MCF-7 and MDA-MB-231 cells were treated with the chemical PHD inhibitor, dimethyloxalylglycine (DMOG; 1 mM) in normoxia for up to 72 hours (0, 2, 4, 8, 16, 24, 48 and 72 hour time course). Western blot was performed to identify HIF-1α stabilisation. RT-qPCR was used to assess changes in VGSCs (***SCN5A***, ***SCN8A*** and ***SCN9A***) and ***NHE1*** mRNA expression. Data were analysed using one-way ANOVA, with post-hoc Dunnett's tests as appropriate.

Hypoxic MCF-7 cells displayed significantly increased expression of ***SCN5A*** (6.03 ± 1.60 fold at 24 hours $p < 0.0001$; n = 6, mean ± SD) and ***SCN8A*** (87.04 ± 32.28 fold at 24 hours, $p < 0.05$, n = 3; mean ± SD). However, ***SCN9A*** was not significantly altered (p = 0.48, n = 3). Preliminary data indicate that ***NHE1*** transcription was also increased at 24 hours (n = 2). Hypoxic MDA-MB-231 cells showed significantly increased expression of ***SCN8A*** (4.79 ± 0.13 fold at 4 hours, $p < 0.05$; 8.78 ± 1.92 fold at 24 hours, $p < 0.001$, n = 3, mean ± SD) but not ***SCN5A*** (p = 0.30, n = 6), ***SCN9A*** (p = 0.32, n = 3), or ***NHE1*** (p = 0.27, n = 3). DMOG-dependent stabilisation of HIF-1α peaked at 4 hours in both MCF-7 and MDA-MB-231 cells, with protein levels decreasing after 16 hours (western blot, n=3). ***SCN5A*** expression was increased in MCF-7 cells after DMOG treatment, reaching a significant fold change in transcript levels at 48 hours (3.74 ± 2.19 fold at 48 hours; $p < 0.05$ n = 3, mean ± SD). However, no significant increase in ***SCN8A*** (p = 0.51, n = 3), ***SCN9A*** (p = 0.17, n = 3) or ***NHE1*** (p = 0.25, n = 3) was observed within the 72 hour DMOG treatment time course.

These findings suggest hypoxia enhances expression of VGSC and ***NHE1*** transcripts in a breast cancer subtype specific manner. Further work is required to depict the involvement of HIF-1α in aberrant sodium transporter expression.

1. Jewell, U. R., I. Kvietikova, A. Scheid, C. Bauer, R. H. Wenger, and M. Gassmann. 2001. "Induction of HIF–1α in Response to Hypoxia Is Instantaneous." FASEB Journal: Official Publication

of the Federation of American Societies for Experimental Biology 15 (7): 1312–14. 2. Fraser, Scott P., James K. J. Diss, Athina-Myrto Chioni, Maria E. Mycielska, Huiyan Pan, Rezan F. Yamaci, Filippo Pani, et al. 2005. “Voltage-Gated Sodium Channel Expression and Potentiation of Human Breast Cancer Metastasis.” Clinical Cancer Research: An Official Journal of the American Association for Cancer Research 11 (15): 5381–89. 3. Brackenbury, William J., Athina-Myrto Chioni, James K. J. Diss, and Mustafa B. A. Djamgoz. 2007. “The Neonatal Splice Variant of Nav1.5 Potentiates in Vitro Invasive Behaviour of MDA-MB-231 Human Breast Cancer Cells.” Breast Cancer Research and Treatment 101 (2): 149–60. 4. Larissa A. Shimoda, Michele Fallon, Sarah Pisarcik, Jian Wang, and Gregg L. Semenza 2006. “HIF-1 regulates hypoxic induction of NHE1 expression and alkalinization of intracellular pH in pulmonary arterial myocytes.” American Journal of Physiology-Lung Cellular and Molecular Physiology 291 (5), L941-L949 5. Weidemann, A., Johnson, R. Biology of HIF-1α. Cell Death Differ 15, 621–627 (2008).

C25

Lithium Attenuates AVP-dependent Calcium Signaling in the Intercalated Cells and Impairs the Regulation of Acid-Base Handling in the Collecting Duct

Mykola Mamenko[1], Alena Cherezova[1], Vadym Buncha[1], Nichole Mumuney[1], Irina Baranovskaya[1]

[1]*Augusta University, Augusta, United States*

INTRODUCTION. Lithium salts are prescribed as mood stabilizers to treat mental disorders. It has been widely reported that lithium therapy negatively affects collecting duct principal cells resulting in reduced urinary concentrating ability. Less is known about the effects of lithium salts on the intercalated cells and acid-base transport in the collecting duct. Previous studies have shown that activation of G_q-coupled vasopressin 1a receptors (V1aR) in type A intercalated cells stimulates luminal H^+ secretion resulting in urinary acidification, while lithium therapy increases baseline urine pH. We hypothesize that lithium administration markedly reduces V1aR-dependent Ca^{2+} signaling in intercalated cells impairing the regulation of acid-base transport in the collecting duct.

METHODS. We combined immunofluorescent imaging in freshly isolated collecting duct segments with metabolic cage studies in C57BL/6NJ (Jackson Labotatory) mice receiving a regular chow (Teklad 2918) or a diet containing 0.3% of lithium carbonate (added to the base Teklad 2918 chow) to assess the effects of lithium on V1aR-mediated Ca^{2+} signal, H^+ transport by intercalated cells, as well as urinary pH, ammonia and acid excretion.

RESULTS. We found that application of arginine-vasopressin (AVP, 1 nM) elicits a transient calcium response in the aquaporin-2 (AQP2) negative cells from the collecting duct segments isolated from the mice on a regular chow. Calcium in response to AVP was mobilized from the intracellular stores as the AVP-dependent calcium response was preserved in 0 Ca^{2+} extracellular solution and ablated upon pretreatment of collecting duct segments with SERCA pump inhibitor, thapsigargin, 500 nM. The amplitude of AVP-induced calcium transient was markedly reduced in the AQP2-negative cells isolated from lithium-treated mice when compared to controls (39±5 vs 163±40 nM, respectively). The reduction of AVP-mediated Ca^{2+} signaling in the AQP2-negative collecting ducts cells was paralleled with significant changes in proton extrusion rates and acid excretion with urine.

CONCLUSIONS. Our findings reveal that AVP-stimulated intracellular Ca^{2+} signaling in intercalated cells is an important determinant of acid transport in the collecting duct and urinary acid excretion at the systemic level. Lithium treatment significantly impairs AVP-dependent intracellular Ca^{2+} signaling in the collecting duct intercalated cells, significantly altering H^+ handling by intercalated cells and acid excretion with urine.

ETHICAL STANDARDS. All animal procedures were approved by the Institutional Animal Care and Use Committee of the Medical College of Georgia at Augusta University (AUP 2017-0844) and were conducted in accordance with the National Institutes of Health Guide for the Care and Use of Laboratory Animals.

C26

Developing a method to map corticosteroid-regulated sodium transport in the distal nephron using multiplex IF and IHC imaging.

Morag Milne[1], In Hwa Um[1], Robert Hunter[2], David Harrison[1], Matthew Bailey[2], Morag Mansley[1]

[1]University of St Andrews, St Andrews, United Kingdom, [2]The University of Edinburgh, Edinburgh, United Kingdom

The aldosterone (ALDO)-sensitive distal nephron is typically defined as: the late distal convoluted tubule (DCT), connecting tubule (CNT) and cortical collecting duct (CD). ALDO-sensitivity is defined by 11βHSD2 (11β) activity (which inactivates corticosterone, CORT); mineralocorticoid (MR) rather than glucocorticoid receptor (GR) expression; and the target epithelial sodium channel (ENaC). Recent studies have reported ALDO-insensitive, but MR-dependent ENaC activity in DCT2/CNT [1,2] and that CORT-stimulated ENaC may be relevant in MR antagonism as 4th line anti-hypertensive therapy [3]. Whilst functional evidence of ALDO-insensitive ENaC activity is compelling, corticosteroid-regulated Na^+ transport along the distal nephron is not fully defined. AIM: To develop a method enabling an unbiased measurement of 11βHSD2, MR and GR expression alongside Na^+ transporter localisation in murine distal nephron.

Male C57BL/6 mouse kidney sections were subject to multiplex immunofluorescence (11β, MR and GR) and immunohistochemical labelling (NCC, TRPV5, γ-ENaC and AQP2), Hoechst was used as a nuclear counterstain with the former. All primary antibodies were recognised by either anti-rabbit or anti-mouse polymer HRP and visualised either by tyramide signal amplification with associated fluorophores (Fluorescein, Cy3 or Cy5) for multiplex IF, or respective chromagens (red, green, blue, brown) for multiplex IHC. Images were co-registered, annotated and analysed using Halo® software. At least 2 users annotated each kidney section. Data are shown as mean±SD.

Distal nephron segments were defined by the presence of transporter/channel: DCT - NCC; DCT/CNT - NCC and TRPV5; CNT - TRPV5; CNT/CCD - TRPV5 and γ-ENaC/AQP2; CCD - γ-ENaC/AQP2. We did not detect NCC and γ-ENaC co-localisation. Average cells/section: DCT - 1165±131; DCT/CNT - 329±81; CNT - 242±50; CNT/CCD - 878±246; CCD - 2247±341 (n=3). 2 additional annotations were made as controls: 11β/MR negative and GR negative cells where at least 100 cells of each criteria were identified from each section. Raw signal intensity for 11β, MR and GR were plotted and thresholds for a positive signal were set using the negatively labelled cells, for each section analysed.

DCT was predominantly 11β- (~80%) and GR dominant (GR:MR ratio ~8:1). In 11β+ cells (~20%), GR was also dominant (GR:MR ratio ~7:1). DCT/CNT and CNT were mainly 11β- (~75 and ~60%, respectively), where MR and GR were similar. In 11β+ cells, MR and GR were similar in DCT/CNT but MR was greater in CNT (MR:GR ratio ~4:1). CNT/CCD contained a greater proportion of 11β+ (~65%) cells. MR and GR were similar in 11β- cells, but 11β+ cells were almost exclusively MR (MR:GR ratio ~12:1). In CCD, ~30% of cells were 11β-, GR were greater (GR:MR ratio ~4:1), and ~70% cells were 11β+, these were predominantly MR (MR:GR ratio ~15:1).

This methodology has enabled an unbiased assessment of the molecular machinery underpinning corticosteroid-regulated Na^+ transport in the distal nephron. Our data suggest that the DCT is a glucocorticoid-responsive segment, with 11β+ cells becoming progressively more dominant from CNT to CCD. The appearance of ENaC in the late CNT and particularly CCD, alongside 11β and MR, suggest these segments reflect the mineralocorticoid-responsive, and thus aldosterone-sensitive distal nephron.

[1] Nesterov, V et al. (2012). Amer J Physiol – Renal Physiol 303: F1289-F1299. [2] Nesterov, V et al. (2021). Amer J Physiol – Renal Physiol 321: F257-F268. [3] Maeoka, Y et al. (2022). Hypertension 79: 1423-1434.

C27

Identification and examination of Mitsugumin 23 within platelets

Jordan Marsh[1], Juan Varela[2], Samantha Pitt[1], Alan Stewart[1]

[1]School of Medicine, University of St Andrews, St Andrews, United Kingdom, [2]School of Physics and Astronomy, University of St Andrews, St Andrews, United Kingdom

Introduction: Intracellular zinc and calcium dynamics are important for both platelet activation and function. We have recently shown that the Ca^{2+} permeable cation channel mitsugumin 23 (MG23), found in the endoplasmic/sarcoplasmic reticulum of other cell types, is Zn^{2+}-sensitive and may facilitate crosstalk between the two metal ions [1]. The role of MG23 in platelet responses has never been explored but given its suggested role as a Ca2+ leak channel we suggest that MG23 may contribute to the elevation of intracellular Ca^{2+} resulting in hyperactive platelets.

Aim: The aim of this study was to confirm the presence the MG23 in platelets, identify its subcellular localization and evaluate the role of MG23 in platelet aggregation by comparing the aggregatory responses of platelets prepared from wild type and MG23-KO mice.

Methods: Expression of MG23 was assessed using RT-PCR and western blotting using mRNA and protein extracted from healthy donor platelets and megakaryocyte-like cells (MEG-01 cell line). Platelet aggregation assays were carried out on washed platelets from both WT and MG23-KO mice to evaluate the effect of MG23 knockout on platelet clotting. The institutional ethics committee at the University of St. Andrews approved the study. Work was carried out under project licence P82006EDF. Subcellular localization of MG23 within platelets was assessed by confocal microscopy using fixed MEG-01 cells.

Results: MG23 mRNA and protein were identified in both platelets and MEG-01 cells. The staining of platelets with antibodies directed against SERCA2 ATPase and MG23 yielded colocalized fluorescence, indicative of MG23 localization to the dense tubular system. Both WT and MG23-KO murine platelets aggregated in response to various platelet agonists.

Conclusion: MG23 expression was confirmed within platelets and is present in the dense tubular system. Though it has been proposed to serve as a Ca^{2+} leak channel in other cell types, its specific role in platelets is less clear.

Acknowledgements: We are grateful to the British Heart Foundation (grant no FS/19/69/34639) for funding this work.

References: [1] Reilly-O'Donnell, B., Robertson, G.B., Karumbi, A., McIntyre, C., Bal, W., Nishi, M., Takeshima, H., Stewart, A.J. and Pitt, S.J. (2017) Dysregulated Zn(2+) homeostasis impairs cardiac type-2 ryanodine receptor and mitsugumin 23 functions, leading to sarcoplasmic reticulum Ca^{2+} leakage. *J Biol Chem*, **292**, 13361-13373.

Ethical statement: The institutional ethics committee at the University of St Andrews approved the use of murine blood in this study (Ethics Approval Code: PS16369). The sacrifice and care of

animals met the guidelines from Directive 2010/63/EU of the European Parliament on the protection of animals used for scientific research purposes. Dr Samantha J. Pitt holds the project licence (Project Licence: P82006EDF) for the breeding and maintenance of MG23 KO mice.

[1] Reilly-O'Donnell, B., Robertson, G.B., Karumbi, A., McIntyre, C., Bal, W., Nishi, M., Takeshima, H., Stewart, A.J. and Pitt, S.J. (2017) Dysregulated Zn(2+) homeostasis impairs cardiac type-2 ryanodine receptor and mitsugumin 23 functions, leading to sarcoplasmic reticulum Ca2+ leakage. J Biol Chem, 292, 13361-13373.

C28

Identifying putative transporters of volume-regulating corticosteroids in the collecting duct of the kidney.

Morag Milne[1]

[1]*University of St Andrews, St Andrews, United Kingdom*

Corticosteroids are volume-regulating hormones which modulate Na^+ reabsorption *via* the epithelial sodium channel (ENaC) in principal cells (PCs) of the collecting duct (CD). Classically, these lipophilic hormones are thought to passively diffuse into target cells, however there is evidence that mediated transport can occur *via* transporters including the ABC and OCT/OAT superfamilies [1]. This has been shown in several tissues including adrenal glands, brain and adipose tissue [2,3] and may reflect a mechanism underpinning intracellular bioavailability. The role of mediated transport in the CD remains unclear. Recent transcriptomic analysis of corticosteroid-treated murine $mCCD_{cl1}$ collecting duct cells [4] identified several transporters with modulated expression including: *Abce1*, *Abcc1*, *Abca2*, *Slc22a5*. The aim of this study was to determine if corticosteroid hormones are actively transported in a cellular model of the CD and to determine localisation of putative transporters in mouse kidney.

$mCCD_{cl1}$ cells [5] were cultured on permeable supports for 9-11 days to form polarised, transporting monolayers. Steroid hormone concentration in media samples was measured following solid-liquid phase extraction and LC-MS/MS analysis, data are mean±SD. Immunofluorescence labelling of putative transporters was carried out on transverse sections of wild-type male and female mouse (C57BL/6) kidneys with antibodies against SLC22A5, ABCA2, ABCE1, ABCC1, as well as 11ßHSD2 as a marker of PCs of the CD. Sections were imaged using a Zeiss AxioScan slidescanner.

$mCCD_{cl1}$ cells were treated with corticosterone (CORT, 150nM, 3h, basolateral bath) following preincubation with carbenoxlone (10µM, 30min) to inhibit 11ßHSD2 activity. Previous work has shown that this treatment causes a robust stimulation of ENaC activity [4]. Media collected at time 0, revealed [CORT] was 144.7±9.9nM in the basolateral bath and below the limit of detection (BLD) in the apical bath. After 3h30, [CORT] was 100.0±3.5nM and 43.2±1.3nM in the basolateral and apical baths, respectively, and BLD in the cell lysate (n=8). Assessment of putative steroid transporters in murine kidney sections (n=3), revealed SLC22A5 and ABCA2 colocalised with 11bHSD2. SLC22A5 localised to the apical membrane of tubular cells, whereas ABCA2 showed nuclear expression. ABCE1 was localised to tubules expressing 11ßHSD2 cells, but in adjacent 11bHSD2 negative cells - likely intercalated cells of the CD. Finally, ABCC1 did not co-localise to tubules expressing 11bHSD2 in either male or female wild-type kidney sections. Further co-labelling studies were carried out and revealed ABCC1 partially co-localised with NaPi-2a, a marker of the proximal tubule.

Together these data provide evidence that mediated transport of a physiological concentration of CORT occurs across the apical membrane of polarised CD epithelia. The lack of detectable CORT in cell lysates suggests this likely occurs across the basolateral membrane as well, though further experiments are required. Of the identified putative transporters, only SLC22A5 and ABCA2

localised to PCs of the CD in mouse kidney, the apical localisation of SLC22A5 suggests this transporter may play a role in steroid transport. Further work aims to assess the localisation of these transporters following manoeuvres to alter plasma concentrations of corticosteroids, as well as assessing the potential for transport of physiological concentrations of aldosterone.

[1] Ueda K et al. (1992). J Biol Chem 267, 24248-24252. [2] Nixon M et al. (2016). Sci Trans Med 8, 352ra109-352ra109. [3] Meijer OC et al. (1998). Endocrinology 139, 1789-1793. [4] Loughlin S et al. (2023). Kidney360 4, 226-240. [5] Gaeggeler HP et al. (2005). J Am Soc Nephrol 16, 878-891.

C29

Back to the future – mathematical models to capture ion channel kinetics using short high-information voltage clamp protocols

Gary Mirams[1]

[1]*University of Nottingham, Nottingham, United Kingdom*

Introduction: since the work of Hodgkin & Huxley, mathematical models of ion channel gating have been used to understand and predict the effects of ion currents in action potential formation. Today we still tend to use the same approach to voltage-clamp protocol design that Hodgkin & Huxley used: designs based on simple square waves, with large gaps to return to steady states, that enable model parameter values to be estimated manually from graph paper.

Aims/Objectives: to use short high-information voltage clamp protocols in partnership with computational modelling to characterise ion currents. To allow a model (Figure 1A) to be fitted, and tested as well as multiple experimental interventions in the same cell. Here we show results of using short protocols to capture the kinetics of I_{Kr} / K_V11.1 / hERG currents in a range of settings.

Method: we apply either a short sinusoidal voltage clamp protocol (Figure 1B, [1]) or a square wave 'staircase' version [2] to CHO cells stably expressing hERG1a at room temperature or physiological temperature in manual and automated patch settings. We then use computational optimisation to fit a simple mathematical model for hERG to the resulting currents, and use it to predict the results of conventional voltage clamp protocols and physiological action potentials.

Results: the short protocols result in highly predictive mathematical models: Figure 1C shows a prediction from a model fitted to the sinusoidal protocol shown in Figure 1B against experimental data. The parameter values within these models then capture our knowledge of channel gating more accurately than a series of Current-Voltage or Time Constant-voltage curves, with the benefit they can be re-used to predict currents in new situations/voltage-clamp protocols that were not examined in the original experiment. There are also opportunities to use mathematical models to account for patch clamp artefacts [3] to consolidate information from different patch clamp recordings more reliably.

Conclusions: this approach offers the opportunity to intervene and reassess currents multiple times in one experiment, and to generate a mathematical model that quantitatively captures our understanding about channel gating. For instance, we can alter temperature to examine the temperature dependence at the level of individual rate and voltage-dependence parameters within a model, rather than at the level of processes such as 'activation' or 'recovery from inactivation' [4]. We can also build models of mutant channels, and/or characterise changes in currents in the presence of drug compounds that alter channel gating [5].

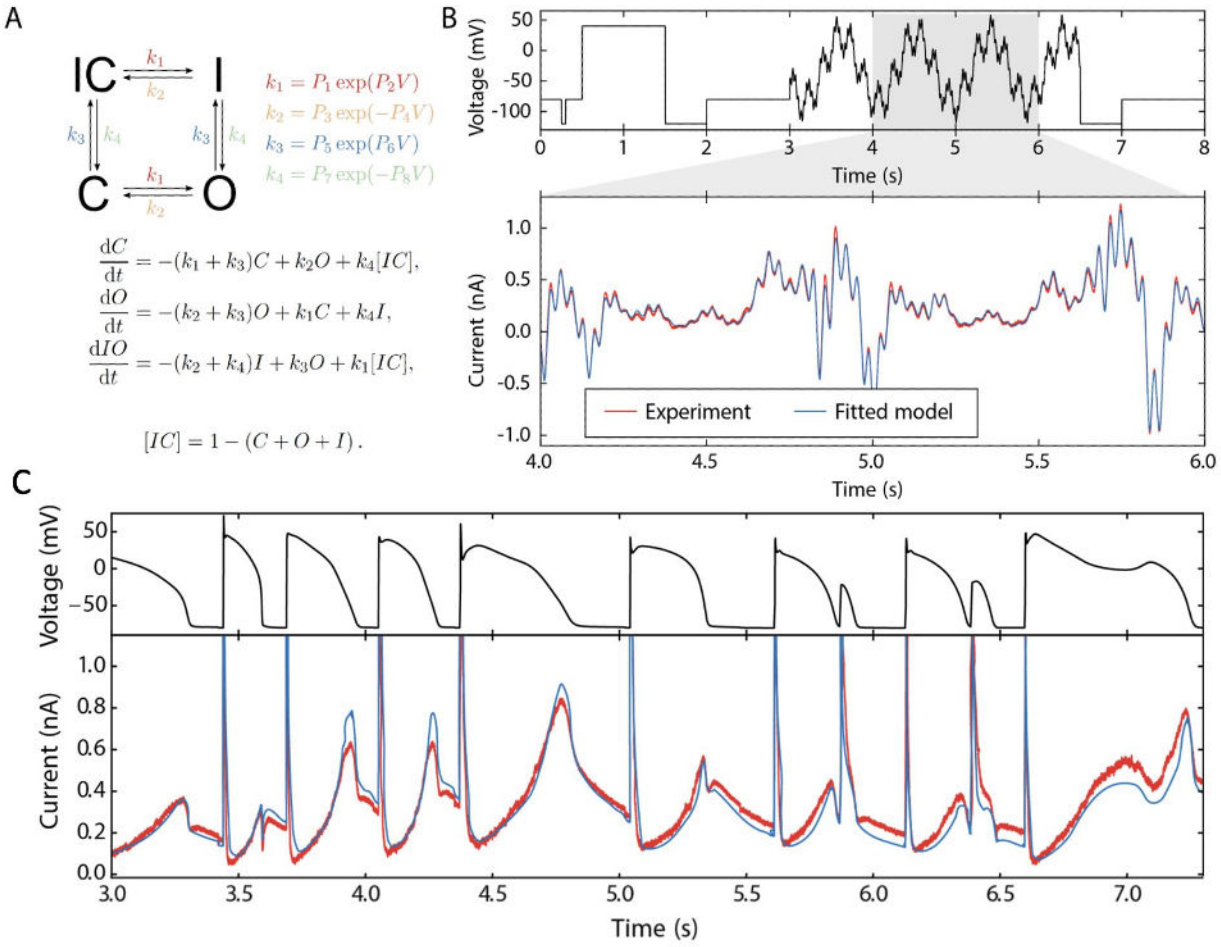

[1] K. A. Beattie et al., “Sinusoidal voltage protocols for rapid characterisation of ion channel kinetics,” J Physiol, vol. 596, no. 10, pp. 1813–1828, May 2018, doi: 10.1113/JP275733. [2] C. L. Lei, M. Clerx, D. J. Gavaghan, L. Polonchuk, G. R. Mirams, and K. Wang, “Rapid Characterization of hERG Channel Kinetics I: Using an Automated High-Throughput System,” Biophys J, vol. 117, no. 12, pp. 2438–2454, Dec. 2019, doi: 10.1016/j.bpj.2019.07.029. [3] C. L. Lei, M. Clerx, D. G. Whittaker, D. J. Gavaghan, T. P. de Boer, and G. R. Mirams, “Accounting for variability in ion current recordings using a mathematical model of artefacts in voltage-clamp experiments,” Philosophical Transactions of the Royal Society A: Mathematical, Physical and Engineering Sciences, vol. 378, no. 2173, p. 20190348, Jun. 2020, doi: 10.1098/rsta.2019.0348. [4] C. L. Lei et al., “Rapid Characterization of hERG Channel Kinetics II: Temperature Dependence,” Biophys J, vol. 117, no. 12, pp. 2455–2470, Dec. 2019, doi: 10.1016/j.bpj.2019.07.030. [5] J. M. Kemp et al., “Electrophysiological characterization of the hERG R56Q LQTS variant and targeted rescue by the activator RPR260243,” Journal of General Physiology, vol. 153, no. 10, Oct. 2021, doi: 10.1085/jgp.202112923.

C30

P2X7 receptor knockout does not alter physiological tubular sodium reabsorption or renal haemodynamics and fails to prevent angiotensin II-induced kidney injury in F344 rats

Josselin Nespoux[1], Marie-Louise Monaghan[1], Natalie Jones[1], Kevin Stewart[1], Laura Denby[1], Alicja Czopek[1], John Mullins[2], Robert Menzies[2], Andrew Baker[2], Matthew Bailey[1]

[1]Edinburgh Kidney Research Group; British Heart Foundation Center for Cardiovascular Science, The University of Edinburgh, Edinburgh, United Kingdom, [2]British Heart Foundation Center for Cardiovascular Science, The University of Edinburgh, Edinburgh, United Kingdom

Purinergic signalling regulates renal vascular and tubular functions. P2X7 receptor (P2X7) is a non-selective cation channel activated by extra-cellular ATP which plays an important role in immune cell response and inflammation. Endothelial cells also express P2X7, including in the kidney. Studies also detected P2X7 expression in the renal tubular epithelium, notably in disease. Acute pharmacological blockade increases renal blood flow (RBF) and glomerular filtration rate (GFR), suggesting that P2X7 receptor activation promotes tonic vasoconstriction. Here, we generated a novel P2X7 global knockout (KO) rat on the F344 background, hypothesising that these rats would have enhanced RBF and would be protected from the injury caused by chronic angiotensin II (ANG II) infusion.

CRISPR/Cas9 technology introduced an early stop codon into exon 2 of *P2rx7*. In male and female KO and WT rats, renal P2X7 expression was measured by RTqPCR (n=4-5/group) and western blotting (n=3/group). Bone marrow-derived macrophages (BMDM) were used to assess P2X7 function by measuring interleukin (IL)-1β release (ELISA) after stimulation with lipopolysaccharide (LPS) (1µg/mL, 4h) and ATP (3mM, 1h) (n=5-6/group). In vivo kidney function was assessed in anesthetized rats (thiopental, 50mg/kg, i.p.) at baseline and following serial arterial ligation to induce acute pressure natriuresis (n=9-10/group). Arterial blood pressure (BP) was measured directly, and urine was collected via tube cystotomy. RBF was measured using a Transonic Doppler flow probe placed around the main renal artery, and cortical and medullary flux by laser Doppler needle probes. GFR was determined by FITC-inulin clearance. Urinary sodium was measured by sodium-selective electrode analysis. Finally, male KO and WT rats (n=9-10/group) were infused with ANG II (250ng/kg/min, s.c.) for ~6 weeks. At end, one renal artery was isolated and vascular reactivity to phenylephrine (PE), acetylcholine (ACh) and sodium nitroprusside (SNP) determined by wire myography. Bladder urine was collected to measure albumin/creatinine ratio (n=4-7/group)., and kidneys were harvested for histological analyses (n=6/group). Data were analysed with unpaired t-test (two groups compared) or two-way ANOVA (two variables), with $P<0.05$ statistically significant.

P2rx7 mutation was confirmed by genome sequencing (Sanger). *P2rx7* mRNA abundance was partially decreased in kidney from male (-54%) and female (-25%) KO vs WT. P2X7 protein was detected in kidneys from WT but not from KO rats. In BMDM from WT rats, LPS+ATP stimulation induced IL-1β release; this response was markedly suppressed in KO BMDM (males: 2577±140 vs 413±175pg/mL, $P<0.0001$; females: 1889±394 vs 265±121pg/mL, $P<0.0001$). In vivo BP, renal haemodynamics and tubular sodium handling were not different between genotypes for either sex ($P>0.05$). Following chronic ANG II infusion, KO and WT rats had no renal artery dysfunction but

showed similar increases in albuminuria (P=0.3587), renal perivascular fibrosis (Picrosirius Red, P=0.5393), cortical interstitium CD68-positive area (p=0.6546) and tubular casts (Periodic acid-Schiff, P=0.8803), compared with naïve controls.

Contrary to our hypothesis, global genetic deletion of P2X7 did not affect renal hemodynamics and we found no significant role for P2X7 in the modulation of tubular sodium reabsorption in health. Our data do not support a major role of P2X7 in causing renal vascular and tubular injury.

C31

Thrombin-activated calcium oscillations in renal mesangial cells

Mykhailo Fedoriuk[1], Mariia Stefanenko[1], Marharyta Semenikhina[1], Mykola Mamenko[2], Tamara Nowling[1], Joshua Lipschutz[1], Alexander Staruschenko[3], Oleg Palygin[1]

[1]Medical University of South Carolina, Charleston, United States, [2]Medical College of Georgia, Augusta, United States, [3]University of South Florida, Tampa, United States

Mesangial cells provide structural support to the glomerular tuft and modulate the glomerular capillary flow via their contractile properties. The mesangial cells' phenotypic changes to myofibroblast-like cells, such as proliferation, mesangial expansion, abnormal glomerular tuft formation, and reduced numbers of capillary loops, are present in several glomerular diseases, including diabetic nephropathy and glomerulonephritis. In addition, thrombin-induced mesangial remodeling was found in diabetic patients, and expression of the corresponding protease-activated receptors (PARs) in the renal mesangium was reported. However, the functional PAR-mediated signaling and mechanisms in mesangial cells were not studied. This study aims to investigate protease-activated mechanisms regulating mesangial cell contraction and glomerular capillary flow.

We used the human renal mesangial cell (HRMC) line to determine the signaling mechanisms mediated by PAR1 thrombin-activated receptors. Confocal fluorescent microscopy was utilized to detect changes in intracellular Ca^{2+} response to specific PAR1 modulators. Pharmacology and patch clamp electrophysiology was further applied to reveal downstream signaling mechanisms responsible for intracellular Ca^{2+} oscillations. PAR1-mediated Ca^{2+} response display high sensitivity to specific agonist (TFLLR-NH_2) with EC_{50} values of 3 and 6.3 nM for male and female cultured cells, respectively (the competition of a ligand for receptor binding fit converged; adj. R^2=0.98). The response to PAR1 activation promotes initial cytosolic Ca^{2+} increase followed by synchronized, damped Ca^{2+} oscillations with a lag of 6.74±0.84 min between peaks. The pre-application of a specific inhibitor (RWJ56110) eliminated PAR1-mediated response, and oscillations were blocked by the changes of an extracellular solution to zero Ca^{2+}. The specific inhibitors for store-operated calcium (SOCs) (Pyr6) and TRPC3 (GSK 2833503A) channels strongly attenuated oscillation behavior (up to 40% when added separately and up to 65% when applied both; two-way ANOVA, * $p<0.0001$). In addition, the effect of a specific inhibitor of TRPC6 channels (BI-749327) on Ca^{2+} flux was minimal. Further single-channel electrophysiology experiments in HRMC cells confirmed the involvement of SOC and TRPC3 channels in PAR1-mediated GPCR activation.

Our results indicate that coagulation proteases like thrombin may strongly regulate mesangial cell contraction and corresponding glomerular capillary flow by PAR1 GPCRs-related activation. The contraction mechanism is mediated presumably through SOCs entry and TRPC3 channels. Since high thrombin levels are linked to poor diabetic control, the described signaling may play a crucial role in the development of diabetic glomerular disease.

C32

Two rare variants that affect the same amino acid in CFTR have distinct response to ivacaftor

Mayuree Rodrat[1,2], Hongyu Li[1], Sangwoo T. Han[3], Garry R Cutting[3], David N. Sheppard[1]

[1]School of Physiology, Pharmacology and Neuroscience, University of Bristol, Bristol, UK, Bristol, United Kingdom, [2]Center of Research and Development for Biomedical Instrumentation, Institute of Molecular Biosciences, Mahidol University, Nakhon Pathom, Thailand, Nakhon Pathom, Thailand, [3]McKusick-Nathans Department of Genetic Medicine, Johns Hopkins University School of Medicine, Baltimore, Maryland, USA, Maryland, United States

Some amino acids in the epithelial anion channel cystic fibrosis transmembrane conductance regulator (CFTR) are the site of more than one CFTR variant that cause the genetic disease cystic fibrosis. Here, we investigate the function of two rare missense substitutions of the serine residue at codon 1159 in the pore-lining twelfth transmembrane segment, S1159F and S1159P and their response to the clinically-approved CFTR potentiator ivacaftor. To study the single-channel behaviour of CFTR, we used excised inside-out membrane patches from CHO cells transiently expressing the CFTR variants that were incubated at 27 °C for 7-12 days to enhance channel trafficking to the plasma membrane. S1159F- and S1159P-CFTR formed Cl^- channels activated by cAMP-dependent phosphorylation and gated by ATP that exhibited thermostability at 37 °C. At –50 mV in the presence of a large Cl^- concentration gradient ($[Cl^-]_{int}$, 147 mM; $[Cl^-]_{ext}$, 10 mM), ATP (1 mM) and protein kinase A (75 nM), both variants modestly reduced single-channel current amplitude (i), but severely decreased open probability (P_o) (S1159F, n = 21; S1159P, n = 25). Ivacaftor (10 – 100 nM) doubled the P_o of both CFTR variants, but did not restore P_o values to wild-type levels (S1159F, n = 3–5; S1159P, n = 8–9). Interestingly, higher concentrations of ivacaftor (0.5 – 1 μM) had little effect on S1159P-CFTR, but reduced the i of S1159F-CFTR (S1159F, n = 3; S1159P, n = 8). To investigate further the action of ivacaftor on S1159F-CFTR, we used excised membrane patches bathed in symmetrical 147 mM Cl^--rich solutions. For wild-type CFTR, ivacaftor potentiation of P_o was concentration-dependent, but voltage-independent, while its current-voltage (i-V) relationship was linear and unaffected by increasing concentrations of the drug (n = 5). Although ivacaftor potentiation of the P_o of S1159F-CFTR was voltage-independent, P_o values were maximal at ivacaftor (100 nM) and not further increased at ivacaftor (1 μM) (n = 3–6). However, ivacaftor (1 μM) caused voltage-independent inhibition of the i-V relationship of S1159F-CFTR (control, $\gamma = 9.63 \pm 0.49$ pS; ivacaftor, $\gamma = 5.55 \pm 0.97$ pS (n = 4); $P < 0.001$; means ± SD, Student's paired t-test), revealing that the drug's action on this CFTR variant is reduced by allosteric channel inhibition. In conclusion, the molecular basis of CFTR dysfunction caused by the S1159F and S1159P variants is class II (defective processing), III (defective regulation) and IV (defective conduction), necessitating the use of combinations of CFTR modulators to optimal restore their channel activity. Supported by the NIH, CF Foundation Therapeutics and CF Trust.

C34

Investigating the effect of HIF-1α on voltage-gated Na+ channel activity in triple-negative breast cancer cells

Nattanan Sajjaboontawee[1], Katherine Bridge[1], William Brackenbury[1]

[1]*University of York, York, United Kingdom*

Triple-negative breast cancer (TNBC) does not express hormone receptors, making it more aggressive and challenging to treat compared to estrogen receptor-positive breast cancer **(Hartkopf et al., 2020)**. In TNBC, the $Na_v1.5$ isoform of voltage-gated sodium channels (VGSCs), encoded by ***SCN5A***, is up-regulated and promotes invasion and metastasis **(Nelson et al., 2015)**. TNBCs often develop intratumoral hypoxic microenvironments. The hypoxic response is regulated transcriptionally by hypoxia-inducible factors (HIFs), most critically the HIF-1α subunit. HIFs bind to hypoxia-response elements (HREs) and activate target genes that are critical for tumour progression **(Semenza, 2016)**. Given that hypoxia plays a key role in up-regulating $Na_v1.5$ activity in the ischaemic heart **(Plant et al., 2020)** and HIF-1α significantly enhances breast cancer metastasis **(Liao et al., 2007)**, we sought to investigate whether HIF-1 might regulate $Na_v1.5$ in TNBC.

To identify whether hypoxia/HIF-1 regulates VGSC expression in TNBC, an in silico analysis was performed to identify HRE consensus motifs (ACGTG) in key VGSC genes expressed in breast cancer. The mRNA expression levels of ***SCN5A*** and ***SCN1B*** (encoding the VGSC β1 subunit also expressed in TNBC) were quantified using rt-qPCR in MDA-MB-231 cells treated with dimethyloxalylglycine (DMOG; 1 mM), a chemical stabiliser of HIF-1α, for 0, 24, 48, and 72 hours. $Na_v1.5$ channel activity was studied using the whole-cell patch clamp technique. Cell proliferation and viability were measured using the RealTime-Glo™ MT cell viability assay and trypan blue exclusion assay, respectively.

In silico HIF binding site prediction showed 4 putative HREs in the ***SCN5A*** promoter and 4 HREs in the 5 kb upstream of its transcription start site (TSS). 1 HRE was found in the 5 kb upstream of the ***SCN1B*** TSS. ***SCN1B*** was upregulated in DMOG-treated cells in a time-dependent manner (2.54±0.46 fold at 72 hours; $p<0.001$) while ***SCN5A*** expression was not affected by DMOG (1.08 ± 0.26 fold at 72 hours; $p>0.05$, one-way ANOVA, n=4, mean±S.D.). Transient and persistent Na^+ currents were not significantly different between control and DMOG-treated cells after 24 or 48 hours of treatment ($p>0.05$, t-test, n=4-11). The RealTime-Glo™ results showed significant decreases in cell proliferation in DMOG-treated cells at all time points (24, 48, and 72 hours); this reduction is likely unrelated to VGSC signalling since the combination of DMOG (1 mM) and tetrodotoxin (TTX; 30 μM), a VGSC blocker, did not alter cell proliferation when compared to cells treated with DMOG alone. The trypan blue exclusion assay confirmed that the decrease in cell proliferation after 72 hours of DMOG treatment was not due to cell death. Cell viability was not statistically different between control (99.12±0.74%) and DMOG-treated cells (98.23±1.78%) ($p>0.05$, t-test, n=3). Overall, this study suggests that HIF stabilisation using DMOG in MDA-MB-231 cells increases ***SCN1B*** expression but does not alter ***SCN5A*** expression or $Na_v1.5$ activity. Further work is required to establish whether hypoxia may affect $Na_v1.5$ activity independent of HIF-1 stabilisation in TNBC.

Hartkopf AD, Grischke E-M, Brucker SY (2020) Endocrine-Resistant Breast Cancer: Mechanisms and Treatment. Breast Care 15:347–354. Liao D, Corle C, Seagroves TN, Johnson RS (2007) Hypoxia-inducible factor-1alpha is a key regulator of metastasis in a transgenic model of cancer initiation and progression. Cancer Res 67:563–572. Nelson M, Yang M, Millican-Slater R, Brackenbury WJ (2015) Nav1.5 regulates breast tumor growth and metastatic dissemination in vivo. Oncotarget 6:32914–32929. Plant LD, Xiong D, Romero J, Dai H, Goldstein SAN (2020) Hypoxia Produces Pro-arrhythmic Late Sodium Current in Cardiac Myocytes by SUMOylation of NaV1.5 Channels. Cell Rep 30:2225–2236.e4. Semenza GL (2016) The hypoxic tumor microenvironment: A driving force for breast cancer progression. Biochim Biophys Acta 1863:382–391.

C35

The pore loop residue R518 is critical for calcium permeability of the polycystin-2L1 channel (PKD2L1)

Tobias Staudner[1], Juthamas Khamseekaew[1], Christoph Korbmacher[1], Alexandr Ilyaskin[1]

[1]*Institute of Cellular and Molecular Physiology, Friedrich-Alexander-Universität Erlangen-Nürnberg, Erlangen, Germany*

Polycystin-2L1 (PKD2L1) belongs to the family of transient receptor potential (TRP) ion channels and bears 76% protein sequence similarity to polycystin-2 (PKD2) [1]. Mutations of the latter cause autosomal dominant polycystic kidney disease (ADPKD). PKD2L1 is characterized by a large permeability for Ca^{2+} [2], which has been attributed to the structure of its selectivity filter [3]. Interestingly, structural information of PKD2L1 suggests that a selectivity filter residue D523 forms a salt bridge interaction with a pore loop residue R518 [4]. Thus, R518 might stabilize the selectivity filter thereby affecting PKD2L1 ion channel properties. Here we investigate the relevance of R518 for the ion channel function of PKD2L1.

To eliminate its potential salt bridge interaction with D523, R518 was substituted with a cysteine residue using site-directed mutagenesis. Mutant $PKD2L1_{R518C}$ and wildtype PKD2L1 constructs were heterologously expressed in *Xenopus laevis* oocytes for functional analysis using the two-electrode voltage clamp (TEVC) technique. To assess calcium entry into oocytes in a qualitative manner, a fluorescent assay was established using the calcium-sensitive dye Fluo-4 and 50mM $CaCl_2$ bath solution. Values are presented as mean +/- SEM and ANOVA with Bonferroni post-hoc-test was used for statistical analysis.

In control experiments, application of calcium ionophore ionomycin in 50 mM $CaCl_2$ bath solution resulted in a ~4-fold increase of fluorescence intensity in Fluo-4-injected oocytes [n=47]. Injecting the Ca^{2+} chelator EGTA into oocytes prevented the ionomycin-induced fluorescence increase, confirming that this was due to Ca^{2+} influx [n=48]. Importantly, PKD2L1 expressing oocytes placed in 50 mM $CaCl_2$ bath solution [n=42] demonstrated a similar increase of fluorescence as ionomycin-treated oocytes [n=40]. In contrast, the $PKD2L1_{R518C}$ failed to produce an increase in fluorescence, indicating reduced Ca^{2+} permeability of the mutant channel [n=29]. In parallel TEVC experiments, application of 50 mM $CaCl_2$ resulted in large inward currents due to activation of calcium-activated chloride channels (CaCC) in PKD2L1 expressing oocytes [n=32, -2.49 µA +/- 0.18 µA]. This was not observed in oocytes pre-injected with EGTA [n=31, -0.33 µA +/- 0,02 µA] or when 50 mM $MgCl_2$ was applied instead of $CaCl_2$ [n=25, -0.22 µA +/- 0.03 µA]. Similarly, oocytes expressing $PKD2L1_{R518C}$ did not reveal a measurable activation of CaCC currents in 50 mM $CaCl_2$ [n=38, - 0.23 µA +/- 0.01 µA, n.s.], further supporting reduced calcium permeability of the mutant channel. Interestingly, in a solution containing 96 mM Na^+ $PKD2L1_{R518C}$ exhibited significantly larger Na^+-inward currents than wildtype PKD2L1 [-1.00 µA +/- 0.08 µA, n=22 *versus* -0.53 µA +/- 0.05 µA, n=23; $p<0.001$]. This suggests that R518C selectively reduces PKD2L1 permeability for divalent but not for monovalent cations.

Taken together, our data indicate that the pore loop residue R518 is essential for Ca^{2+} permeability of PKD2L1, probably due to its role in stabilizing the selectivity filter. Interestingly, this arginine

residue is conserved in PKD2 (R638) and the corresponding mutation R638C has been reported to be associated with the ADPKD [5]. Therefore, our findings regarding PKD2L1 may help to understand functional consequences of disease causing PKD2 mutations which remain to be explored in future studies.

1. Wu, G., et al., Identification of PKD2L, a human PKD2-related gene: tissue-specific expression and mapping to chromosome 10q25. Genomics, 1998. 54(3): p. 564-8. 2. Shen, P.S., et al., The Structure of the Polycystic Kidney Disease Channel PKD2 in Lipid Nanodiscs. Cell, 2016. 167(3): p. 763-773.e11. 3. DeCaen, P.G., et al., Atypical calcium regulation of the PKD2-L1 polycystin ion channel. Elife, 2016. 5. 4. Hulse, R.E., et al., Cryo-EM structure of the polycystin 2-l1 ion channel. Elife, 2018. 7. 5. Grieben, M., et al., Structure of the polycystic kidney disease TRP channel Polycystin-2 (PC2). Nat Struct Mol Biol, 2017. 24(2): p. 114-122.

C36

Piezo1 as a force-through-membrane sensor in red blood cells

George Vaisey[1], Priyam Banerjee[2], Alison North[2], Christoph A Haselwandter[3], Roderick MacKinnon[1]

[1]Laboratory of Molecular Neurobiology and Biophysics, Howard Hughes Medical Institute, The Rockefeller University, New York, United States, [2]Bio-Imaging Resource Center, The Rockefeller University, New York, United States, [3]Department of Physics and Astronomy and Department of Quantitative and Computational Biology, University of Southern California, Los Angeles, United States

Abstract

Piezo1 is the stretch activated Ca^{2+} channel in red blood cells that mediates homeostatic volume control. Here, we study the organization of Piezo1 in red blood cells using a combination of super-resolution microscopy techniques and electron microscopy. Piezo1 adopts a non-uniform distribution on the red blood cell surface, with a bias toward the biconcave 'dimple'. Trajectories of diffusing Piezo1 molecules, which exhibit confined Brownian diffusion on short timescales and hopping on long timescales, also reflect a bias toward the dimple. This bias can be explained by 'curvature coupling' between the intrinsic curvature of the Piezo dome and the curvature of the red blood cell membrane. Piezo1 does not form clusters with itself, nor does it colocalize with F-actin, Spectrin, or the Gardos channel. Thus, Piezo1 exhibits the properties of a force-through-membrane sensor of curvature and lateral tension in the red blood cell.

Statistical Analyses

For all comparative analyses n > 10 and the mean and standard deviation is given.

The one-way analysis of variance (ANOVA) with Tukeys post hoc analysis is used to test statistical significance.

Ethics

All animal procedures were reviewed and approved by the Institutional Animal Care and Use Committee at The Rockefeller University, protocol # 22056.

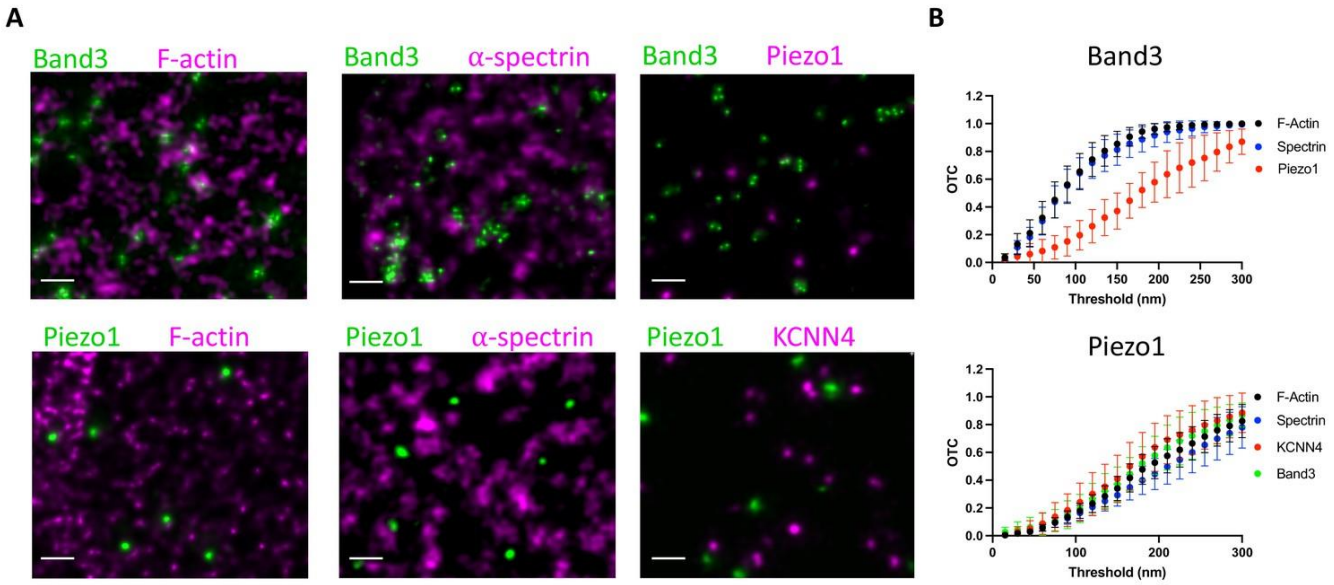
A
Band3 F-actin
Band3 α-spectrin
Band3 Piezo1
Piezo1 F-actin
Piezo1 α-spectrin
Piezo1 KCNN4
B
Band3
OTC
Threshold (nm)
F-Actin
Spectrin
Piezo1
Piezo1
KCNN4
Band3

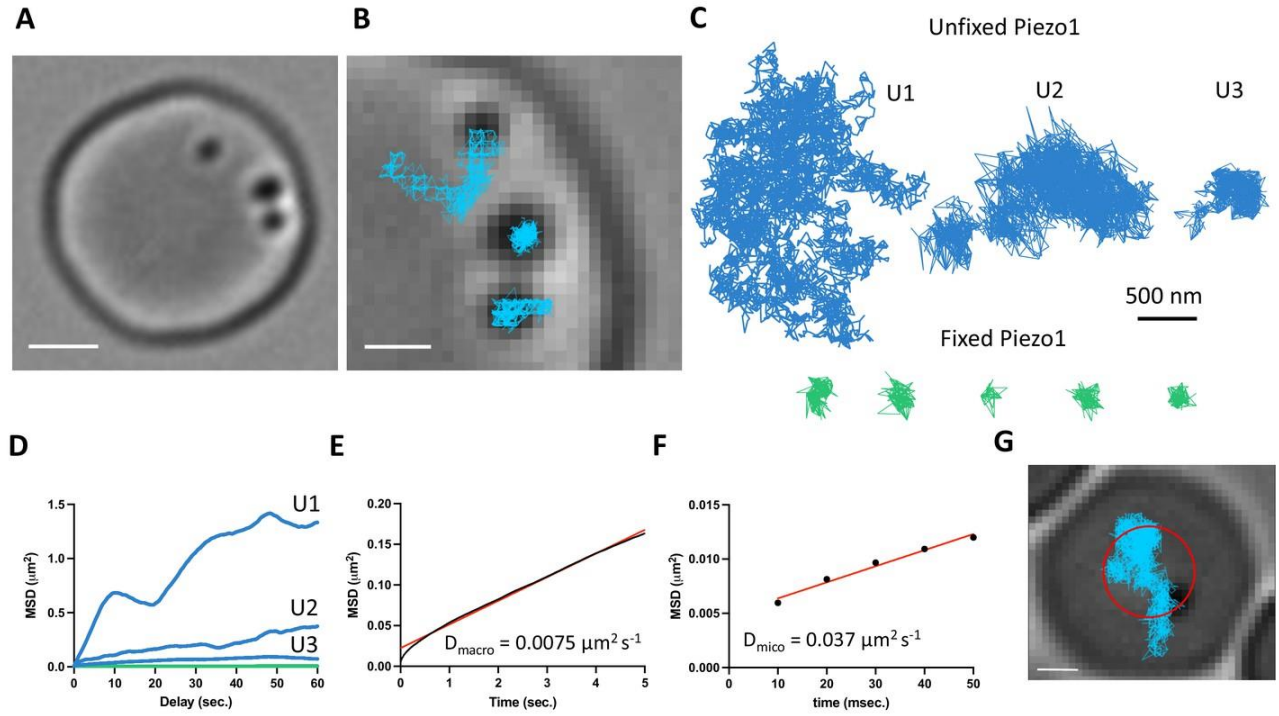
A
B
C
Unfixed Piezo1
U1
U2
U3
500 nm
Fixed Piezo1
D
MSD (μm²)
Delay (sec.)
E
Time (sec.)
D_macro = 0.0075 μm² s⁻¹
F
time (msec.)
D_mico = 0.037 μm² s⁻¹
G

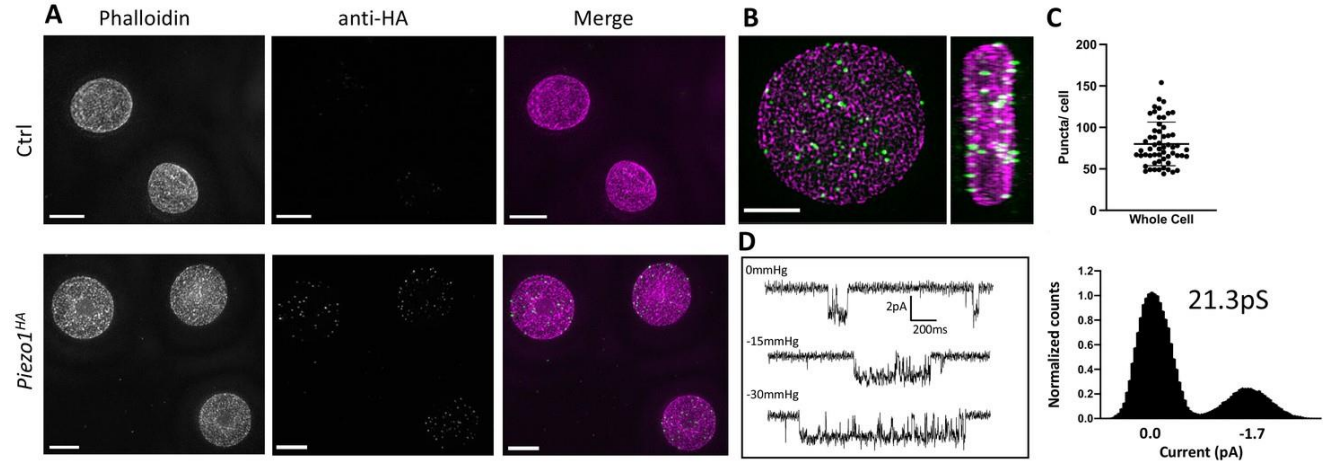
A
Phalloidin
anti-HA
Merge
Ctrl
Piezo1HA
B
C
Punctal/ cell
Whole Cell
D
0mmHg
2pA
200ms
-15mmHg
-30mmHg
Normalized counts
21.3pS
0.0
-1.7
Current (pA)

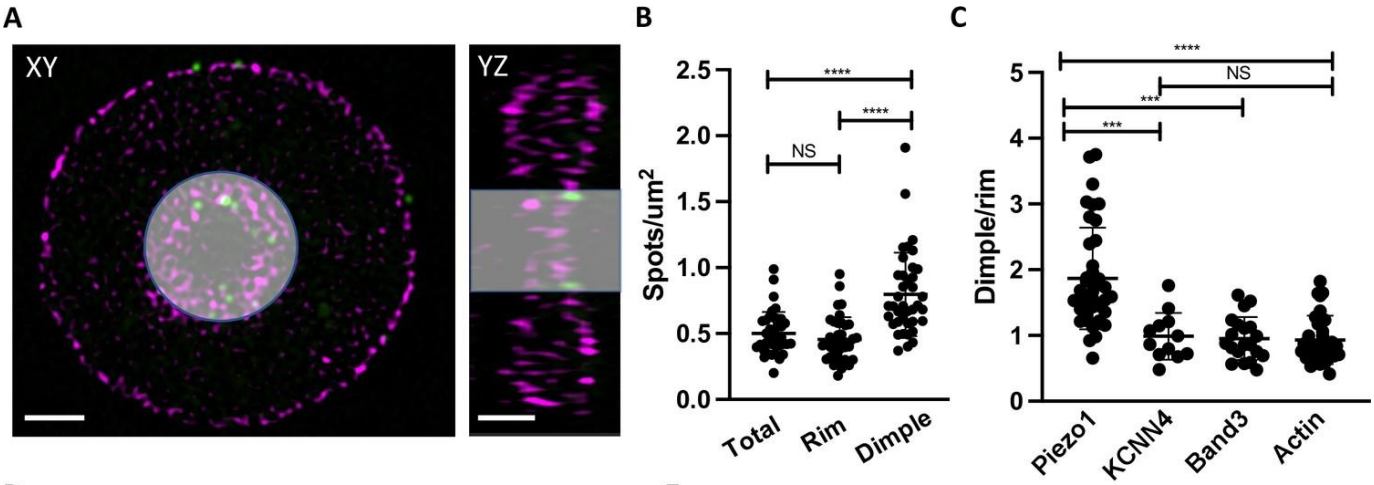
A
XY
YZ
B
Spots/um2
NS
Total
Rim
Dimple
C
Dimple/rim
Piezo1
KCNN4
Band3
Actin

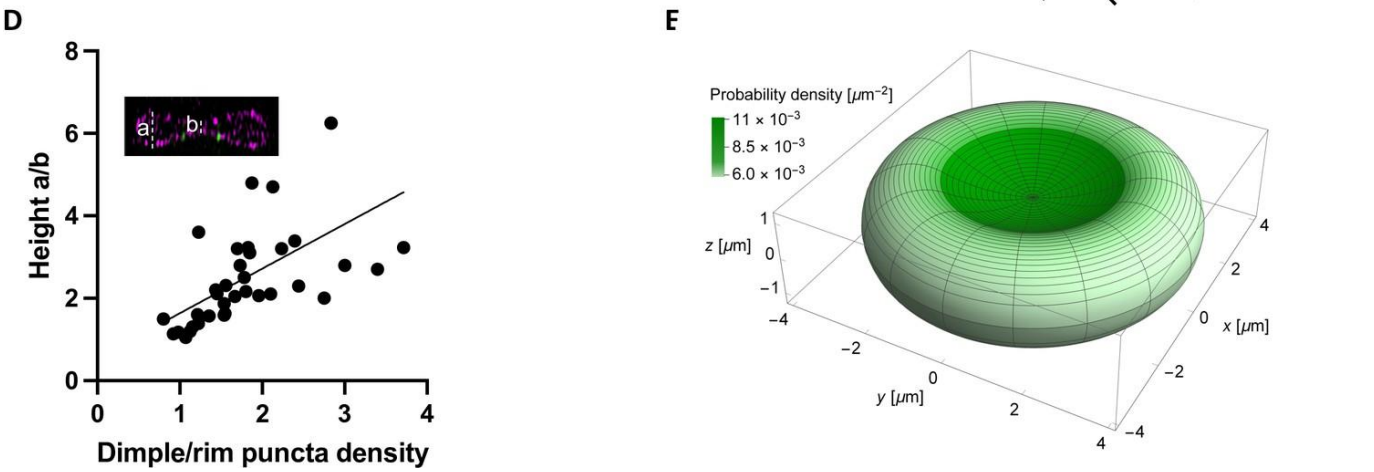
D
Height a/b
Dimple/rim puncta density
E
Probability density [μm−2]
11 × 10−3
8.5 × 10−3
6.0 × 10−3
z [μm]
y [μm]
x [μm]

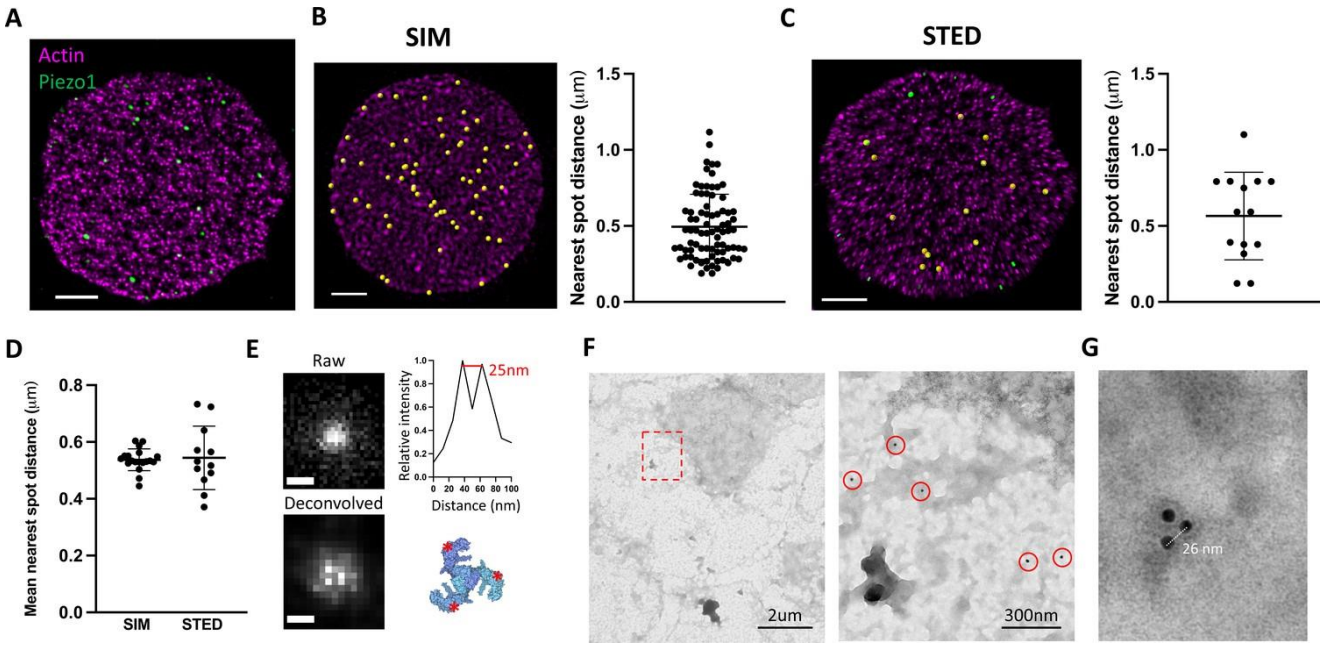
A
Actin
Piezo1
B
SIM
Nearest spot distance (μm)
1.5
1.0
0.5
0.0
C
STED
Nearest spot distance (μm)
1.5
1.0
0.5
0.0
D
Mean nearest spot distance (μm)
0.8
0.6
0.4
0.2
0.0
SIM
STED
E
Raw
Deconvolved
Relative intensity
1.0
0.8
0.6
0.4
0.2
0.0
0 20 40 60 80 100
Distance (nm)
25nm
F
2um
300nm
G
26 nm

C37

Why do some ABC transporter inhibitors activate CFTR?

Maria-Cristina Ardelean[1], Hannah J. Eldred[1], Paola Vergani[1]

[1]*Neuroscience, Physiology and Pharmacology, UCL, London, United Kingdom*

Introduction

CFTR is an anion-selective channel which plays important roles, regulating fluidity and pH of luminal secretions. New modulator drugs targeting CFTR have highlighted previously unexpected involvement of CFTR in physiological and pathological processes [1-4]. CFTR-targeting drugs also have the potential to help improve our mechanistic understanding of CFTR gating function and biogenesis, especially when structural details of binding are known [5, 6].

To improve our molecular understanding of CFTR function and pharmacology we tested compounds known to inhibit MsbA and P-glycoprotein, both Type IV ABC transporters [7], like CFTR. Quinoline inhibitors bind on MsbA at positions homologous to CFTR's portals. In the open channel conformation CFTR's portals are thought to be part of the permeation pathway connecting the inner pore vestibule to the cytosol. Inhibitors Elacridar and Zosuquidar occupy the substrate-binding cavity in P-glycoprotein, structurally homologous to CFTR's inner vestibule.

Methods

We tested the ABC transporter inhibitors on CFTR using a high-content fluorescence assay [8]. YFP-CFTR, an N-terminal fusion of an iodide-sensitive YFP [9] to CFTR, was coexpressed in HEK293 cells with a cytosolic mCherry. Exploiting a microscopic image-acquisition system and watershed image-segmentation algorithms (relying on mCherry fluorescence), we monitored the time course of YFP quenching in individual cells, following extracellular iodide addition. The amount of iodide entering each cell was estimated from the integral of the relative YFP fluorescence decrease following iodide addition (area above the curve over 39 s, AAC_{39}), providing a robust readout of CFTR activity.

Results

Upon activation of CFTR by addition of forskolin (at EC_{50}, 0.3 μM), frequency distributions of the AAC_{39} metric shift towards higher values (figure 1A), reflecting increased PKA-dependent CFTR phosphorylation. In the presence of 0.5 μM forskolin, 10 μM BPO-27 or 3 μM VX-770, CFTR-specific inhibitor and potentiator, respectively, shifted AAC_{39} distributions to lower and higher values, as expected (figure 1B). Activation of CFTR in the presence of inhibitors of MsbA (10 μM G592 (*S*)-enantiomer [10], figure 1A) or P-glycoprotein (10 μM Elacridar, figure 1C, or 10 μM Zosuquidar, figure 1D) resulted in more cells populating histogram bins corresponding to larger integral areas above the quenching curve. Activation in the presence of G593 ((*R*)-enantiomer) resulted in a significantly smaller AAC_{39} (0.3 μM forskolin + G592: 25.02±0.90 RFU*s (n=6) vs. 0.3 μM forskolin + G593: 22.24±0.89 RFU*s (6), P=0.039, paired t-test) inconsistent with non-specific action at the membrane [10]. Moreover, the activating effect of Elacridar or Zosuqidar disappeared when P-

glycoprotein inhibitors were combined with VX-770 (0.5 μM forskolin + VX-770: 29.68±1.33 RFU*s (4); 0.5 μM forskolin + VX-770 + Elacridar: 28.03±1.03 RFU*s (4); 0.5 μM forskolin + VX-770 + Zosuquidar: 28.58±1.35 RFU*s (4)). The lack of additivity suggests that both potentiator and P-glycoprotein inhibitors bind to CFTR.

Conclusion

P-glycoprotein and MsbA are ATPase-driven pumps, while hydrolysis of bound ATP controls the rate of channel closing in CFTR. Obstructing the ATP hydrolysis step could inhibit substrate transport in pumps and increase open probability in CFTR. Yet why the binding of compounds at CFTR's portals and inner vestibule increases cellular anion conductance, rather than hinder anion permeation, remains unclear.

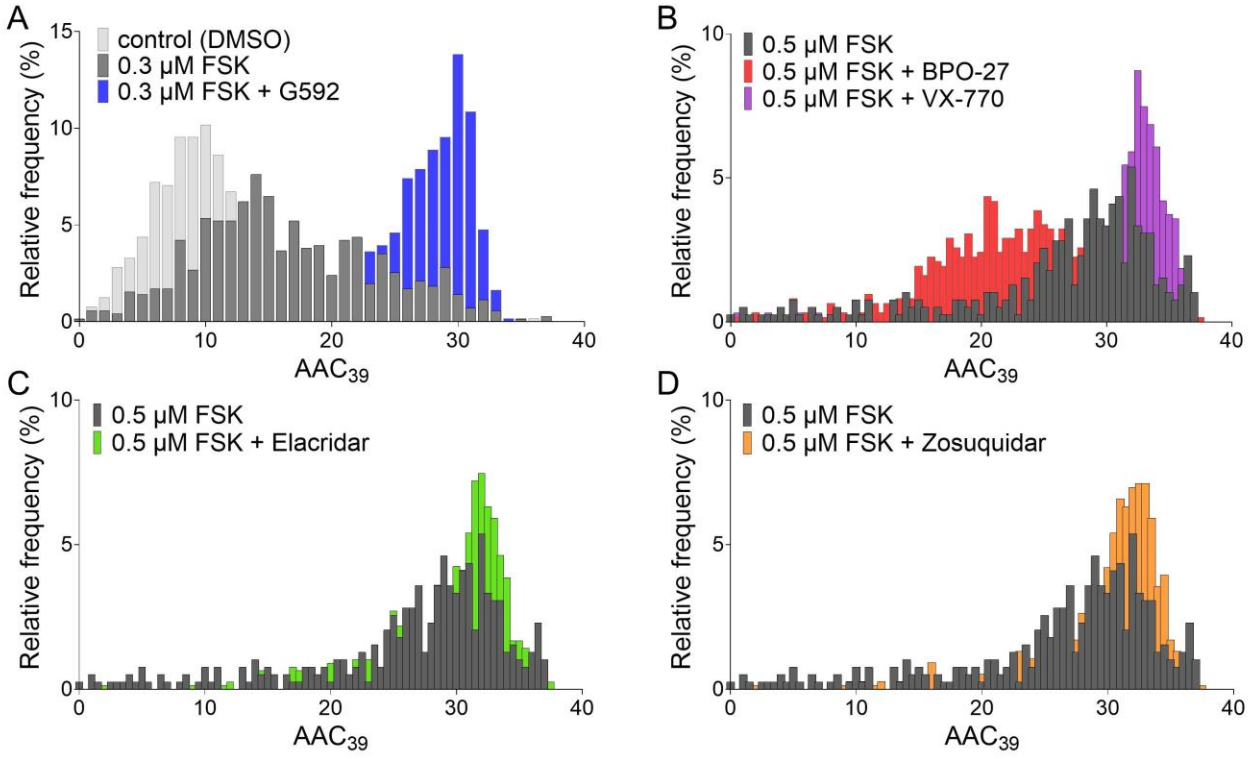

1. Erfinanda, L., et al., Loss of endothelial CFTR drives barrier failure and edema formation in lung infection and can be targeted by CFTR potentiation. Sci Transl Med. , 2022. 14(674): p. eabg8577. 2. Vanherle, L., et al., Restoring myocardial infarction-induced long-term memory impairment by targeting the cystic fibrosis transmembrane regulator. eBioMedicine, 2022. 86: p. 104384. 3. Harwood, K.H., et al., Ivacaftor Alters Macrophage and Lymphocyte Infiltration in the Lungs Following Lipopolysaccharide Exposure. ACS Pharm & Transl Sci, 2022. 5(6): p. 419-428. 4. Liu, M., et al., Treatment of human T-cell acute lymphoblastic leukemia cells with CFTR inhibitor CFTRinh-172. Leuk Res, 2019. 86: p. 106225. 5. Fiedorczuk, K. and J. Chen, Molecular structures reveal synergistic rescue of Δ508 CFTR by Trikafta modulators. Science, 2022. 378(6617): p. 284-290. 6.

Fiedorczuk, K. and J. Chen, Mechanism of CFTR correction by type I folding correctors. Cell, 2022. 185(1): p. 158-168.e11. 7. Thomas, C., et al., Structural and functional diversity calls for a new classification of ABC transporters. FEBS Lett, 2020. 594(23): p. 3767-3775. 8. Prins, S., et al., Fluorescence assay for simultaneous quantification of CFTR ion-channel function and plasma membrane proximity. J Biol Chem, 2020. 295(49): p. 16529-16544. 9. Galietta, L.J., P.M. Haggie, and A.S. Verkman, Green fluorescent protein-based halide indicators with improved chloride and iodide affinities. FEBS Lett, 2001. 499(3): p. 220-224. 10. de Jonge, H.R., et al., Strategies for cystic fibrosis transmembrane conductance regulator inhibition: from molecular mechanisms to treatment for secretory diarrhoeas. FEBS Lett, 2020. 594(23): p. 4085-4108.

C38

Familial Hyperkalaemic Hypertension is associated with Immunodeficiency

Rhys Evans[1], Elizabeth R Wan[1], Viola D'Ambrosio[1,2], Keith Siew[1], Stephen Walsh[1]

[1]University College London, London, United Kingdom, [2]Università Cattolica del Sacro Cuore, Rome, Italy

Introduction
Familial hyperkalaemic hypertension (FHHt) is also known as Gordon syndrome or pseudohypoaldosteronism type II. It is an autosomal dominant condition that leads to salt retention through over activation of the sodium chloride co-transporter (NCC) in the distal convoluted tubule causing salt-sensitive hypertension. Pathogenic mutations in WNK1, WNK4, CUL3 and KLHL3 cause FHHt. Our recent study on patients with salt-losing tubulopathies (SLTs e.g. Gitelman syndrome) found significantly altered immunity, predisposing patients to a variety of infections1. We studied whether FHHt (a salt retaining tubulopathy) also led to an altered immune phenotype.

Methods
12 patients with FHHt were studied. Information such as past medical history, medications, autoimmunity, atopy, allergy status, childhood infections, recurrent adult infections were collected amongst other data. This was compared to 24 healthy controls and 47 patients with salt losing tubulopathy.

Results
Patients with FHHt were found to have significantly more viral (p=0.0094) and fungal infections (p=0.04) compared to healthy controls. They also experienced more recurrent upper respiratory tract infections (p=0.04) and urinary tract infections (p=0.04). Compared to patients with salt losing nephropathy, FHHt patients suffered significantly more recurrent viral infections (p=0.0021) but less allergic disease (p=0.03).

Conclusion
Our data suggests altered immunity in patients with FHHt. Their phenotype and range of infections were different to both healthy controls and patients with salt losing nephropathy. Further work is required to replicate these differences in larger cohorts and to investigate underlying mechanisms that may explain changes in immunity and whether this can be corrected with treatment

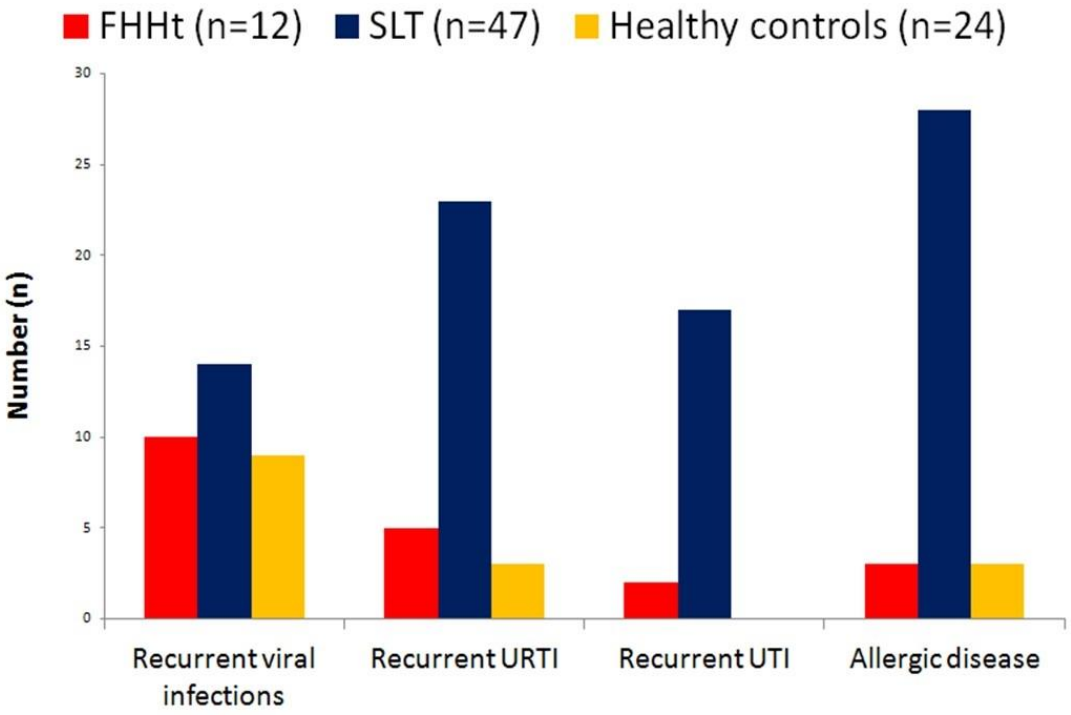

[1] Evans RDR et al. Nat Commun 2020; 11: 4368

C39

Rare tubular disorders and dyslipidaemia: the good, the bad and the unexplained.

Elizabeth Wan[1], Keith Siew[1], Stephen Walsh[1]

[1]*Department of Renal Medicine, University College London, London, United Kingdom*

Introduction: It has long been recognised that thiazide therapy can raise serum cholesterol, specifically low density lipoprotein (LDL), in contradiction to their well evidenced benefit to cardiovascular outcomes[1]. This has also been recognised in those receiving loop diuretics, to a lesser extent[2]. The cause of this is unclear, although it has previously been attributed to serum volume contraction. The rare genetic salt-losing tubulopathies – Gitelman and Bartter syndromes – are equivalent to chronic thiazide and loop diuretic use, respectively[3], but the lipid profiles of these patients have not been explored.

Aims/Objectives: We sought to describe lipid profiles in patients with genetically confirmed Gitelman and Bartter syndromes.

Method: Patients attending a specialist Renal Tubular Clinic were prospectively enrolled in the study over a six month period. 'Control' patients included those with nephrogenic diabetes insipidus, distal renal tubular acidosis, recurrent renal stones, and EAST syndrome. Data were compared using Mann Whitney U Tests.

Results: We recruited 54 patients with Gitelman syndrome, 36 with Bartter syndrome and 139 controls. The mean serum total cholesterol for Gitelman patients was 4.9mmol/L, HDL 1.41mmol/L, LDL 2.68mmol/L and triglycerides 1.94mmol/L. Whilst these are in the normal ranges, both total cholesterol and LDL are significantly higher than in control tubular patients (p=0.029 and p=0.031 respectively). In the case of Bartter syndrome (types 1 to 4 grouped), the mean total cholesterol was 5.38mmol/L, HDL 1.48mmol/L, LDL 3.08mmol/L and triglycerides 1.98mmol/L. Again, both total cholesterol and LDL were significantly higher than in the controls (p=0.00973 and 0.00858). There was no significant difference in weight or HbA1c between patients with Gitelman syndrome and the control group, or patients with Bartter syndrome and the control group.

Conclusions: Findings in patients with rare genetic salt-losing tubulopathies mirror those previously described in cohorts taking diuretic therapy, specifically thiazides and loop-diuretics. This is interesting, and further establishes their role in studying the physiology of the wider population, especially those with hypertensive disease. This study has not established *why* this should be the case, since we do not think patients with Gitelman or Bartter syndrome are chronically volume contracted. We therefore hope this small study acts as a catalyst for further enquiry.

1. Weidmann, Peter, Gerber, Andreas & Mordasini, Rubino. Effects of antihypertensive therapy on serum lipoproteins. Hypertension 5, (1983). 2. Campbell, N. R. C., Wickert, W. A. & Shumak, S. L. Frusemide causes acute increases in lipid concentrations. British Journal of Clinical Pharmacology 36, 607–609 (1993). 3. Mumford, E., Unwin, R. J. & Walsh, S. B. Liquorice, Liddle, Bartter or Gitelman—how to differentiate? Nephrology Dialysis Transplantation 34, 38–39 (2019).

C40

Can whales and dolphins taste salt? Pseudogenisation of a candidate salt taste receptor gene in cetaceans

Fynn Zahnow[1], Chiara Jäger[1], Yassmin Mohamed[1], Stephan Maxeiner[2], Mike Althaus[1]

[1]Bonn-Rhein-Sieg University of Applied Sciences, Institute for functional Gene Analytics, Rheinbach, Germany, [2]Saarland University, Institute for Anatomy and Cell Biology, Homburg, Germany

Introduction
The epithelial sodium channel (ENaC) plays a key role in salt and water homeostasis in tetrapod vertebrates and is also suggested as a candidate receptor for salt taste sensation in rodents. There are four ENaC subunits (α, β, γ, δ) which form heterotrimeric αβγ- or δβγ-ENaCs. Whereas αβγ-ENaC mediates appetitive salt taste in mice, the *SCNN1D* gene, coding for δ-ENaC, is absent in Myomorpha (mice, rats and hamsters) but δ-ENaC appears to be present in human taste buds. The ancestors of modern cetaceans (whales/dolphins) transitioned from a terrestrial to a marine environment 40-50 million years ago. The transition to a marine environment was associated with extensive loss of chemoreceptor genes, including genes coding for olfactory receptors and the receptors mediating bitter and sweet taste. The genes coding for αβγ-ENaC are intact in cetaceans, thereby leading to the wide-spread assumption that cetaceans can only taste salt.

Methods
Using genome information in the National Center for Biotechnology Information (NCBI) database, we analysed the genes coding for the four ENaC subunits, *SCNN1A* (α-ENaC), *SCNN1B* (β-ENaC), *SCNN1G* (γ-ENaC) and *SCNN1D* (δ-ENaC) in 21 cetacean species, belonging to 12 families and 23 sister species of the Artiodactyla (even-toed ungulates), belonging to 9 families.

Results
Whereas *SCNN1A*, *SCNN1B* and *SCNN1G* are intact in species of all investigated cetacean and artiodactylan families, the *SCNN1D* gene displayed multiple insertions/deletions or loss of splice donor-acceptor sites, causing disruption of *SCNN1D* open reading frames across all investigated cetacean families. *SCNN1D* is intact in the investigated artiodactylan families. Pseudogenisation of *SCNN1D* is evident in toothed whales (Odontoceti) and baleen whales (Mysticeti), suggesting that loss of the *SCNN1D* gene occurred early in cetacean evolution. Interestingly, like the previously reported exon 11/12 fusion in the rodent infraorder Hystricognathi (Gettings et al. 2021), a fusion of exons 11 and 12 of the *SCNN1D* gene was observed in the Bovidae (cloven-hoofed, ruminants), with exception of the subfamily Bovinae (bison, buffalos, cattle, and relatives).

Conclusion
These data indicate that there is no functional δ-ENaC in cetaceans, excluding a role for this ENaC isoform in cetacean salt taste. Given the importance of αβγ-ENaC in mammalian renal and lung physiology, the presence of this ion channel does not necessarily point to a role in salt taste physiology and the ability of cetaceans to taste salt.

Gettings, S. M., Maxeiner, S., Tzika, M., Cobain, M. R. D., Ruf, I., Benseler, F., Brose, N., Krasteva-Christ, G., Vande Velde, G., Schönberger, M., & Althaus, M. (2021). Two functional epithelial sodium channel isoforms are present in rodents despite pronounced evolutionary pseudogenisation and exon fusion. Molecular Biology and Evolution, 1, 1–42. https://doi.org/10.1093/molbev/msab271

C41

Tubule-on-a-Chip: Culture and Analysis of a Novel Immortalised Human Distal Convoluted Tubule Cell Line in an Organ-on-a-Chip System

Chutong Zhong[1], Alessandra Grillo[1], Keith Siew[1], Stephen Walsh[1]

[1]*Department of Renal Medicine, Division of Medicine, University College London, London, United Kingdom*

Introduction

The kidney maintains blood pressure and electrolyte balance through the entwined actions of the tubular nephron segments and ion transporters. Recent investigations into rare monogenic diseases, specifically Gordon and Gitelman syndromes, occurring in the distal convoluted tubule (DCT) segment of the kidney, underline the critical physiological role of this segment as well as a DCT-specific membrane protein, sodium chloride cotransporter (NCC, *SLC12A3*), in regulating blood pressure. Despite its crucial significance, no well-characterized and independently validated human DCT cell lines have been identified, with only a limited number of murine DCT cell lines available for *in vitro* studies. To date, none have been incorporated into the Organ-on-a-Chip (OOaC) system. This study aims to employ a novel, immortalized human DCT cell line into a multi-channel OOaC culture system, with the ultimate goal of creating the first human DCT Tubule-on-a-chip (TOaC).

Method

Immortalised hDCT cells characterised in our lab (gifted from Dr Kusaba, Kyoto Prefectural University of Medicine, Japan) were cultured as previously described (Ikeda et al., 2020). Cells were applied in a three-lane, micro-plate-based microfluidic chip platform OrganoPlate (Mimetas, Leiden, Netherland) following manufacture's protocol with modifications on the constitution of the extracellular matrix gel. Tubules formed in the OrganoPlate channel on an average of 5-7 days of culture. TOaCs were fixed using 4% w/v formaldehyde-PBS for 15min at room temperature or lysed with TRI reagent for RNA isolation. Segment specific marker expression was confirmed by staining with fluorescently tagged antibodies/lectins and qPCR.

Result

Barrier integrity assay in the OrganoPlate using fluorescent probes confirmed tight junctions between cells. qPCR of the cell lysate showed these TOaCs expressed the DCT-specific marker NCC (*SLC12A3*). NCC antibody showed positive staining localised to the apical membrane.

Discussion

These preliminary data demonstrate that this novel hDCT cell line is able to form tubule-like structures in the OrganoPlate. Given this cell line were derived from primary human DCT cells, we propose this TOaC model will better reflect *in vivo* human DCT physiology, especially useful in exploring the functionality of membrane transporters and replicating the fluidic movement in the

kidney, comparing to conventional iPSC-based systems. Tubular function will be validated by ion transport assays and pharmacological responses. In the future, we aim to create patient-specific TOaC from urine-derived cells and conduct therapeutic optimisation, thereby bringing true personalised medicine to nephrology.

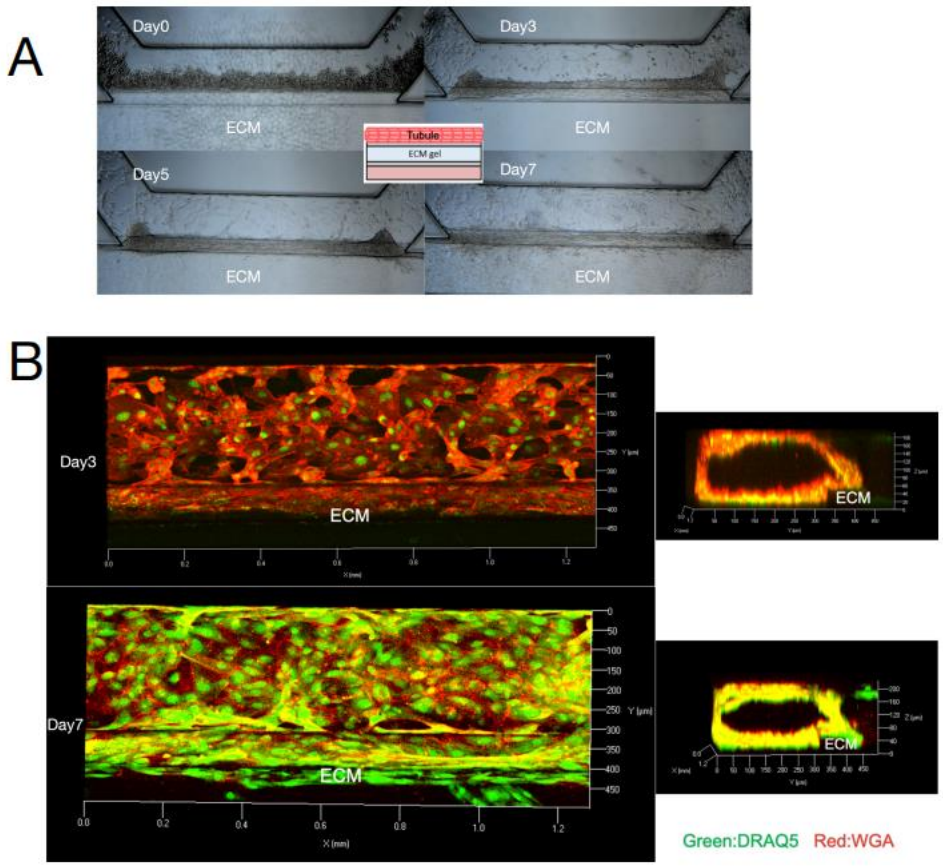

Figure 1. Culture of a novel immortalised hDCT cell line on the 3-lane Organ-On-a-Chip(OOaC) systems. A) The bright field images of the hDCT cells cultring on the OOaC system from Day0 to Day 7. A schematic illustration of the 3-lane design was shown in the middle. **B)** The 3D confocal imaging of the projection and cross-sectional views of the hDCT Tubule-On-a-Chip on Day 3 and Day 7 with immunofluorescence stains DRAQ5 (nuclei) and WGA (membrane) to demonstrata the gradual completion of the tubule.

Ikeda, K., Kusaba, T., Tomita, A., Watanabe-Uehara, N., Ida, T., Kitani, T., Yamashita, N., Uehara, M., Matoba, S., Yamada, T., & Tamagaki, K. (2020). Diverse Receptor Tyrosine Kinase Phosphorylation in Urine-Derived Tubular Epithelial Cells from Autosomal Dominant Polycystic Kidney Disease Patients. Nephron, 144(10), 525–536. https://doi.org/10.1159/000509419

C43

Regulation of WNK-SPAK-NKCC1 pathway by NRBP1-TSC22D2/4 complex

Ramchandra Amnekar[1]

[1]*MRC-PPU University of Dundee, UK*

C44

Golgi-IP: A novel tool for multimodal analysis of Golgi molecular content

Rotimi Fasimoye[1]

[1]MRC Protein Phosphorylation and Ubiquitylation Unit, University of Dundee